Materials Horizons

ROYAL SOCIETY OF CHEMISTRY

REVIEW

View Article Online
View Journal | View Issue

Cite this: *Mater. Horiz.*, 2025, **12**, 4573

Photo-crosslinkable organic materials for flexible and stretchable electronics

Minsung Kim, † Hayeong Park, † Eunjin Kim, Minji Chung and Joon Hak Oh *

As technology advances to enhance human perceptual experiences of the surrounding environment, significant research on stretchable electronics is actively progressing, spanning from the synthesis of materials to their applications in fully integrated devices. A critical challenge lies in developing materials that can maintain their electrical properties under substantial stretching. Photo-crosslinkable organic materials have emerged as a promising solution due to their ability to be precisely modified with light to achieve desired properties, such as enhanced durability, stable conductivity, and micropatterning. This review examines recent research on photo-crosslinkable organic materials, focusing on their components and integration within stretchable electronic devices. We explore the essential characteristics required for each device component (insulators, semiconductors, and conductors) and explain how photo-crosslinking technology addresses these needs through its principles and implementation. Additionally, we discuss the integration and utilization of these components in real-world applications, including physical sensors, organic field-effect transistors (OFETs), and organic solar cells (OSCs). Finally, we offer a concise perspective on the future directions and potential challenges in ongoing research on photo-crosslinkable organic materials.

Received 5th December 2024,
Accepted 19th March 2025

DOI: 10.1039/d4mh01757a

rsc.li/materials-horizons

Wider impact

In flexible and stretchable electronics, photo-crosslinking technology is a powerful technique that enables precise control over the structure of organic materials using specific wavelengths of light. This technique allows for achieving an optimal balance between the mechanical durability and electrical properties. However, there remains a lack of comprehensive reviews summarizing the role of photo-crosslinking in the design of organic materials and their integration into electronic devices. This review aims to fill that gap by analysing key challenges faced by components in stretchable electronics and demonstrating how photo-crosslinking strategies can be used to overcome these obstacles. It also examines recent breakthroughs in material integration, illustrating how this technology enhances the reliability and performance of the devices. By combining structural precision with advanced functionalities, particularly when coupled with additive manufacturing techniques like 3D printing, photo-crosslinking holds immense potential to accelerate the development of stretchable electronics. These advancements are anticipated to drive innovation across diverse industries, including healthcare, environmental monitoring, and energy, ultimately contributing to improving quality of life. We hope this review inspires novel approaches in materials science and provides researchers with valuable insights to propel the advancements in next-generation stretchable electronics.

1. Introduction

The digital revolution is fundamentally transforming our lifestyles and redefining how we interact with technology and communicate with one another. These changes are driving significant advancements in the design and functionality of electronic devices, making them more versatile and user-friendly than ever before. Among these developments, stretchable electronics are leading the way, providing immersive experiences that distinguish them from traditional rigid devices.[1–3] Stretchable electronics represent not just a gradual improvement in performance, but also a paradigm shift that fundamentally changes our approach to electronic interfaces and applications.

Unlike traditional rigid electronic devices, stretchable electronics can adapt to various shapes and surfaces, allowing them to be attached anywhere and worn comfortably. This flexibility enables an unprecedented user experience and functionality, leading to innovative applications across various fields. For example, in the medical and healthcare field, body-attached electronic devices are utilized in wearable health monitors that

School of Chemical and Biological Engineering, Institute of Chemical Processes, Seoul National University, 1 Gwanak-ro, Gwanak-gu, Seoul 08826, Republic of Korea. E-mail: joonhoh@snu.ac.kr

† These authors contributed equally to this work.

track vital signs in real time, providing valuable data for both patients and healthcare providers.[4–6] In robotics, these devices enhance the responsiveness of robots, allowing for more refined interactions with their environments.[7,8] Furthermore, in the field of energy storage, stretchable batteries and supercapacitors are integrated into flexible materials, offering more efficient and adaptable energy solutions.[9–11] Additionally, stretchable electronics play a crucial role in environmental monitoring,[12–14] enabling the collection of air and water quality data across various environments to facilitate rapid responses to ecological changes. In this way, the emergence of stretchable electronics has a wide-ranging impact across industries and daily life.

For the development of stretchable electronics, two different approaches have been primarily investigated: *i.e.*, structure-based approaches and material-based approaches.[15] The structure-based approaches achieve stretchability through geometric patterns and structure designs such as kirigami, origami, and mesh structures.[16–22] However, the complexity of structure designs can complicate the manufacturing process,

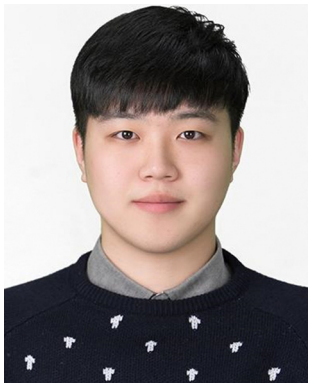

Minsung Kim

Minsung Kim received his BS degree from the School of Chemical and Biological Engineering at Seoul National University in 2021. He is currently enrolled in the MS/PhD program in the School of Chemical and Biological Engineering at Seoul National University, under the supervision of Prof. Joon Hak Oh. His research interests include synthesis of elastomers and their applications.

Hayeong Park

Hayeong Park received her BS degree from the School of Chemical Engineering at Sungkyunkwan University in 2021. She is currently enrolled in the MS/PhD program in the School of Chemical and Biological Engineering at Seoul National University, under the supervision of Prof. Joon Hak Oh. Her research interests include fully stretchable OFETs and circuit applications.

Eunjin Kim

Eunjin Kim received her BS degree from the Department of Chemical Engineering at Pohang University of Science and Technology in 2023. She is currently enrolled in the MS program in the School of Chemical and Biological Engineering at Seoul National University, under the supervision of Prof. Joon Hak Oh. Her research focuses on stretchable OFETs and circuit applications.

Minji Chung

Minji Chung received her BS degree from the School of Chemical and Biological Engineering at Seoul National University in 2024. She is currently enrolled in the MS/PhD program in the School of Chemical and Biological Engineering at Seoul National University, under the supervision of Prof. Joon Hak Oh. Her research interests include the processing of organic/polymer semiconductors for stretchable field-effect transistors.

Joon Hak Oh

Joon Hak Oh is a professor at the School of Chemical and Biological Engineering, Seoul National University, where he received his PhD degree (2004). He conducted his postdoctoral research in the Department of Chemical Engineering at Stanford University (2006–2010). He worked as an assistant professor at the School of Energy and Chemical Engineering at Ulsan National Institute of Science and Technology (2010–2014) and an associate professor in the Department of Chemical Engineering at Pohang University of Science and Technology (2014–2018). His research interests include organic/polymer electronics, advanced optoelectronics with chiral and perovskite materials, and multifunctional sensors.

making it less suitable for large-scale production.[23] Moreover, geometric design typically restricts deformation to specific directions, which limits the potential for multi-directional flexibility.[24,25]

On the other hand, the material-based approaches focus on the precise design of material structures and compositions to obtain desired properties. These approaches allow for the adjustment of the inherent characteristics of the materials through molecular design, ensuring that electronic devices maintain stability even under continuous deformation.[26] Notably, this approach can be tailored to consider biocompatibility with human tissues, thereby contributing to the reliability and safety of electronic devices, particularly in medical and biomedical implant applications.[27–29]

In the material-based approaches, organic materials have become essential materials due to their unique intrinsic properties: excellent elasticity, light weight, and durability.[30] These superior properties of polymers allow devices remain durable under mechanical stimuli. This capability allows for a wide range of applications, from smart clothing to implantable devices that conformally attach to internal organs.

Currently, many researchers are making continuous efforts to balance the mechanical and electrical properties of organic materials for stretchable electronics. Among the various methods to achieve this balance, photo-crosslinking is gaining significant attention. Photo-crosslinking utilizes light with specific wavelengths to rapidly form covalent bonds between organic materials. This technique allows for precise tuning and low-temperature processing, making it easy to modify the properties of soft materials. As a result, it is widely used in the research of stretchable electronics.

In the following, we will explore the utilization of photo-crosslinking technology in stretchable electronic devices (Fig. 1). We will begin by outlining the strategies for incorporating photo-crosslinkable components in stretchable electronics into three main categories: insulators, semiconductors, and conductors. We will discuss the chemical structures and mechanisms behind the application of photo-crosslinking technology to each component. Next, we will highlight how these three elements integrate into a combined device, working together to optimize performance. Through various applications of stretchable electronic devices – such as physical sensors, organic field-effect transistors (OFETs), and organic solar cells (OSCs) – we will examine how these elements interact to enhance the performance of the integrated system, thereby demonstrating the practicality and potential of photo-crosslinking technology. Finally, we will discuss the opportunities that photo-crosslinking technology offers in the field of stretchable electronics.

2. Photo-crosslinking technology mechanisms

Photo-crosslinking technology is a simple method to modify the physical and chemical properties of organic materials by employing light to induce covalent bonds between polymer chains or molecular components (Fig. 2). Typically, this process involves the generation of reactive intermediates (*e.g.*, radical, ion, carbene, *etc.*) *via* light activation. These intermediates then engage in subsequent reactions to form robust crosslinks, setting the stage for a wide variety of material transformations.

A common example of this approach is free radical polymerization. In such systems, a photoinitiator absorbs UV or visible light and transitions to an excited state. This excited state weakens internal bonds, leading to their cleavage and the formation of free radicals. These radicals then add to C–C unsaturated bonds, initiating chain propagation and eventually combining to form a stable crosslinked network.[41,42] Similarly, benzophenone-based hydrogen abstraction utilizes light in a related mechanism. Upon absorbing light, benzophenone reaches an excited triplet state that abstracts a hydrogen atom from a nearby polymer chain's C–H bond. The resulting polymer radical can then either couple with another radical or participate in further reactions, effectively forming crosslinks without requiring an additional initiator.[43–45]

Expanding on radical-based processes, the thiol–ene reaction represents another effective photo-crosslinking pathway. Here, light activates a thiol (–SH) group to produce a thiyl radical. This radical promptly adds to a C–C unsaturated bond, generating a carbon-centered radical that subsequently reacts with another thiol. Through repeated cycles, this mechanism gradually builds a uniform and resilient crosslinked network.[46,47]

Beyond these radical mechanisms, diazirine and azide-based photocrosslinking reactions exploit light to generate highly reactive intermediates without the need for a separate initiator. Upon exposure to light, these functional groups release small molecules such as nitrogen, thereby producing reactive carbene or nitrene intermediates. These intermediates rapidly insert into C–H bonds or other reactive sites on the polymer chain, directly forming crosslinks.[48–52]

Photoacid-mediated crosslinking represents a unique strategy for forming covalent polymer networks through the controlled release of acid. In this process, the photoacid generator (PAG) absorbs light to reach a high-energy state and subsequently undergoes bond cleavage to release acid. This acid protonates acid-sensitive monomers (*e.g.*, epoxides, vinyl ethers, *etc.*), generating active intermediates that react with adjacent monomers to gradually build a covalent network. This mechanism can initiate either ring-opening or step-growth polymerization *via* nucleophilic substitution. Unlike radical polymerization, photoacid-mediated reactions are insensitive to atmospheric oxygen and do not involve termination reactions, resulting in high curing efficiency and the formation of diverse polymer backbones.[53] PAGs are generally classified into ionic and non-ionic types. Ionic PAGs are typically based on onium salt derivatives (*e.g.*, diaryliodonium salts, sulfonium salts, *etc.*). When exposed to light, they generate acid *via* direct π–σ^* or π–π^* transitions or by intersystem crossing to the

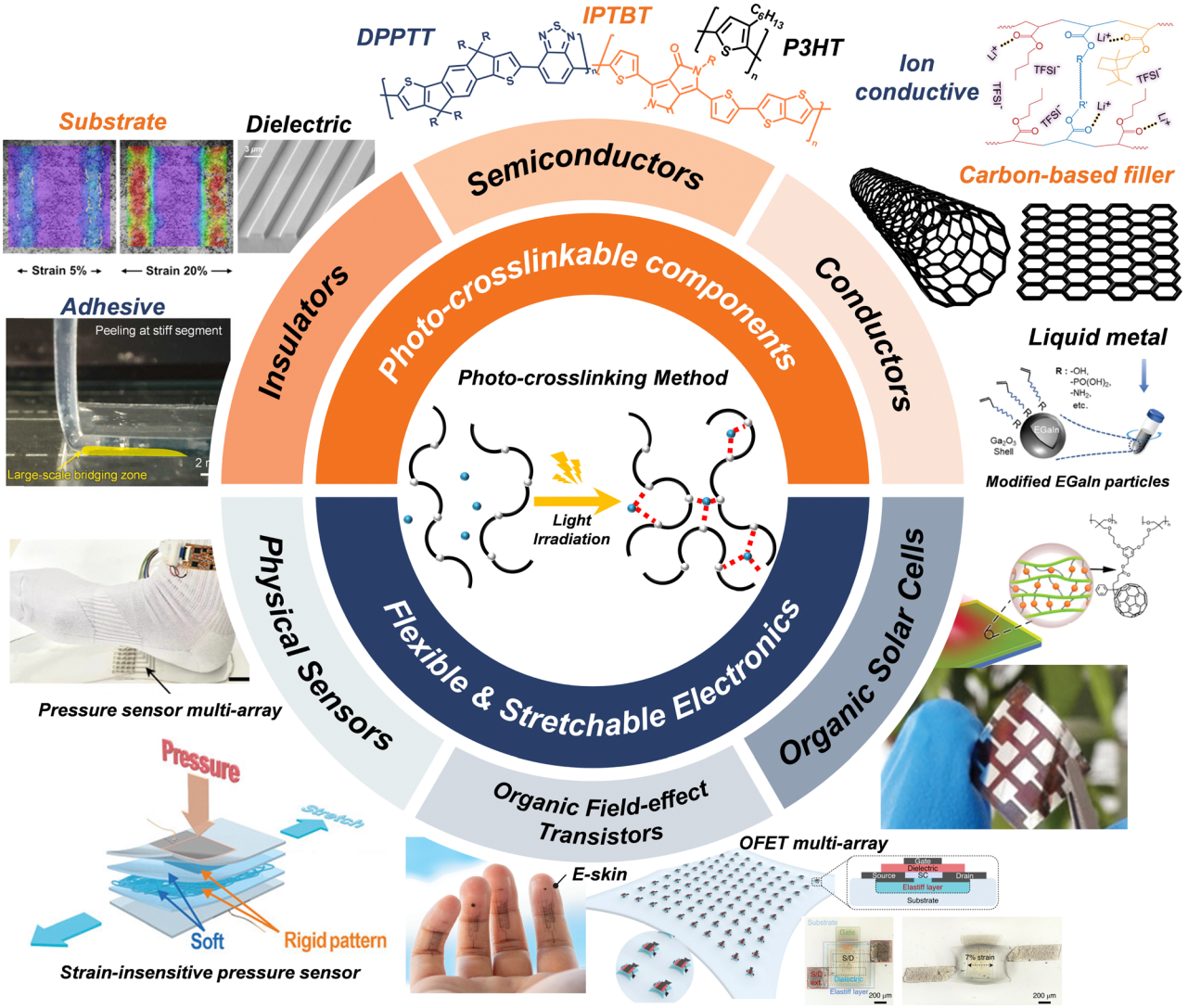

Fig. 1 Schematic illustration of photo-crosslinkable components and their applications in flexible and stretchable electronics. Image of "substrate"[31] Copyright 2021, The American Association for the Advancement of Science. Image for "dielectric"[32] Copyright 2017, American Chemical Society. Image for "adhesive"[33] Copyright 2024, Elsevier. Image for "ion conductive"[34] Copyright 2022, American Chemical Society. Image for "liquid metal"[35] Copyright 2023, Wiley-VCH. Image for "organic solar cells"[36] Copyright 2019, Wiley-VCH. Image for "OFET multi-array"[37] Copyright 2021, Springer Nature. Image for "E-Skin"[38] Copyright 2023, The American Association for the Advancement of Science. Image for "strain-insensitive pressure sensor"[39] Copyright 2024, Wiley-VCH. Image for "pressure sensor multi-array"[40] Copyright 2022, American Chemical Society.

triplet state, followed by either heterolytic or homolytic bond cleavage.[54,55] In these systems, the cation determines the photochemical reactivity and thermal stability, while the counter-anion (*e.g.*, BF_4^-, PF_6^-, and SbF_6^-) controls the acid strength and the rate of polymerization initiation.[56,57] However, ionic PAGs often exhibit limited solubility in reactive monomers or organic solvents.[53,58] Additionally, they often require thicker films to ensure sufficient radiation absorption and may pose potential issues related to toxicity and external band reactivity.[59–61] To overcome these limitations, non-ionic PAGs have attracted significant attention. Under illumination, the C–O, S–O, and N–O bonds in non-ionic PAGs (*e.g.*, imido sulfonate, arylsulfonate esters, *etc.*) undergo dissociation, forming structurally stabilized radicals. These radicals then extract hydrogen from protic solvents, leading to the generation of acidic compounds. Their excellent solubility in various solvents and polymer matrices makes them particularly useful for photopolymerization and surface curing applications.[62–64] Although non-ionic PAGs are generally less thermally stable than their ionic PAGs, this drawback has been effectively mitigated through careful modification of pendant structures within their molecular frameworks.[65]

Photomedicated redox catalysts provide an alternative pathway for generating active intermediates that lead to crosslink formation. In this method, catalysts (*e.g.*, $Ru(bpy)_3^{2+}$, $Ir(ppy)_3$, *etc.*) absorb light and transition to an excited state, resulting in significant changes in their electronic structures that enhance

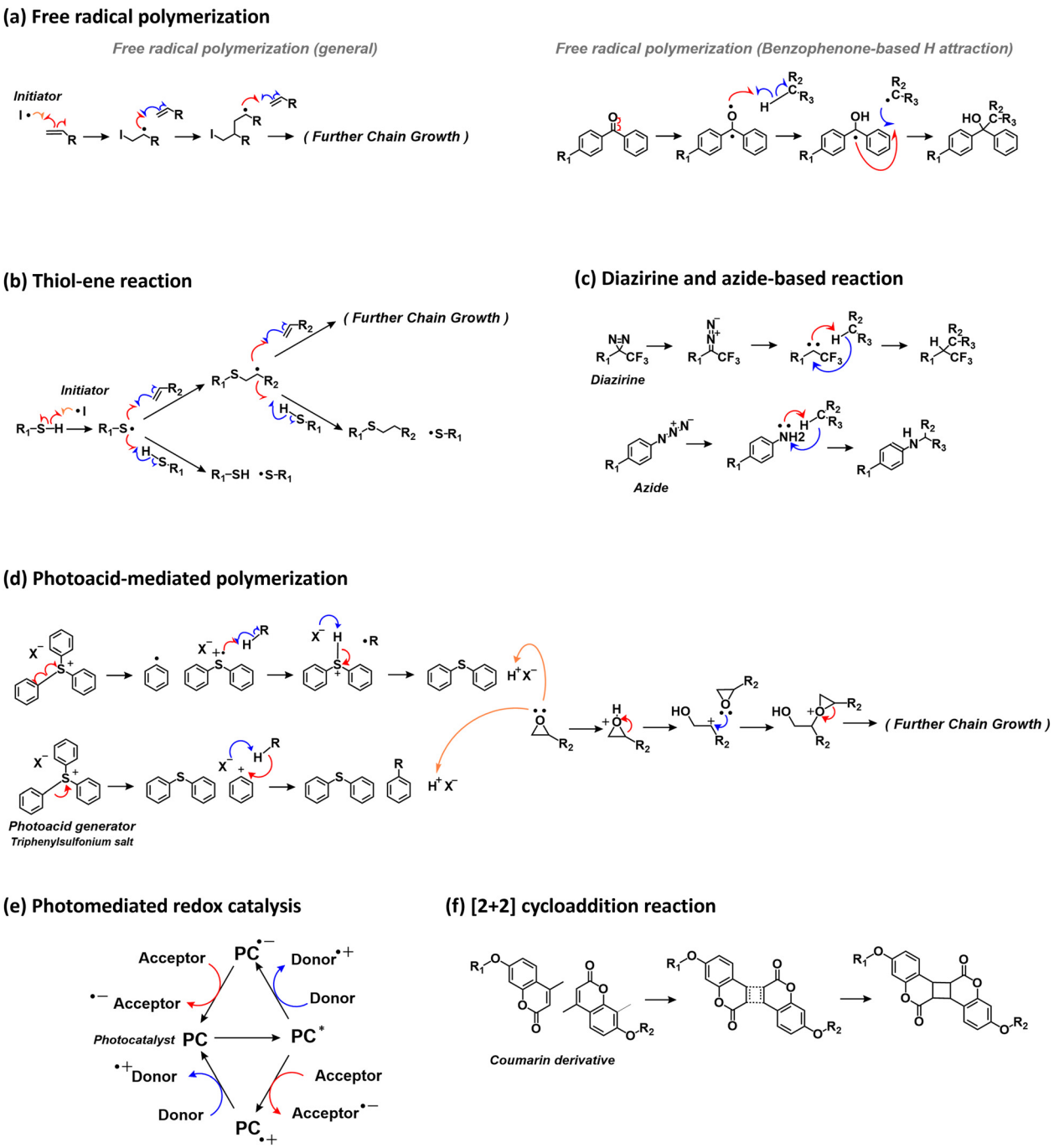

Fig. 2 Schematic representation of various photo-crosslinking mechanisms. (a) Free radical polymerization. (b) Thiol-ene reaction. (c) Diazirine and azide-based reaction. (d) Photoacid-mediated polymerization. (e) Photomediated redox catalysis. (f) [2+2] cycloaddition reaction.

their electron-donating and electron-accepting abilities. The excited catalyst interacts with redox-active groups in the reactants, inducing electron transfer that converts stable reactants into highly reactive radical species or radical ions. These reactive intermediates combine to form crosslinks, while the catalyst is regenerated through additional electron transfer, thereby sustaining an efficient polymerization cycle.[66–68] For optimal performance, the redox potentials of the catalyst and reactants must be well-matched to facilitate efficient electron transfer and selective crosslinking while minimizing side reactions. Furthermore, a sufficiently long excited state lifetime is essential to enable efficient electron or hydrogen transfer between donors and acceptors. Additionally, achieving both high photoluminescence quantum efficiency and excellent reversibility is essential for efficient catalyst recycling.[66,68–71]

Table 1 Summary of the advantages and applications of representative photo-crosslinkable organic materials: insulators and semiconductors

Functional role	Materials	Crosslinking agent	Mechanism	Application	Max. stretchability	ref.
Insulator Substrate	POSS-grafted acrylate PEG	Acrylate	Free radical	Substrate	9455%	74
	PP/mSEBS	PP/mSEBS	Free radical	Substrate	700%	75
	Polyepoxy acrylate/polyurethane acrylate	Acrylate	Free radical	Transistor array, circuit	50%	76
	Acrylate	Acrylate	Free radical	Physical sensor	100%	39
Dielectric	PVDF-HFP/COC/FPA azide	FPA azide	Azide	OFET	Flexible	77
	P(NB/VNB)/PETMP	PETMP	Thiol–ene	OFET	Flexible	78
	PVDF-CTFE/thiol-modified $BaTiO_3$	Thiol-modified $BaTiO_3$	Thiol–ene	Dielectric	400%	79
	ZrTA	ZrTA	Free radical	OFET	Flexible	80
	$ZrCl_4$/HDDA	HDDA	Free radical	OFET	Flexible	81
	Polystyrene/PEG-azide	PEG-azide	Azide	OFET	Flexible	82
	SEBS/azide	Azide	Azide	Transistor array, circuit	100%	83
	PVDF-TrFE-CTFE-azide	PVDF-TrFE-CTFE-azide	Azide	Dielectric	Flexible	84
	Parylene-OH	Parylene-OH	Free radical	Transistor array/ inverter	Flexible	85
	PMMA/BBP-4	BBP-4	Free radical	OFET	Flexible	86
	PEG-SH/acrylate/BMITFSI	PEG-SH/acrylate	Photoacid/thiol–ene	OFET	130%	87
	PDMS/BP	PDMS/BP	Free radical	Physical sensor	Flexible	40
	PAAm/$CaCl_2$	PAAm/$CaCl_2$	Free radical	Physical sensor	55.64%	88
Adhesive	Disulfide-based dynamic material	Disulfide-based dynamic material	Free radical	Adhesive	Flexible	89
	Acrylate/PEGDMA	PEGDMA	Free radical	Adhesive	Flexible	90
	PAAm/P(BA-*co*-IBA)	Acrylate	Free radical	Adhesive	200%	33
	Polyurethane acrylate	Acrylate	Free radical	Physical sensor	Flexible	91
	Acrylate	Acrylate	Free radical	Adhesive	Flexible	92
Semiconductor	DPP based polymer	Butadiyne functionalized polymer	Free radical	OFET	Flexible	93
	PDPP4T-N_3	PDPP4T-N_3	Azide	OFET	Flexible	94
	Coumarin functionalized DPP based polymer	Coumarin	[2+2] cycloaddition	OFET	Flexible	95
	P3HT-azide	P3HT-azide	Azide	OFET	Flexible	96
	IDTBT/*n*-NIPS	*n*-NIPS	Azide	OFET	80%	51
	P4TDPP/SBS/TRIS	SBS/TRIS	Thiol–ene	OFET	100%	97
	PDPP4T/PDPP3T-2F/N2200/PN3	PN3	Azide	OFET/inverter	Flexible	98
	PTDPPTFT4/Acrylate/TRIS	Acrylate	Free radical	OFET/inverter	Flexible	99
	DPP/N2200/SU8/Pcell	Pcell/SU8	Cycloaddition/ photoacid	OFET/inverter	Flexible	100
	Vinyl functionalized N2200/PBDBT	Vinyl functionalized polymer	Free radical	OSC	Flexible	101
	PM6/BAC	BAC	Azide	OSC	20%	102

While many photo-crosslinking reactions proceed generating reactive intermediates that then form crosslinks, some reactions rely on direct bonding between excited state groups. A prominent example of this is the [2+2] cycloaddition reaction. In this process, a light-activated functional group undergoes a $\pi \rightarrow \pi^*$ transition, and when two such excited groups are correctly aligned, they simultaneously form two σ bonds to create a four-membered cyclobutane ring.[72] Notably, certain [2+2] cycloaddition systems (*e.g.*, coumarin, cinnamate, thymine, *etc.*) are reversible. Under specific wavelengths of light, the cyclobutane ring can reopen to restore the original double bonds, a feature that is particularly advantageous for developing self-healing materials or for fine-tuning material properties under various conditions.[73]

Through various mechanisms, photo-crosslinking technology offers a powerful method for material scientists. In flexible and stretchable electronic devices, techniques such as employing photoinitiators to generate free radicals or using diazirine and azide groups to readily form reactive intermediates are widely adopted. This precise control over covalent bond network formation enables the custom fabrication of photo-crosslinkable materials, allowing fine-tuning of their properties and driving significant advancements across a broad spectrum of stretchable device applications (Tables 1 and 2).

3. Photo-crosslinkable insulators for stretchable electronics

In stretchable electronic devices, insulators are utilized in three key components: (i) substrates; (ii) dielectrics; (iii) adhesives. Each of these components plays a crucial role in ensuring the flexibility, durability, reliability of the devices. This chapter outlines how photo-crosslinking method enhances performance and functionality of each component for stretchable electronics.

3.1. Substrates

The substrates in stretchable electronic devices play a vital role in supporting electronic components while accommodating

Table 2 Summary of the advantages and applications of representative photo-crosslinkable organic materials: conductors and multiple roles

Functional role		Materials	Crosslinking agent	Mechanism	Application	Max. stretchability	ref.
Conductor		PEDOT:PSS/PR-PEGMA	PR-PEGMA	Free radical	Electrode	150%	103
		Acrylate functionalized EDOT:PSS	Acylate	Free radical	Electrode	Flexible	104
		Doped cinnamate polythiophene	Cinnamate polythiophene	[2+2] cycloaddition	OFET	Flexible	105
		Epoxy grafted P3HT	Epoxy grafted P3HT	Photoacid	Electrode	150%	106
		Modified EGaIn particle	Acrylate	Free radical	Electrode	2200%	35
		Graphene oxide/acrylate	Acrylate	Free radical	Electrode	Flexible	107
		MWCNT/acrylate	Acrylate	Free radical	Electrode	60%	108
		Acrylate/EMIMDCA	Acrylate	Free radical	Physical sensor	1500%	109
		$Al(OH)_3$/acrylate/EMIES	Acrylate	Free radical	Physical sensor	487%	110
		LiTFSI/acrylate	Acrylate	Free radical	Physical sensor	1300%	34
		Acrylate/LiCl	Acrylate	Free radical	Physical sensor	Flexible	111
		Acrylate/$MgCl_2$	Acrylate	Free radical	Physical sensor	Flexible	112
		V-POSS/acrylate/$EMIM(EtO)_2PO_2$	V-POSS/acrylate	Free radical	Physical sensor	1200%	113
		Acrylate/PVA/NaCl	Acrylate	Free radical	Physical sensor	Flexible	114
		PDMMAm/TEOS/$BMIMTf_2N$	Acrylate	Free radical	Physical sensor	210%	115
		Acrylate/LiTFSI	Acrylate	Free radical	Physical sensor	>1000%	116
		Acrylate/ChCl/tannic acid-encapsulated cellulose nanocrystals	Acrylate	Free radical	Physical sensor	2400%	117
		Acrylate/cellulose nanofibril/PBA-IL	Acrylate	Free radical	Physical sensor	1810%	118
		Acrylate/PVA/KCl	Acrylate	Free radical	Physical sensor	>500%	119
		Acrylate/$BMIMBF_4$	Acrylate	Free radical	Physical sensor	>1000%	120
		Acrylate/$EMIMBF_4$	Acrylate	Free radical	Physical sensor	30%	121
		PEDOT:PSS/PEGDE	PEGDE	Photoacid	Physical sensor	50%	122
Multiple roles	Substrate/dielectric/electrode	SBS/NBR/PEDOT:PSS/PETMP, C10-azide,PR-PEGMA	PETMP/C10-azide/PR-PEGMA	Thiol–ene, azide, free radical	Transistor array, circuit	100%	123
	Semiconductor/dielectric	DPPTT/IDTBT/SEBS/FPA end-capped BA/FPA end-capped BH	Azide	Azide	Transistor array	100%	124
	Semiconductor/dielectric/electrode	P(DPP2DT-TVT)/P(NDI3OT-Se2)/PMMA/PS/PVDF-HFP/AgNP/4Bx	4Bx	Azide	Transistor array, circuit	Flexible	125
	Semiconductor/dielectric/electrode	PEGDMA/PEDOT:PSS/diazirine/DPPTT/PMMA	Diazirine/PEGDMA	Diazirine/free radical	Transistor array, circuit	100%	126
	Semiconductor/dielectric/encapsulation	DPP/BA azide/PFDT	BA aizde/PFDT	Azide/thiol–ene	OFET	100%	127

mechanical deformations. To ensure both performance and reliability, the substrate must effectively dissipate repeated mechanical stress, thereby protecting the integrated electronics. Achieving this requires a delicate balance between mechanical durability to support and stabilize components and flexibility to withstand deformation. However, mechanical durability and flexibility are often in a trade-off relationship, making it challenging to optimize both requirements simultaneously.[128]

To resolve these conflicting demands, researchers have proposed two promising strategies. The first strategy focuses on improving stretchability through polymer interactions, which promote even energy dissipation, enabling the substrate to absorb and distribute external forces effectively. The second strategy involves incorporating rigid structures into the substrate which primarily serve as supportive elements, while the surrounding softer parts provide flexibility. These rigid islands protect electronic components by resisting external forces. Photo-crosslinking techniques offer a powerful means of achieving these strategies by precisely tuning the mechanical characteristics of organic materials. By controlling crosslinking density, it is possible to modulate the modulus, elasticity, and toughness of the substrate, allowing for improved stretchability and mechanical robustness. Additionally, photo-crosslinking enables the formation of interfacial crosslinked networks, which enhance energy dissipation, and facilitates the fabrication of rigid-island architectures, providing localized mechanical reinforcement without sacrificing overall flexibility.

This chapter will outline how these two strategies can be applied using photo-crosslinking techniques: (i) increasing energy dissipation through polymer entanglement or interfacial crosslinking; (ii) facilitating the formation of rigid islands using photo-crosslinking methods.

3.1.1. Blending photo-crosslinkable polymers. Blending different polymer chains is an effective strategy for energy dissipation. Physical entanglement and interactions between polymer chains help distribute mechanical stress during deformation. Pruksawan *et al.* developed a hydrogel crosslinking system using polyhedral oligomeric silsesquioxane (POSS)-grafted acrylated polyethylene glycol (PEG) as a crosslinker.[74] This approach achieved uniform crosslinking and maximized physical entanglement (Fig. 3a). The study highlighted two main energy dissipation mechanisms. The first was energy dissipation through the silica core of POSS. The nanoscale silica core formed a rigid structure within the hydrogel, distributing external stress evenly across the material and reducing stress concentration in specific areas, which strengthens the hydrogel. The second mechanism involved energy dissipation through the physical entanglement of PEG chains. The long PEG chains attached to POSS created a complex network within the hydrogel that absorbs and distributes energy when subjected to external forces. This mechanism allowed the hydrogel to maintain high elongation while effectively absorbing impact and resisting deformation. As a result, the POSS-PEG-based hydrogel achieved a high energy dissipation capacity of up to 6531 kJ m^{-3} and an elongation rate of up to 9455% (Fig. 3b).

Additionally, crosslinking between polymer plays an important role in energy dissipation. For example, Xu *et al.* enhanced the mechanical performance of a blend of polypropylene (PP) and maleic anhydride-crosslinked styrene-ethylene-butylene-styrene (mSEBS) through photo-crosslinking.[75] The study presented two main energy dissipation mechanisms. First, photo-crosslinking increased the rigidity of mSEBS, enabling the absorption and dissipation of strain through a cold drawing process. The second mechanism occurred at the interface between the PP and the mSEBS. Photo-crosslinking formed chemical bonds between the PP and mSEBS, resulting in strong interfacial bonds between the two phases, leading to effective stress transfer and distribution of external stress. Consequently, the strong interfacial bond significantly enhanced the material's tensile strength and resistance to external impacts.

3.1.2. Rigid island technology. The rigid island technique involves creating rigid structures on a soft substrate.[37,129] The rigid parts can support electronic components, while the surrounding soft material remains deformable to withstand repeated strain. A crucial aspect of this technique is ensuring a distinct modulus difference between the rigid islands and the soft substrate,[130,131] while simultaneously preventing delamination between these two regions.[132,133] To meet these requirements, researchers have developed various strategies, such as embedding of rigid polymers,[134,135] incorporation of curing inhibitors,[136,137] and geometric structuring.[138–140] However, the complexity of these processes highlights the necessity for more straightforward alternatives. In this regard, photo-crosslinking presents a viable solution.

Park *et al.* synthesized a photo-crosslinkable polymer based on acrylates that enables the simultaneous formation of rigid and soft regions.[39] The polymer was functionalized by grafting additional double bonds onto the acrylate backbone using a urethane reaction, specifically by incorporating 2-isocyanatoethyl acrylate (IEA). Upon exposure to UV light, these double bonds selectively crosslinked, forming rigid islands on the substrate. A significant advantage of this polymer was its ability to create fine rigid islands (7 μm) directly on the substrate using a UV mask, eliminating the need for additional processing steps. The researchers demonstrated that by

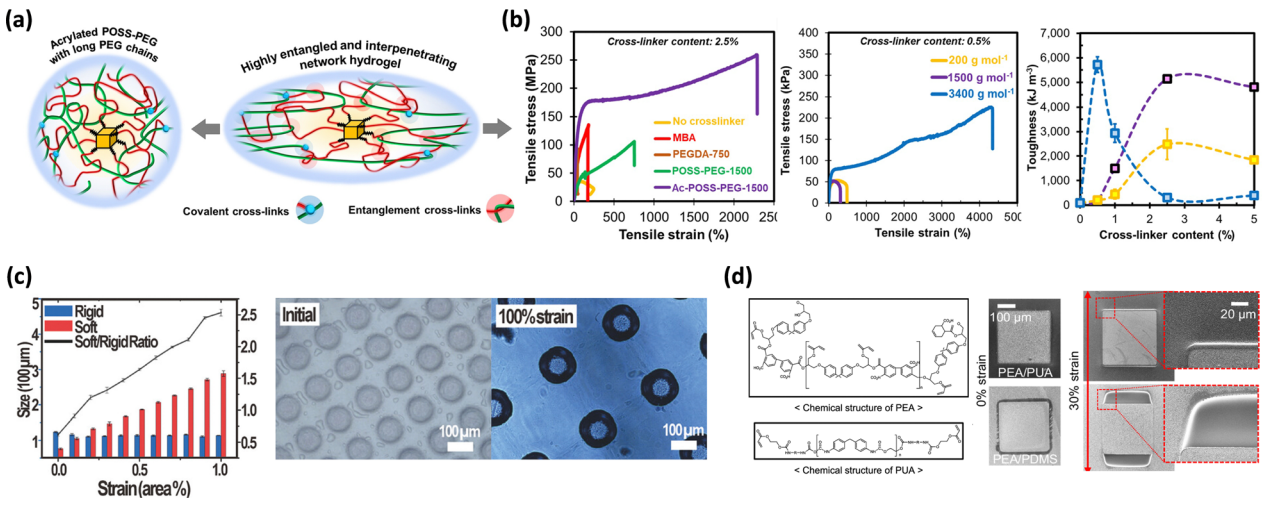

Fig. 3 Enhancement of the mechanical properties of polymeric materials using photo-crosslinkers. (a) Schematic illustration of toughening achieved using the Ac-POSS-PEG crosslinker. (b) Mechanical properties of PAM-Ac-POSS-PEG hydrogels with different molecular weights of PEG.[74] Copyright 2023, Springer Nature. (c) The ratio of rigid/soft regions and optical images of the patterned substrate.[39] Copyright 2024, Wiley-VCH. (d) Chemical structure of PEA/PUA and the optical image of PEA/PUA and PEA/PDMS substrates.[76] Copyright 2024, Springer Nature.

controlling the crosslinking sites of the photo-crosslinkable polymer, they could achieve a modulus increase of up to 38 000%, confirming its suitability for use as rigid islands. When the substrate, which includes circular rigid islands (100 μm in diameter) and soft regions (50 μm in diameter), was stretched, only the distance between the rigid islands changed, while their size and shape remained consistent (Fig. 3c). This observation demonstrated the effectiveness of this technique in rigid island formation.

Additionally, Kang *et al.* successfully established a strong interfacial bond between the rigid and soft regions through simultaneous crosslinking.[76] This approach effectively prevented delamination while leveraging the modulus difference between polyepoxy acrylate (PEA) and polyurethane acrylate (PUA) (Fig. 3d). The resulting structure exhibited exceptional durability, capable of withstanding structural defects even at a strain of 50%. The residual acrylate groups in PEA bonded with the acrylate groups in PUA, creating robust interfacial adhesion that integrated the two materials into a cohesive unit.

3.2. Dielectric materials

Stretchable electronics now require organic dielectrics to outperform traditional oxide-based dielectrics. While maintaining a high-dielectric constant and lowering dielectric loss is still essential, the organic dielectric must also form stable interfaces with electronic components and withstand various environmental conditions. These requirements underscore the need for more comprehensive molecular design research to meet the high-performance demands of modern devices. Crosslinking is an effective approach to addressing these challenges.[141–143] By restricting the mobility of molecular chains, crosslinking reduces orientation polarization and blocks impurity movement, thereby improving dielectric properties.[144] Additionally, it enhances solvent resistance and prevents defects at the semiconductor interface.[145,146] Furthermore, the smoother surface created through crosslinking can improve the crystalline morphology of the semiconductor, leading to more reliable device performance.[147]

This chapter will discuss how photo-crosslinking can enhance dielectric properties without complex processes: (i) enhancing dielectric properties through adjusting crosslink density; (ii) achieving uniform dispersion of inorganic oxides within the dielectric; and (iii) improving the interface between dielectrics and semiconductors. Finally, we introduce photo-patterning technique for dielectrics through improved solvent resistance.

3.2.1. Enhancing dielectric properties through adjusting crosslink density. Photo-crosslinking has emerged as a promising method to significantly enhance the performance of polymer dielectrics. Recent studies have shown that adjusting the crosslink density in dielectrics can effectively influence the electrical properties.[86,148] For example, Kwon *et al.* introduced a photo-crosslinking technique to improve the performance of a high-*k* dielectric material, poly(vinylidene fluoride-*co*-hexafluoropropylene) (PVDF-HFP).[77] PVDF-HFP exhibited ferroelectric behavior, which caused hysteresis due to the reorientation of C–F dipoles under an electric field. To address this issue, the researchers applied a fluorophenyl azide crosslinker (FPA) to PVDF-HFP through photo-crosslinking to modify the crystalline structure of the polymer (Fig. 4a). As the crosslink

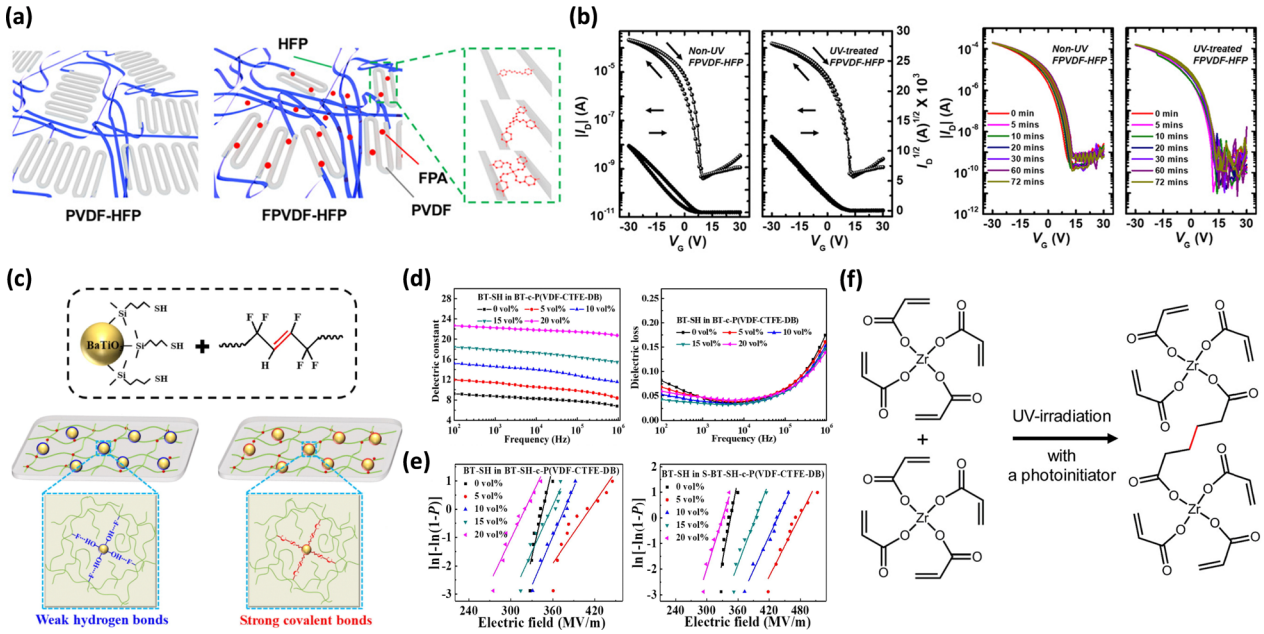

Fig. 4 Enhancement of dielectric properties. (a) Schematic illustration of photo-crosslinking in a PVDF-HFP crystalline structure. (b) Transfer characteristics of the C10-DNTT OFETs with FPVDF-HFP.[77] Copyright 2020, American Chemical Society. (c) Schematic illustration of the crosslinking between BT-SH and P(VDF-CTFE-DB). (d) Dielectric properties as a function of frequency for BT-SH-c-P(VDF-CTFE-DB). (e) Breakdown strength of BT-SH-c-P(VDF-CTFE-DB) before (left) and after 400% strain (right).[79] Copyright 2022, Elsevier. (f) Schematic illustration of photo-crosslinking of ZrTA.[80] Copyright 2016, American Chemical Society.

density increased in PVDF-HFP, the size of the VDF crystalline grains decreased. This reduction in the grain size suppressed the reorientation of C–F dipoles, leading to a decrease in ferroelectric domains and thus reducing hysteresis (Fig. 4b). Furthermore, the increased crosslink density resulted in denser and more closely packed dielectric layer, which decreased leakage current density and consequently increased the on/off ratio.

Similarly, Kim *et al.* demonstrated that increasing the crosslinking density through thiol–ene click reaction improved the dielectric properties of vinyl-addition polynorbornene copolymers (P(NB/VNB)).[78] By adjusting the amount of pentaerythritol tetrakis(3-mercaptopropionate) (PETMP), they found that adding up to 3 wt% of the crosslinker enhanced the dielectric properties without causing film defects. The crosslinked P(NB/VNB) films with 3 wt% PETMP (cP(NB/VNB)-3) showed a significant increase in the dielectric constant from 2.25 to 3.39 and breakdown electric field from 2.46 MV cm^{-1} to 3.27 MV cm^{-1}. Moreover, the cP(NB/VNB)-3 exhibited minimal hysteresis during OFET operation, which was due to the reduction of free volume and charge trapping resulting from the high crosslinking density.

3.2.2. Uniform dispersion of inorganic oxides within the dielectric materials. Organic dielectrics have often been created by blending high-performance SiO_2 and other inorganic oxides to enhance their dielectric constant.[149–151] However, the high surface energy of nanoparticles can lead to agglomeration and uneven distribution, which may increase dielectric loss.[152,153] This non-uniformity complicates the formation of thin high-dielectric constant layers. Therefore, it is essential to improve the interface between nanoparticles and the polymer matrix. Strong crosslinking at the interface between particles and polymers can positively influence the uniform dispersion of particles.[154,155] Zhang *et al.* explained that the chemical bond between nanoparticles and the polymer matrix limits charge carrier movement and minimizes dielectric loss.[156] This crosslinked network structure also prevented dipolar disorder and charge trapping, leading to higher dielectric constant and greater thermal stability.

In this context, photo-crosslinking can be employed as an effective method to enhance the interface between nanoparticles and the polymer matrix. For example, Ma *et al.* functionalized barium titanate nanoparticles with thiol groups (BT-SH) to enable crosslinking with a polymer matrix (P(VDF-CTFE-DB)) (Fig. 4c).[79] The resulting thiol–ene reaction formed strong bond between BT-SH and P(VDF-CTFE-DB), which improved nanoparticle dispersion and reduced defects within the polymer. As a result, this process could stabilize the dielectric constant and reduce dielectric loss (Fig. 4d). Notably, the crosslinking improved the breakdown strength from 366.7 MV m^{-1} to 409.2 MV m^{-1}, because BT-SH acted as traps for charge carrier and a scattering center for electrical stress. Additionally, when the film was stretched by 400%, the breakdown strength further increased to 476.6 MV m^{-1} (Fig. 4e). This notable improvement was due to the orderly alignment of polymer chains and BT-SH during stretching, which prevented the electrical stress concentration.

Recently, organometallic monomers have been utilized to achieve uniform dispersion of inorganic components within the dielectric. Kim *et al.* introduced a photo-crosslinkable organic–inorganic hybrid gate dielectric based on zirconium tetraacrylate (ZrTA) (Fig. 4f).[80] ZrTA consisted of Zr^{4+} cations and acrylate anions, where the acrylate groups undergo photo-crosslinking to form high-dielectric constant materials (k = 5.48). This hybrid structure combined the benefits of both organic and inorganic materials, resulting in low leakage current (10^{-7} A cm^{-2} at 2 MV cm^{-1}) and excellent surface properties, including a very low roughness (0.449 nm), which promoted favorable semiconductor growth. The crosslinked ZrTA film also showed enhanced hydrophobicity due to its organic acrylate matrix, which minimizes polar surface groups like hydroxyls. This reduction in polar groups helped to reduce charge trapping, leading to more efficient charge carrier transport.

3.2.3. Improvement of semiconductor/dielectric interfaces. Introducing polar functional groups, such as hydroxyl and cyanoethyl groups, is a common strategy to enhance the dielectric constant.[157–159] However, these groups can create charge trapping sites that reduce mobility and induce hysteresis behavior.[160,161] To tackle these issues, researchers are exploring methods that involve crosslinked low-dielectric constant interface layers as a charge trapping barrier onto the polar polymers.[162]

Tousignant *et al.* fabricated a bilayer dielectric structure by photo-crosslinking a polyvinyl alcohol (PVA) surface (Fig. 5a).[163] They used 2,2-dimethyl benzodioxinone terminated polycaprolactone (UV-PCL), which effectively crosslinked with the hydroxyl groups of PVA. The UV-PCL layer acted as a protective coating for PVA, providing moisture resistance (Fig. 5b). The crosslinking occurred only at the interface, preventing a decrease in the number of hydroxyl groups in PVA and allowing the dielectric to maintain a high-dielectric constant of 14.5. Additionally, the crosslinking process created a low-polarity environment at the interface, reducing direct interactions between the hydroxyl groups of PVA and the semiconductor (Fig. 5c). As a result, the performance of single-walled carbon nanotube (sc-SWCNT) thin film transistors (TFTs) improved significantly. Devices with the UV-PCL layer exhibited a four-fold improvement in an average hole mobility of 2.8 $cm^2 V^{-1} s^{-1}$ compared to devices using PVA alone. Furthermore, the UV-PCL dielectric increased the on/off current ratio by ten times, leading to a marked improvement in overall device performance.

Perinot *et al.* reported another bilayer dielectric structure, demonstrating that the device characteristics depend on the crosslinking of the low-permittivity dielectric layer (Fig. 5d).[82] The study employed 1,11-diazido-3,6,9-trioxaundecane (Bis-PEG3-Azide) as the crosslinking agent in a photo-crosslinked polystyrene (XLPS) layer. This crosslinked dielectric effectively suppressed charge injection into the interface or bulk of cyanoethylated pullulan (CEP), even under high electric fields. As a result, TFTs achieved optimal operation at gate voltages below 10 V, with leakage currents kept under 1 nA cm^{-2}

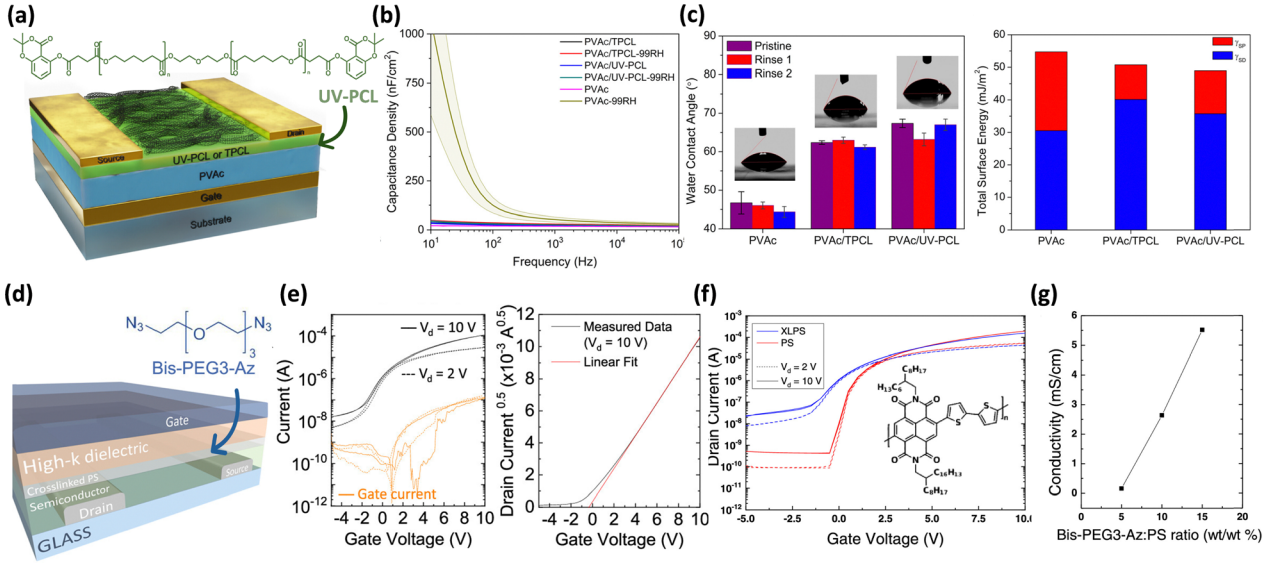

Fig. 5 Improvement of the organic semiconductor/dielectric interface through low-permittivity dielectric crosslinking. (a) Schematic illustration of the TFT with a PVAc/UV-PCL dielectric. (b) Moisture-dependent capacitance density of PVAc and PVAc/UV-PCL. (c) Water contact angle and total surface energy for PVAc, and PVAc/UV-PCL.[163] Copyright 2023, American Chemical Society. (d) Schematic illustration of the TFT with a CEP/XLPS dielectric. (e) Transfer curve of the OFET based on the CEP/XLPS dielectric. (f) Transfer curves of p-type FETs (DPP–TTT) with the CEP/XLPS and CEP/PS dielectric. (g) Conductivity of n-doped P(NDI2OD-T2) films with crosslinking agent concentration.[82] Copyright 2023, American Chemical Society.

(Fig. 5e). A key finding of the study was the role of the azide-based crosslinker in enhancing n-type doping. During the photo-crosslinking process, the UV activation of azide groups led to the formation of amines, which acted as electron donors. These amines contributed additional electrons to the semiconductor, promoting n-type doping and increasing the overall conductivity of the system (Fig. 5f). When using P(NDI2OD-T2) as the active semiconductor, TFTs with higher concentrations of crosslinkers exhibited a clear linear increase in conductivity (Fig. 5g).

3.2.4. Photo-patterning through improved solvent resistance. Solution processing can expose polymer dielectrics to solvents, potentially degrading their performance. Lee *et al.* demonstrated that photo-crosslinking significantly enhances the chemical durability of polymer dielectrics, preventing leakage currents after solvent exposure.[164] This enhancement in chemical resistance also enables selective crosslinking in specific regions, allowing for precise patterning techniques. Gate dielectric patterning is crucial for integrating large numbers of transistors into complex circuits. By patterning the gate dielectric layer, crosstalk and parasitic capacitance between devices can be reduced.[165,166] Many researchers have simplified the patterning of polymer dielectrics for stretchable devices by introducing photo-crosslinkable agents.[31,32,38] For instance, Zhong *et al.* patterned dielectrics with unsaturated bonds of polymer and thiol terminated additives using thiol–ene reactions (Fig. 6a),[123] while Wang *et al.* employed azide crosslinkers for various polymer dielectric patterning (Fig. 6b).[83] These methods allow for straightforward dielectric patterning using only photomasks, facilitating the development of high-density integrated circuits.

However, the mobility of monomer crosslinkers within dielectrics can negatively impact device performance due to undesired phase separation. As a result, researchers are exploring methods to enhance the chemical resistance of polymer dielectrics without the need for additional crosslinkers, while still enabling photo-patterning.[145,167–169] Kallitsis *et al.* demonstrated that grafting photo-crosslinkable azide groups onto high-*k* fluoropolymer dielectrics enabled direct patterning through photolithography, resulting in films with very low surface roughness (Fig. 6c).[84] More recently, Lee *et al.* fabricated a hydroxy functionalized parylene thin film (parylene-OH) *via* chemical vapor deposition achieving intrinsically photo-patterned high-*k* dielectrics.[85] UV irradiation triggered crosslinking, which strengthened the film mechanically while maintaining precise pattern boundaries with a resolution of approximately 5 μm (Fig. 6d). The surface roughness remained unchanged after UV exposure, ensuring stable interfacial properties and enhancing the mobility and current driving performance in IGZO TFT-based semiconductor devices (Fig. 6e)

3.3. Adhesives

In the manufacturing of stretchable electronics, adhesives are needed to meet two different requirements. First, strong adhesion between electronic components is necessary. The adhesive must ensure that components remain securely bonded during the manufacturing process, including solvent treatments and mechanical stresses.[170–172] Second, it is important that the device can be easily removed from rigid substrates after fabrication without causing damage.[173,174] Stretchable electronics are often fabricated on a rigid supporting substrate; consequently, a method to reduce adhesion strength at a specific

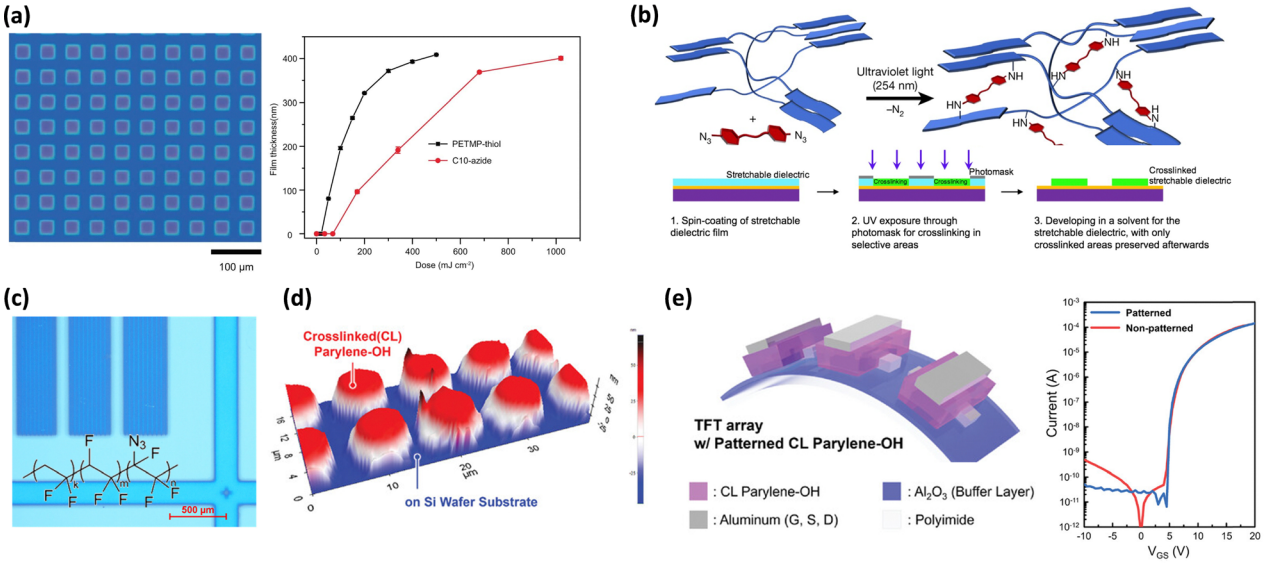

Fig. 6 Enhancement of chemical resistance for dielectric micro-patterning. (a) Optical image of photo-patterned NBR and the thickness of NBR patterns in relation to UV exposure doses.[123] Copyright 2024, Springer Nature. (b) Photo-patterning process of SEBS using azide-crosslinker.[83] Copyright 2018, Springer Nature. (c) Optical image of photo-patterned azide-modified P(VDF-TrFE-CTFE).[84] Copyright 2019, American Chemical Society. (d) AFM 3D topology showing the boundaries of the crosslinked parylene-OH (red) on the Si wafer substrate (blue). (e) Schematic structure and transfer curves of the fabricated TFT array using patterned crosslinked (CL) parylene-OH.[85] Copyright 2024, Wiley-VCH.

stage is necessary. To meet these requirements, adhesive control technologies based on photo-crosslinking have emerged as a promising solution. These technologies facilitate precise spatial control of adhesion through straightforward light exposure, allowing for easy adjustment of adhesive strength.

This chapter will explore strategies for (i) improving adhesion strength and (ii) detachment techniques using photo-crosslinking.

3.3.1. Enhancement of adhesion strength. Recent research has proposed methods to enhance adhesive strength: (i) photo-induced dynamic bond; (ii) pattern design for crack propagation control. First, the light-induced dissociation and reformation of dynamic bonds can modulate the mechanical properties of the adhesive, leading to improved adhesion performance. For example, Michal *et al.* developed a shape memory adhesive that improved adhesion by increasing surface wettability through the dynamic exchange of disulfide bonds, a process induced by UV light (Fig. 7a).[89] This strategy facilitated the modulation of adhesive viscosity, promoting a uniform coating across the entire substrate surface. When subjected to thermal treatment at 80 °C, the crystalline domains of the adhesive melt, but the dynamic exchange of disulfide bonds remained inactive. However, UV light exposure triggered the decomposition and exchange of disulfide bonds, reducing viscosity and increasing the contact area with the substrate. This process enhanced surface wettability and improved adhesive strength, demonstrating remarkable performance across various substrates. These methods provided opportunities to dynamically adjust adhesive strength through modulation of the crosslinked structure.

Second, researchers have explored spatial control of adhesive strength through strategic material design. By increasing bending stiffness in specific areas *via* crosslinking, detachment resistance can be enhanced.[175,176] This approach integrates

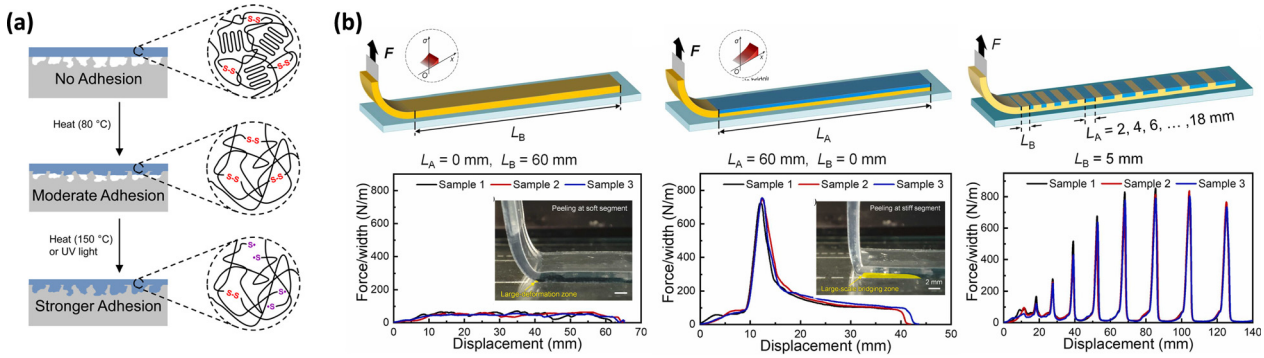

Fig. 7 Enhancement of adhesion strength. (a) Schematic illustration of enhancing surface wetting based on temperature and UV irradiation.[89] Copyright 2016, American Chemical Society. (b) Peel strength for soft and stiff segments.[33] Copyright 2024, Elsevier.

rigid and flexible sections sequentially using photo-patterning, further improving adhesive properties in stretchable devices.[90] Lee *et al.* offered detailed insights into a large-scale bridging mechanism that increased maximum peel strength (Fig. 7b).[33] When a rigid area was encountered, a significant portion of the peel force converts into bending energy, which diminished the force propagating interfacial cracks and effectively prevented their propagation. The rigid area redistributed the force, increasing the area available for crack formation, thereby enhancing peel resistance. To maximize debonding resistance, the length of the rigid segments should match the saturation size of the bridging area. For a heterogeneous adhesive with segment lengths of 10 mm, the debonding resistance measured 642.8 N m^{-1}, approximately 13 times higher than that of a fully ductile adhesive. As the length of the rigid segments increased, the debonding resistance rose to 818.8 N m^{-1} at 14 mm, exceeding that of a fully rigid adhesive.

3.3.2. Adhesion control for safe detachment. In the manufacturing of stretchable electronics, adhesives must maintain strong adhesion during fabrication but allow easy detachment from rigid support substrates after production. To meet this requirement, various methods have been developed to improve adhesive detachment, such as pH adjustment,[177,178] introducing metal ions,[179,180] thermal treatment,[181–183] and electrostatic techniques.[184,185] Recently, light-induced detachment methods, such as photodegradation[186] and photoisomerization,[187–190] have drawn significant attention. However, these methods often involve complex processes and limited control over adhesion strength, leading to inconsistent performance.

Photo-crosslinking offers a simpler solution for effective detachment. Increasing crosslink density typically induces volumetric shrinkage due to internal stress, which enhances detachment at the interface. Many researchers have already utilized photo-crosslinking technology in adhesives to enhance detachment performance.[191–194] For example, Kim *et al.* highlighted the ease of detachment in the manufacturing process of ultrathin devices through the formation of an interpenetrating network (IPN).[91] After UV exposure, the polyurethane acrylate crosslinker formed an interpenetrating network (IPN), reducing adhesion to less than 1%. This structure allowed for the easy separation of a 1.4 μm ultrathin PET film patterned with silver nanowires (AgNW) and graphene from a thick carrier substrate. This reduction in adhesion ensured that the film remained undamaged during detachment, providing high reliability and yield in the production of ultrathin devices (Fig. 8a).

Similarly, Hwang *et al.* developed a photo-crosslinkable adhesive by grafting photosensitive side chains through the ring-opening reaction of *N*-methacryloyl-2-methylaziridine (MAMAz).[195] This adhesive demonstrated a reduction in adhesion by up to 99.2% after UV crosslinking, allowing for the non-destructive separation of devices. The detachment performance improved as the amount of crosslinkable side chains increased and as the curing time progressed. Once a certain threshold was reached, the adhesion strength stabilized, with no further reduction (Fig. 8b).

Recent studies have also focused on incorporating photo-initiating groups into adhesive polymers. Kim *et al.* developed an optically clear adhesive (OCA) by integrating benzophenone derivatives into the polymer network, allowing for easy removal

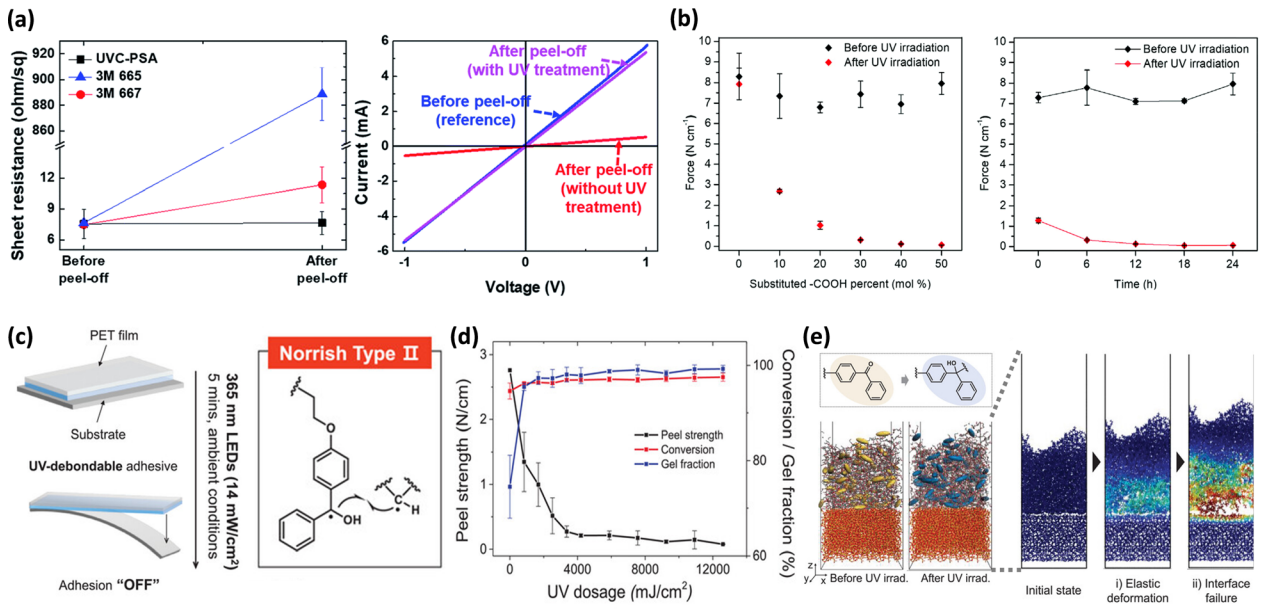

Fig. 8 Adhesion control for safe detachment. (a) Sheet resistance of the AgNW electrode and the *I*–*V* characteristics of graphene.[91] Copyright 2019, Royal Society of Chemistry. (b) Peel strength in relation to the crosslinking site ratio and UV irradiation time.[195] Copyright 2022, Royal Society of Chemistry. (c) Strategies for the selective removal of adhesion through UV irradiation. (d) Evaluation of peel strength, conversion, and gel fraction changes in UV-debondable adhesive with 3 mol% benzophenone content in relation to UV exposure doses. (e) MD simulated illustration of adhesive delamination post-UV irradiation.[92] Copyright 2024, Wiley-VCH.

without residue from foldable displays (Fig. 8c).[92] Benzophenone exhibited low reactivity under visible light, allowing it to be safely used as a monomer in visible light-induced polymerization. In contrast, it facilitated additional crosslinking through UV-induced reactions. After UV exposure at 4200 mJ cm^{-2}, the OCA containing 3 mol% benzophenone showed a sharp decrease in adhesion from 2.44 N cm^{-1} to 0.14 N cm^{-1} (Fig. 8d). Furthermore, the researchers demonstrated through simulations that the increased chain connectivity from crosslinking hindered deformation in the UV-exposed OCA (Fig. 8e). This led to stress concentration at the interface between the OCA and the substrate, enabling easy detachment without residue.

4. Photo-crosslinkable semiconducting polymers for stretchable electronics

Semiconducting polymers have garnered significant attention as promising materials for stretchable electronics due to their inherent mechanical flexibility, tunable properties, solution processability, and cost-effectiveness.[196–199] Despite their theoretical advantages, however, these materials often present a trade-off between key advantages and limitations, such as electrical performance *versus* mechanical durability,[200–202] and solution processability *versus* chemical vulnerability.[203–205] Efforts to increase crystallinity for enhanced electrical conductivity often result in brittle mechanical properties. Similarly, while good solubility in organic solvents aids in processing, it also compromises solvent resistance, thereby limiting the applicability of semiconducting polymers in multilayer tandem structures for integrated circuits, sensor arrays, and display fabrication.

Photo-crosslinkable semiconducting polymers offer a promising solution to these challenges by simultaneously improving mechanical robustness, stretchability and processibility. First, photo-crosslinking allows facile solution process by selectively imparting the chemical robustness of the material through light-induced chemical bonds. Traditional patterning methods often involve complicated steps with harsh conditions which might degrade the composing materials, including the use of high temperature, sacrificial layers, orthogonal solvents and inkjet printing. In contrast, photo-crosslinking provides a simpler and more efficient strategy for fabricating advanced stretchable organic electronic devices. Second, photo-crosslinking can easily enhance the mechanical durability of semiconducting polymers. A key advantage of photo-crosslinking is its ability to modulate the mechanical properties of semiconducting polymers, addressing the inherent trade-off between electrical performance and stretchability. By chemically linking amorphous and flexible polymer segments, photo-crosslinking can effectively enhance mechanical toughness while maintaining electronic function. Wang *et al.* revealed that tuning the crystallinity of the crosslinker affects the morphology of the polymer, which in turn influences both its mechanical and electrical properties.[206] Through precise control of crosslinking density, the polymer network can be tailored to exhibit both high elasticity and durability under mechanical strain, which is essential for wearable applications. Third, photo-crosslinking enables the functionalization of semiconducting polymers through covalent bonding with functional moieties,[127,207,208] imparting desired properties such as enhanced adhesion, passivation, and interfacial compatibility, further improving device reliability and integration.

This section outlines three strategies for rendering semiconducting polymers photo-crosslinkable: (i) molecular engineering of semiconducting polymers by attaching photo-crosslinkable units to the polymer backbone or side chains; (ii) the use of photo-crosslinkable additives that bind directly to the polymer; and (iii) the addition of photo-crosslinkable additives that form covalent bonds exclusively among themselves, without interacting with the semiconductor. Finally, a few research studies to functionalize the surface of semiconductor thin films applying this photo-crosslinking strategy will be discussed

4.1. Molecular design strategies for photo-crosslinking semiconductors

This section will focus on recently reported photo-crosslinkable semiconducting polymers used in OFET applications, following recent reviews of molecular design strategies for crosslinkable conjugated molecules. The incorporation of photo-cleavable or reactive groups into the polymer backbone[93] or side chains[94,96,98,209] has proven to be a highly effective strategy for patterning semiconducting polymers.[203–205,210,211] This approach eliminates the need for additives, which can lead to phase separation and negatively affect the uniformity, morphology, and electrical performance of the material. Various photo-crosslinkable groups, such as azide,[96,212] vinyl,[213,214] alkyne,[215] and oxetane[216,217] can be integrated through molecular engineering. Among these, the azide group is particularly favored due to its simplicity and effectiveness of photo-crosslinking. Upon UV light exposure, azide groups form reactive nitrene species and release nitrogen gas. Nitrene species can readily insert into C–H bonds, allowing them to cross-link various sites. Gao *et al.* utilized this approach by incorporating the azide group into the branching alkyl side chains of a diketopyrrolopyrrole (DPP)-based conjugated polymer, PDPP4T-N_3 (Fig. 9b).[94] This polymer enabled patterning using facile lithographic techniques, as shown in Fig. 9a. Efficient patterning was achieved using a photomask, because selective UV treatment significantly reduced solubility, allowing for precise patterning. After UV exposure, the unexposed area was removed by soaking in chloroform, resulting in uniform thin films with a thickness of 40 nm and feature sizes as small as 5 μm (Fig. 9c). These patterned films exhibited consistent performance, with average charge mobility of 0.61 ± 0.10 cm^2 V^{-1} s^{-1}. Similarly, Kim *et al.* synthesized polythiophene (P3HT) with azide groups partially attached to the end of the alkyl chain.[96] Even with just 10–20% incorporation of azide units, successful photo-crosslinking was achieved, producing an insoluble

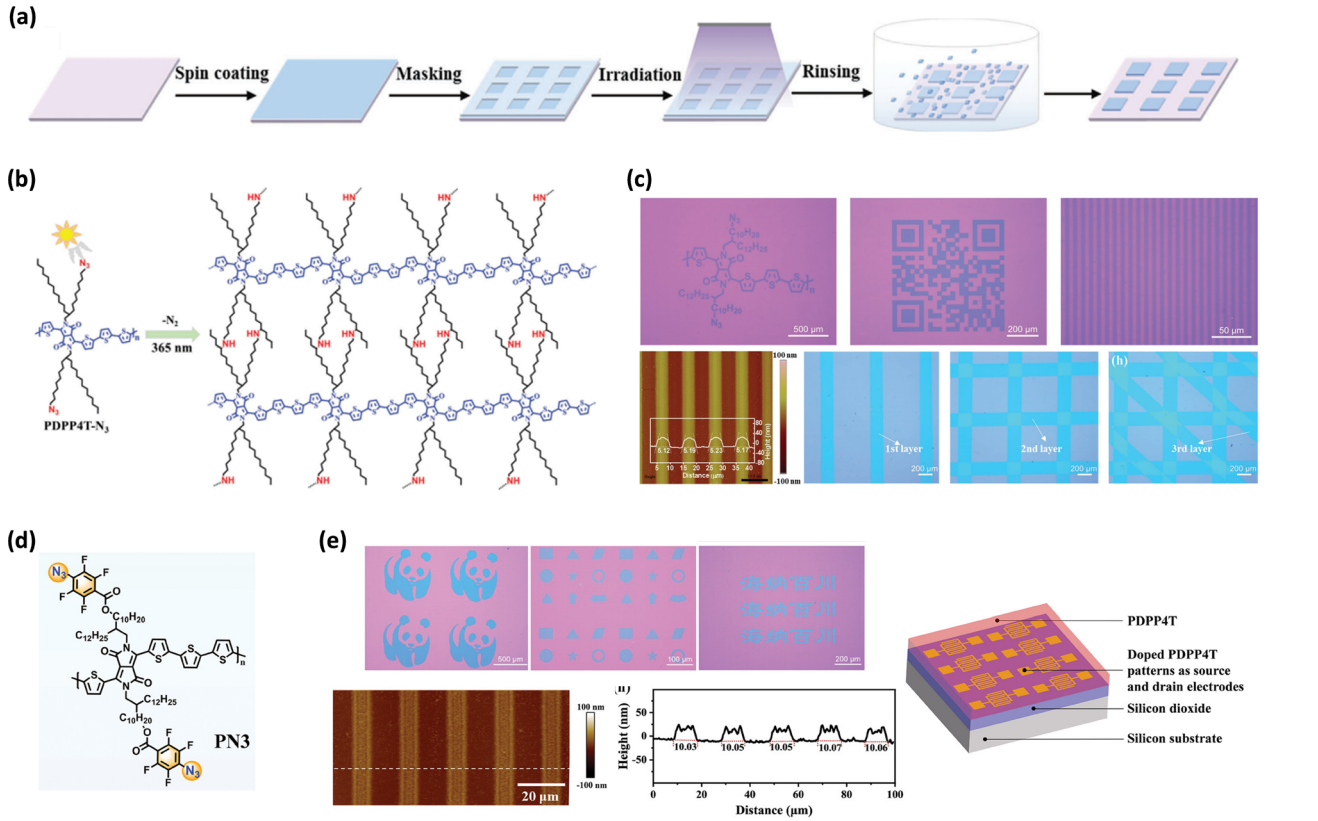

Fig. 9 Molecular design strategies for photo-crosslinking semiconductors. (a) Schematic of the photo-patterning procedure using molecular design strategies. (b) Chemical structure of semiconducting photoresist PDPP4T-N3 and its crosslinking mechanism. (c) Optical and AFM images after the photo-patterning process.[94] Copyright 2022, Wiley-VCH. (d) Chemical structure of PN3. (e) Optical and AFM images after the photo-patterning process and schematic of device structures.[98] Copyright 2024, Wiley-VCH.

semiconducting polymer thin film. They also demonstrated thin film transistors on flexible substrates. This crosslinking method also enhanced the thermal stability of bulk-heterojunction organic photovoltaics (BHJ OPVs) by acting as an *in situ* compatibilizer at the P3HT/PCBM interface, suppressing macrophase separation.

The backbone design strategy offers an alternative strategy to side chain modification for introducing reactive groups into a semiconducting polymer backbone. For example, Nyayachavadi *et al.* developed a DPP-based polymer with 1,3-butadiyne-containing conjugation breaker spacers (CBSs) in the backbone.[93] Upon UV irradiation, these butadiyne CBS units underwent polymerization, forming polydiacetylene crosslinks. The crosslinked polymers exhibited improved mechanical properties, such as increased rigidity and thin film stability, while maintaining a solid-state morphology. However, OFET devices using these crosslinked thin films showed a decrease in charge mobility, from 0.058 to 0.013 $cm^2\ V^{-1}\ s^{-1}$ at best, indicating that crosslinking affected charge transport.

Additionally, the modified polymers can be blended with other conjugated polymers (CPs), serving as the conjugated photo-crosslinker. For example, Xue *et al.* introduced a new conjugated polymer-based photo-crosslinker, PN3, designed for efficient patterning in OFET applications.[98] PN3 features a conjugated backbone made of DPP and bithiophene units, with phenyl-substituted azide groups on its side chains (Fig. 9d). Under UV light, these azide groups crosslink with the alkyl side chains of CP, enhancing the material's solvent resistance. The π–π interactions between PN3 and CP ensure better miscibility, resulting in higher patterning resolution, lower UV exposure doses, and improved sensitivity compared to small molecule-based crosslinkers. PN3 enabled the creation of well-defined patterns with resolutions down to 500 nm, and its doped patterned arrays were used as source-drain electrodes, maintaining excellent charge transport properties (Fig. 9e).

These strategies selectively enhance solvent resistance, enabling efficient photo-patterning and offering significant potential for organic flexible electronics processed through all-photolithography techniques.

4.2. Direct crosslinking *via* functional additives

Photo-crosslinkable additives are compounds that contain photo-reactive groups, typically located at the ends of their molecular structures. Direct crosslinking refers to a photo-crosslinker creating strong covalent bonds with a CP under UV irradiation, providing significant robustness with minimal additive usage. Unlike methods that modify a polymer's side chains or backbones, this approach allows for more flexible

molecular designs, facilitating functionalization without imposing significant synthetic constraints. To maintain effective charge transport, it is essential that additives do not disrupt the polymer's chain packing and aggregation.[124,206] Therefore, careful design of their interaction with the CP is crucial.

A widely used photo-crosslinkable group is FPA.[51,77,218–220] FPAs are favored for their high reactivity and ability to minimize unwanted nitrene attacks on the π-conjugated core, which could otherwise degrade the semiconductor's properties.[221] Research has focused on optimizing the performance of FPAs through variations in azide density and chain linkages. For instance, Kim *et al.* enhanced crosslinking density by using a crosslinker containing four FPAs, facilitating the creation of fully photo-patterned electronics.[125] Tan *et al.* further showed that specific FPAs could achieve unity quantum efficiency for crosslinking, primarily targeting C–H bonds and minimizing side reactions.[219]

Zheng *et al.* demonstrated a molecular design using FPA-based crosslinker additives to achieve stretchable, solvent-resistant, and photo-patternable semiconducting polymers using a covalently embedded *in situ* rubber matrix (iRUM) as shown in Fig. 10a.[124] The iRUM system employs an azide-based crosslinker called a BA crosslinker, particularly FPA end-capped polybutadiene, which undergoes both self-crosslinking through azide/C=C cycloaddition and selective crosslinking with a CP *via* azide/C–H insertion. The researchers systemically compared the impact of crosslinking with the CP and self-crosslinking (Fig. 10b). The researchers revealed that crosslinking with a CP significantly improved patternability but disrupted the aggregation of the CP. On the other hand, self-crosslinking significantly improved chain packing and morphology. Interestingly, both types of crosslinking improved softness and stretchability of the CP by connecting with a long soft chain. Because of dual usage of crosslinking with a specific ratio, determined by different reactivities, BA crosslinkers could facilitate a high charge mobility of 1 $cm^2 V^{-1} s^{-1}$, stretchability, and chemical robustness for the fabricated multilayer device with the all-solution process (Fig. 10c).

Another common example of a photo-crosslinkable group is diazirine,[222–224] because it transforms into reactive carbene

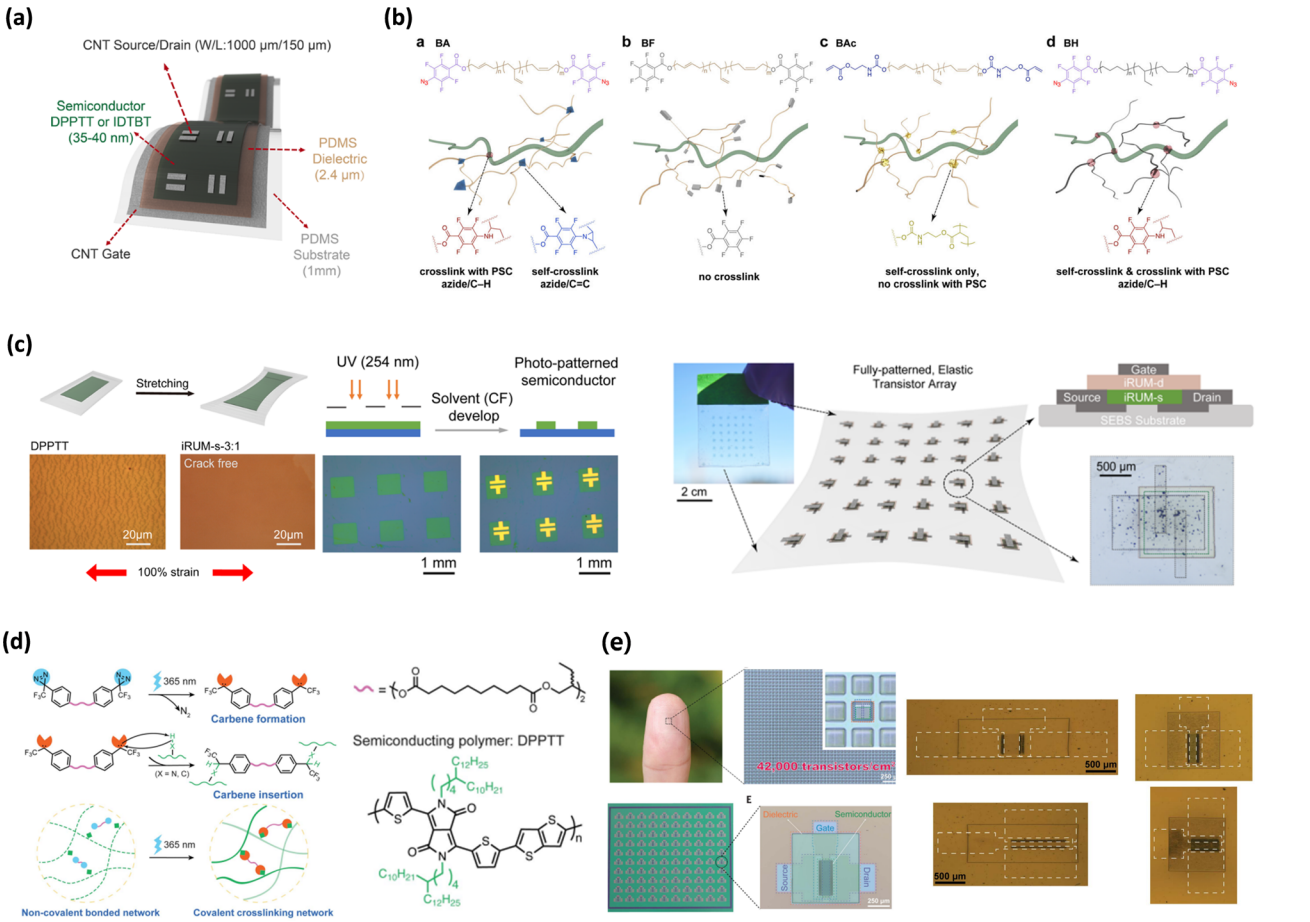

Fig. 10 Direct crosslinking *via* functional additives. (a) Device structure of a fully stretchable transistor using iRUM semiconductors. (b) Chemical structure of the polybutadiene-based precursors for crosslinking with PSC and self-crosslinking. (c) Schematic and optical images of iRUM films during stretching and patterning. Images of the fully patterned, elastic transistor array.[124] Copyright 2021, Springer Nature. (d) Mechanism of UV-triggered carbene insertion crosslinking. (e) Images of the elastic transistor array containing 10 000 transistors and stretched films.[126] Copyright 2021, The American Association for the Advancement of Science.

species, reacting specifically to non-conjugated bonds (Fig. 10d) under UV light irradiation, leading to maintaining the electrical properties. For example, Zheng *et al.* demonstrated a high-resolution, UV-triggered microlithographic process using a trifluoromethyl-substituted diazirine crosslinker to pattern a CP and improve stretchability.[126] They introduced a double-end functionalized trifluoromethyl-substituted diazirine crosslinkers with amorphous branched alkyl chains for semiconducting polymer film patterning. The diazirine unit using less than 10 wt% of the diazirine crosslinker was needed to realize 99% film retention and feature sizes down to 4μm were successfully obtained. Finally, they could fabricate high density transistor arrays with 42 000 transistors per square centimetre (Fig. 10e). Wu *et al.* also presented a diazirine-based four-armed crosslinker (4CNN).[49] With just 3% 4CNN, p-type, n-type, and ambipolar polymers could be patterned with high precision, achieving feature sizes as small as 5 μm without altering thin film morphology or charge transport properties. This method enabled the fabrication of solution-processable multilayer electronic devices with high device performance and solvent resistance.

4.3. Self-crosslinking networks for enhanced performance

Blending self-crosslinking additives, which form covalent bonds exclusively with themselves under UV irradiation, offers a viable method for fabricating photo-crosslinkable semiconducting thin films. These additives create crosslinked interpenetrating networks that intertwine with a CP, enhancing chemical robustness. However, this approach often requires a higher concentration of additives compared to direct crosslinking, which can lead to severe phase separation. A key advantage of self-crosslinking additives is that they do not disrupt the aggregation of a CP or interfere with the π-conjugated core, thereby maintaining electrical performance. In some cases, they can even promote tighter packing of the polymers, improving electrical performance and charge transport. Additionally, the reduced concern about interactions with the π-conjugated core provide greater flexibility in molecular design, allowing the incorporation of various functionalized materials such as long and elastic components. These materials can achieve both stretchability and patternability simultaneously, making them highly versatile for advanced applications.

For example, Tien *et al.* demonstrated a novel approach of scalable patterning using a thiol–ene reaction (Fig. 11a).[97] The process involved blending a high-mobility CP, with elastic rubber like poly(styrene-butadiene-styrene) (SBS). The thiol–ene reaction selectively cross-links the vinyl groups in SBS and a thiol containing additive, trimethylolpropane tris(3-mercapto propionate) (TRIS), creating a semi-interpenetrating polymer network (SIPN) that enhances stretchability and solvent resistance while preserving the electronic properties of the

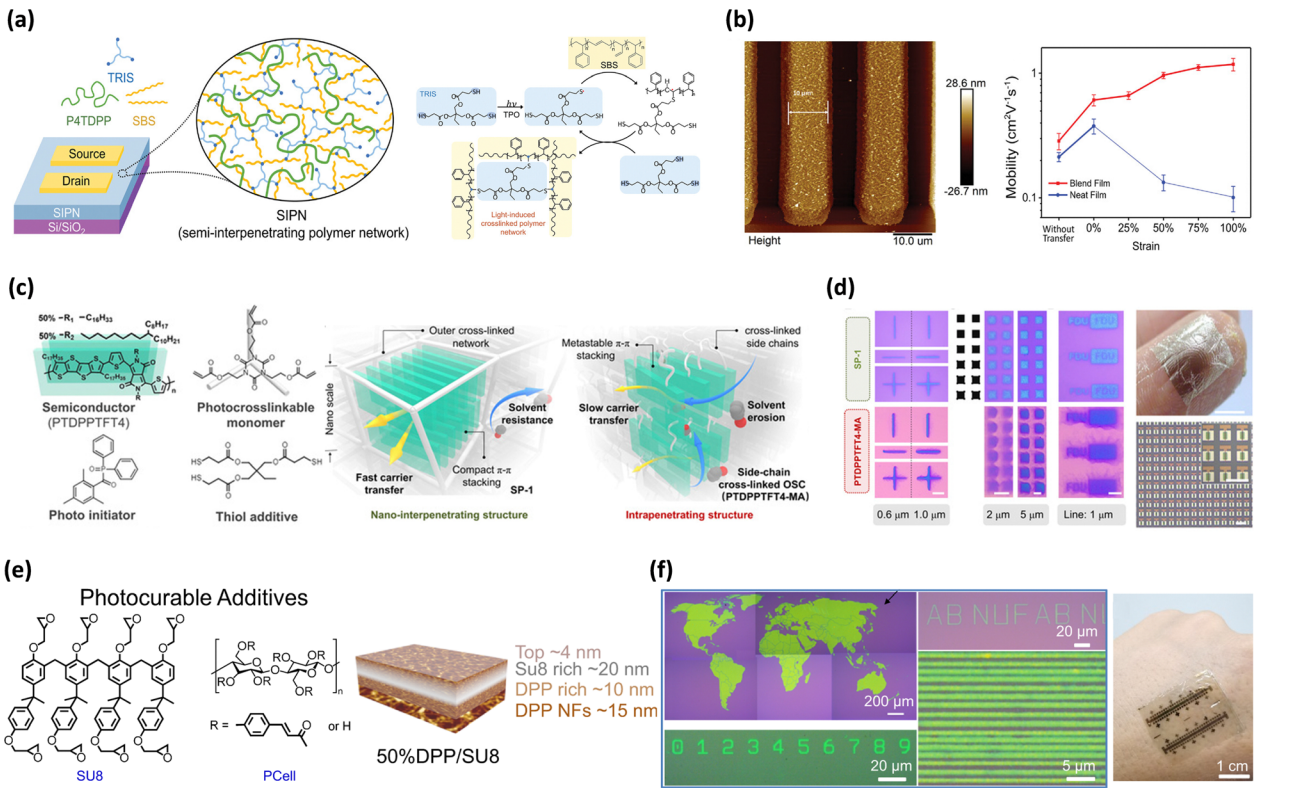

Fig. 11 Self-crosslinking networks for enhanced performance. (a) Chemical structure and illustration of a semi-interpenetrating polymer network. (b) AFM image of a photo-patterned semiconducting polymer and mobilities under strain.[97] Copyright 2023, Wiley-VCH. (c) Chemical structure of and the schematic diagram of photo-crosslinking of SP-1. (d) Images of patterned SP-1 and transistor arrays.[99] Copyright 2021, The American Association for the Advancement of Science. (e) Chemical structure of photocurable additives and schematic of vertical phase separation in 50%DPP/SU8. (f) Images of photo-patterned flexible 50%DPP/SU8.[100] Copyright 2021, Springer Nature.

polymer. The thiol–ene approach selectively targets non-conjugated double bonds in SBS, ensuring minimal disturbance to the conjugated polymer's structure. So, the SIPN-based transistors show increased mobilities from 0.61 to 1.18 $cm^2\ V^{-1}\ s^{-1}$ when applying the strain from 0% to 100% (Fig. 11b). Moreover, the hole mobility could be still maintained after 1000 strain-and-release cycles under a strain of 25%.

Chen *et al.* introduced a novel semiconducting photoresist (SP-1) with a nano-interpenetrating structure, designed for all-photolithography processes (Fig. 11c).[99] SP-1 consists of a DPP-based CP, acrylate-based crosslinkable monomers with a small amount of photoinitiator and thiol additives. Under UV irradiation, arylate undergoes a radical polymerization reaction, forming a stable interpenetrating network. This allowed for submicrometer patterning with high-density OTFT arrays of 1.1×10^5 units cm^{-2} (Fig. 11d) while retaining a high charge mobility of 1.11 $cm^2\ V^{-1}\ s^{-1}$, even after photolithography solution processes. They also demonstrated flexible OFET arrays with a high density OTFT array of 4489 units cm^{-2} and a mobility of 0.471 $cm^2\ V^{-1}\ s^{-1}$, achieving 90.8% mobility retention after 1000 bending cycles, making SP-1 a promising material for advanced organic electronics.

Wang *et al.* presented a wafer-scale, foundry-compatible approach for fabricating polymeric semiconducting layers with 0.5 μm resolution using a three-step photolithographic process (Fig. 11f).[100] The CPs such as DPP-based p-type and n-type N2200, were blended with photo-crosslinkable additives like SU-8 and PCell. The patterned layers are chemically inert to aggressive aqueous and organic solvents and thereby withstand subsequent deposition and patterning of the additional organic layers and/or metal contacts used in the circuitry fabrication. These blends exhibited vertical phase separation and a nanofiber morphology, confirmed *via* AFM, ToF-SIMS, and GIWAXS (Fig. 11e). The resulting OTFTs maintained a high carrier mobility (0.1–0.24 $cm^2\ V^{-1}\ s^{-1}$) with an improved thermal stability of 175 °C, a mechanical durability of 5000 bending cycles at a radius of 1 mm, and efficient switching performance of subthreshold swing to be 1.4 V dec^{-1}.

4.4. Functional additives for advanced applications

Recently, a few research studies have explored utilizing crosslinkers to impart specialized functions to semiconducting layers, such as surface protection, self-healing, and enhanced interfacial adhesion. When activated by UV irradiation, these functional additives can significantly improve the performance and stability of semiconducting polymer thin films.

For example, Zheng *et al.* proposed a novel approach of covalent functionalization to form a molecular protection layer (Fig. 12a).[127] Using a butadiene-azide (BA) crosslinker, the researcher introduced non-conjugated C=C bonds as surface reactive sites in a CP. By drop casting perfluorodecanethiol molecules onto the surface of the CP and applying UV irradiation, they induced a thiol–ene reaction that tethered fluoroalkyl chains onto the surface, creating a molecular protection layer. This functionalized surface exhibited hydrophobic properties,

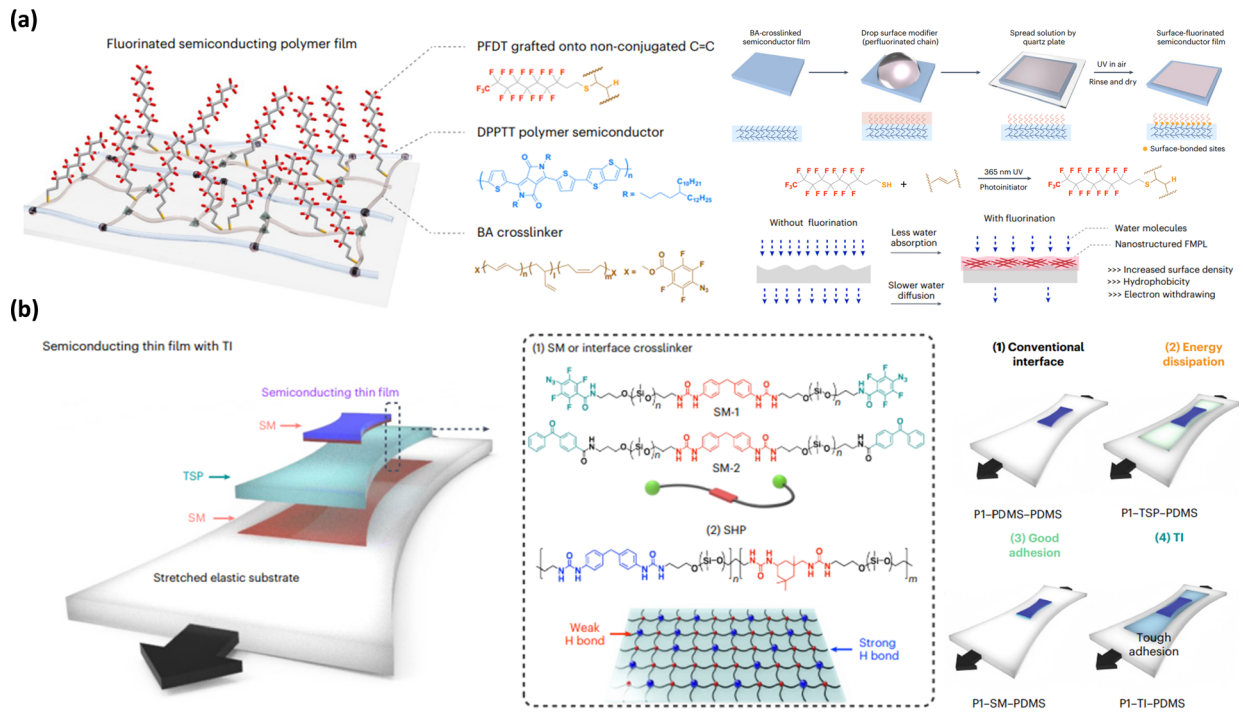

Fig. 12 Functional additives for advanced applications. (a) Schematic of the process of PSC surface fluorination with photo-crosslinking and the mechanism of achieving long-term environmental stability.[127] Copyright 2023, Springer Nature. (b) Schematic of a TI between a semiconducting film and an elastic substrate and schematic of semiconducting thin film on an elastic PDMS substrate with various interface conditions.[207] Copyright 2022, Springer Nature.

preventing water absorption and diffusion, thus maintaining a stable electrical performance of ~ 1 cm^2 V^{-1} s^{-1} in the CP. The fluorinated protection layer outperformed traditional micrometer-thick stretchable polymer encapsulants, showing exceptional stability in harsh environments such as 85–90% humidity for 56 days, and in water or artificial sweat for 42 days.

Additionally, Kang *et al.* demonstrated an interface engineering strategy (Fig. 12b) to enhance the stretchability of brittle semiconducting polymer thin films.[207] They introduced a tough interface (TI) bond, composed of a tough self-healing polymer (TSP) layer and a surface modifier (SM) layer. The TSP, consisting of a 90% self-healing polymer (SHP) and a 10% SM, acted as an energy-dissipating matrix. The SM, based on an FPA crosslinker with a dynamic hydrogen bond and a flexible PDMS backbone, covalently bonded with both the substrate and the semiconducting film under UV irradiation. This interface engineering improved the stretchability of the films from 30% to 110% and enhanced their durability and robustness. It also prevented delamination and delayed crack formation, significantly improving performance in all-polymeric transistor devices.

5. Photo-crosslinking strategy of conductors for stretchable electronics

Intrinsically stretchable conductors are essential components of stretchable electronics, serving as stretchable electrodes and interconnects essential for optimal device performance.[225–227] Traditional rigid metal interconnects, while conductive, often fail due to mechanical mismatches, leading to delamination and performance degradation. The stretchable electrodes that are studied a lot are largely divided into three categories: conductive polymers, liquid metals and composites of elastomer and conductive fillers. These limitations have driven the development of photo-patternable conductors, where *in situ* photo-crosslinking enables precise patterning without the need for complex fabrication processes.[23,24,228,229] Conventional thermal and lithographic methods, however, are unsuitable due to the low thermal stability and solvent resistance of stretchable conductors. Photo-patternable conductors, achieved by a material-based molecular design approach provide an alternative, enabling patterning without complex fabrication methods through *in situ* photo-crosslinking. Such precisely patterned stretchable conductors play a crucial role in the miniaturization of wearable electronics by providing mechanically stable and highly flexible interconnects.

This section will explore two major approaches: (i) photo-patterning strategies for CPs and liquid metals, and (ii) 3D-printable nanocomposite-based conductors with various fillers, leveraging from the *in situ* polymerization. These photo-crosslinkable strategies simplify the fabrication of stretchable, high-performance conductors for flexible electronic applications.

5.1. Photo-crosslinking strategy of stretchable conductors

Some CPs, like poly(3,4-ethylenedioxythiophene):poly styrene sulfonate (PEDOT:PSS),[230–232] polyaniline (PANI)[233] and polypyrrole[234,235] are inherently ductile and conductive due to their energy-band structure.[15] These properties make them ideal candidates for use as stretchable conductors in applications such as electrodes and interconnects in flexible electronic devices. However, one of the primary challenges with these materials has been achieving high-resolution patterning for advanced applications. To address these challenges, PEDOT has been the focus of extensive studies aimed at modifying its chemical structure to enhance its chemical resistance during photo-patterning processes. Efforts such as incorporating photo-crosslinkable groups in the side chain of PEDOT have been explored, albeit with trade-offs such as relatively lower conductivity and pattern resolution.[104,236–238] Recent advancements have shown that a rational design of photo-crosslinkable PEDOT additives can significantly improve conductivity while enabling precise patterning.

For example, Zheng *et al.* employed a rationally designed monolithic optical microlithographic process to fabricate stretchable and patternable conductors by precisely optimizing the chemical structure of PEDOT.[126] In this approach, the conductive PEDOT polymer formed a double-network structure with a polyethylene glycol dimethacrylate (PEGDMA) crosslinker. The strong interaction between PEDOT and PEG linker initiated a microstructural transition in PEDOT from a core–shell structure to a more extended form, thus forming the first conductive network. Upon UV exposure, PEGDMA underwent radical polymerization, creating a secondary network around the entangled PEDOT chains, which enables high-resolution patterning down to 2 μm feature. This technique allowed PEDOT to achieve improved conductivity, reaching up to 52.5 kS m^{-1} after methanol treatment, along with enhanced stretchability. The resulting structure exhibits increased solubility modulation and structural stability, making it well-suited for flexible electronics.

Furthermore, Jiang *et al.* introduced a topological supramolecular network using polyrotaxane (PR) structures to further improve the stretchability and conductivity of PEDOT films (Fig. 13a).[103] This strategy relied on the hypothesis that topological molecular design can decouple competing properties from multiple molecular building blocks, enabling high conductivity, stretchability and patternability in one system (Fig. 13b). The PR-PEGMA additive, composed of a PEG backbone with sliding cyclodextrins (CDs) functionalized with PEG methacrylate (PEGMA) side chains, prevented PEG crystallization, thereby avoiding phase separation and enhancing stretchability of PEDOT. The PR-PEGMA enhanced PEDOT aggregation by replacing the insulating PSS, boosting conductivity to 2700 S cm^{-2} after sulfuric acid treatment while maintaining stretchability up to 150% strain. The acid treatment further enhanced PEDOT's crystallinity, forming interconnected fibers that substantially improved conductivity without compromising mechanical flexibility. The molecular engineering approach facilitated charge transport through PEG's role in promoting PEDOT aggregation, while the sliding CDs prevent phase separation, ensuring a uniform material distribution.

Another effective strategy for enhancing the electrical conductivity of CPs while maintaining their suitability for flexible applications is chemical doping.[98,105,239] This approach plays a

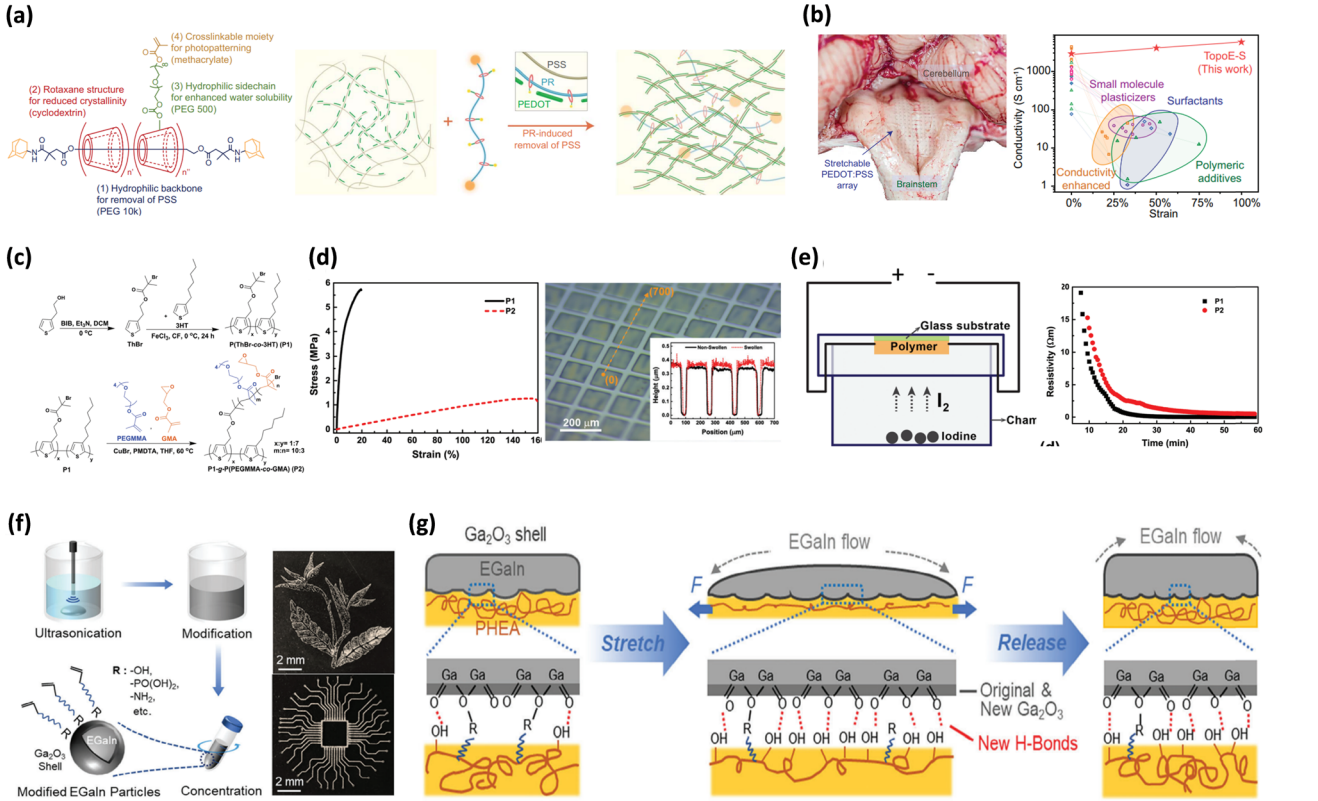

Fig. 13 Photo-crosslinking strategy of stretchable conductors. (a) Chemical structure of PR-PEGMA and illustration of the interaction between PR and PEDOT:PSS for enhanced conductivity. (b) Image showing conformal interface and conductivity over strain plots showing high conductivity *versus* previously reported PEDOT:PSS.[103] Copyright 2022, The American Association for the Advancement of Science. (c) Synthesis route and chemical structure of stretchable and patternable grafted copolymers. (d) Stress–strain curve showing the mechanical properties and images showing patternability. (e) I_2 vapor doping method description and subsequent resistivity.[106] Copyright 2019, Royal Society of Chemistry. (f) Schematic of modified LMP stock solution preparation and patterned LM image. (g) Schematic during stretching process.[35] Copyright 2024, Wiley-VCH.

significant role in converting these polymers into highly conductive materials by increasing their charge carrier density and facilitating efficient charge transport. Chemical doping can be utilized to create photo-crosslinkable and stretchable conductors, which are valuable in stretchable electronics and bioelectronics. For example, Wang *et al.* introduced a multifunctional graft copolymer that combines a conductive P3HT backbone with poly(PEGMMA-*co*-GMA) side chains (Fig. 13c).[106] The P3HT backbone provides electrical conductivity due to its conjugated structure, allowing for efficient charge transport. The poly(PEGMMA-*co*-GMA) side chains added mechanical stretchability and hydrophilicity, while the glycidyl methacrylate (GMA) segments enabled photo-crosslinking (Fig. 13d). Chemical doping with iodine vapor increased the electrical conductivity to 21.5 S m^{-1}, making the material suitable for conductors in stretchable electronics and bioelectronics, retaining conductivity even under deformation and after patterning (Fig. 13e).

Liquid metals, such as eutectic gallium–indium (EGaIn), have recently gained significant attention as highly conductive and stretchable materials due to their exceptional deformability.[240–243] These properties make them promising candidates for use in advanced flexible electronics. However, the inherent challenges with EGaIn—such as its fluidity, extremely high surface tension, and the rapid formation of an oxide layer—complicate its integration as interconnects or direct contact pads in electronic devices. Recent research has focused on overcoming these limitations by utilizing liquid metal particles (LMPs), enabling precise patterning for stretchable electronic applications. For example, Lee *et al.* introduced a novel method for large-area patterning of EGaIn using a conventional photolithographic process.[244] In this approach, the EGaIn particles were encapsulated with PSS, which enhances their mechanical and chemical stability. This encapsulation allowed for uniform thin film coating improving the overall processability of the material. By using dimethyl sulfoxide (DMSO) as a lift-off solvent, the cohesion between the EGaIn particles was increased, enabling a metal-level conductivity of 2.2×10^6 S m^{-1} without requiring an activation step. This technique enabled high-resolution patterning down to 10 μm and supports multilayered fabrication of stretchable electronics.

Similarly, Wu *et al.* introduced stretchable liquid metal pattern fabrication using a chemically functionalized EGaIn particle ink in combination with polymer precursors.[35] The EGaIn particles were chemically modified with a 2-hydroxyethyl

acrylate (2-HEA) ligand, which facilitates strong covalent bonds during the photo-polymerization process (Fig. 13f). Upon exposure to UV light, 2-HEA acted as a polymer precursor, creating a crosslinked network with the modified LMPs with high resolution around 20 μm. Subsequent mechanical sintering broke the oxide barriers between the LMPs, further enhancing their electrical conductivity of 3×10^6 S m^{-1}. When the material was stretched, the poly(HEA) layer, enriched with hydroxyl groups, enables a natural oxide-driven interface reconciliation of the EGaIn particles, which further boosted the stretchability of the material to up to 2500% strain (Fig. 13g).

These innovations in molecular design and crosslinking strategies represent significant advancements in creating stretchable, high-conductivity materials for use in bioelectronic applications, marking a critical step forward in the development of flexible electronic devices.

5.2. Nanocomposite-based conductors for stretchable electronics

Nanocomposite-based conductors, consisting of conductive fillers embedded in an elastomer matrix, present a promising alternative to conventional electronic materials, owing to their enhanced electrical conductivity and mechanical flexibility.[225,245–248] When combined with fast photo-reactive monomers like acrylates, these composites with CNTs,[249–252] silver nanowires,[253–255] graphene oxide[256,257] or ionic liquids[258,259] can be utilized as photo-patternable conductors. Upon exposure to UV light, a percolated network of conductive fillers forms within the elastomer matrix, enabling continuous charge transport even under mechanical deformation, creating flexible pathways for carrier movement. For example, Yi *et al.* developed a technique to fabricate high-resolution conductive films and micropatterns using an acylate based photoresist and reduced graphene oxide (RGO) with UV photolithography (Fig. 14a).[107] In this method, RGO was formed through *in situ* photoreduction of graphene oxide (GO) in photoresist/GO solution, achieving conductivities of up to 9.90 S cm^{-1} for films and 0.98 S cm^{-1} for micropatterns. The photoinitiator XBPO played a crucial role, initiating both the polymerization of photoresists and the reduction of GO, leading to well-dispersed photoresist/RGO (PRGO) and preventing its oxidation. This approach created patterns with a precision of about 30 μm, compatible with various substrates like PET and silicon.

Benefiting from *in situ* photo-crosslinking, high-resolution photo-crosslinkable conductors with excellent mechanical and electrical properties can be rapidly formed, extending beyond traditional 2D conductive electrodes. These conductors create precise percolated networks of conductive fillers, ensuring stable conductivity even under strain. This method greatly improves the scalability, speed, and cost-effectiveness of producing flexible electronics like sensors and smart devices. Additionally, the ability to integrate multiple materials into a single structure enhances design versatility, enabling the development of advanced applications, including flexible capacitive sensors, force sensors, and 4D-printed devices with expanded functionality.

Xiao *et al.* showcased the use of digital light processing (DLP) 3D printing to pattern multiwalled carbon nanotubes (MWCNTs) in a UV-curable elastomer matrix (Fig. 14b and c).[108] This method allowed for precise and scalable fabrication of complex MWCNT patterns, improving the sensitivity and functionality of strain sensors. With 2 wt% MWCNTs, the sensors achieved a high sensitivity of 8.939, a broad strain detection range of 0.01% to 60%, and exceptional durability over 10 000 cycles. This technique is ideal for flexible, high-performance

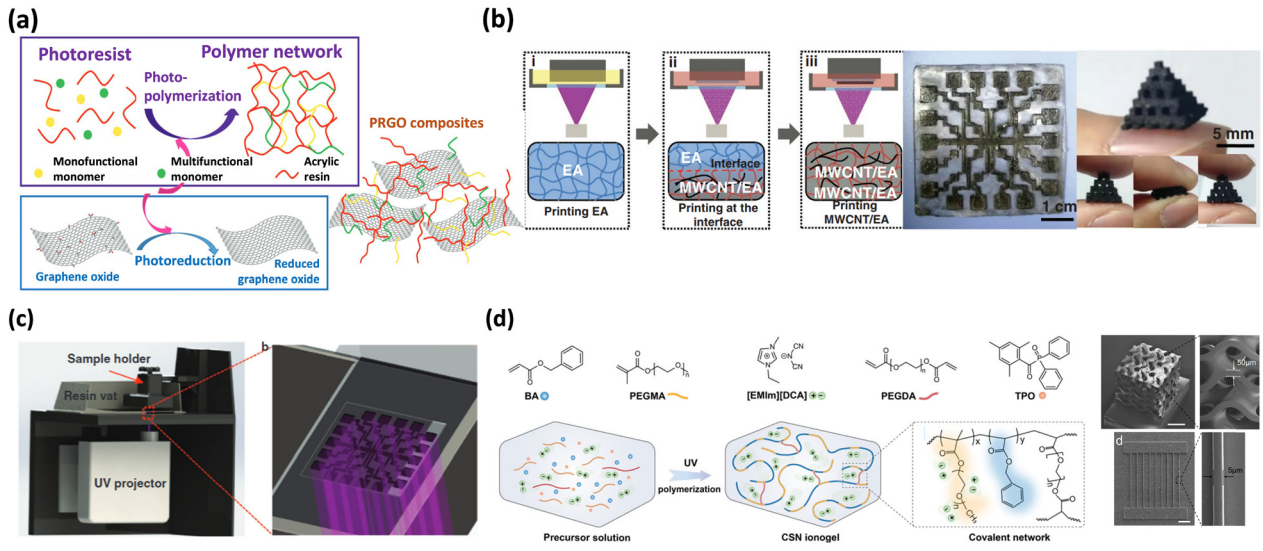

Fig. 14 Nanocomposite-based conductors for stretchable electronics. (a) Schematic illustration of the formation of photoresist/RGO composites through *in situ* photoreduction.[107] Copyright 2023, Wiley-VCH. (b) Schematic showing the 3D printing process of a 4 × 4 strain sensor array and its image. (c) Diagram of the DLP-based 3D printer.[108] Copyright 2021, Wiley-VCH. (d) Chemical structures and photo-polymerization process to prepare a CSN ionogel and SEM images of a 3D printed ionogel.[109] Copyright 2024, Springer Nature.

IoT devices, including human motion detectors and distributed strain sensors.

He *et al.* developed conductive nanostructured ionogels (CSNs) for 3D-printed capacitive sensors, which exhibit a high ionic conductivity of 3 S m^{-1}, an extreme stretchability of 1500%, a low hysteresis of 0.4%, and excellent thermal stability (Fig. 14d).[109] These ionogels were prepared by inducing microphase separation *via* photo-polymerization using acrylate-based monomers and ionic liquids, creating conductive nanochannels intertwined with a crosslinked polymer framework. The use of ionic liquids like [EMIm][DCA] enhanced electrical double layer formation, increasing capacitance and sensitivity up to 15.1 kPa^{-1}. The high printability of CSN ionogels enabled complex geometries to improve sensor performance, making them ideal for wearable and soft electronics.

Similarly, Yu *et al.*[110] and He *et al.*[34] introduced innovative 3D printable nanocomposite ionogels using photo-crosslinkable acrylate-based monomers. Yu *et al.* developed a one-step photopolymerized ionogel incorporating $Al(OH)_3$ nanoparticles as multifunctional crosslinking sites, featuring a high stretchability of 487% and a strength of 2.72 MPa. He *et al.* demonstrated DLP-based multimaterial 3D printing using UV-curable ionic conductive elastomers (UV-ICEs), achieving a high stretchability of 1300% and complex designs for capacitive sensors and 4D printing applications.

6. Applications

In the previous sections, we systematically examined the role of photo-crosslinking at the component level, detailing its impact on mechanical robustness, chemical resistance, and electrical stability. However, beyond the optimization of individual components, it is crucial to understand how these fundamental crosslinking strategies translate into practical benefits at the device level. By leveraging the advantages established at the material level, photo-crosslinking provides a pathway toward the scalable and reliable fabrication of fully integrated flexible and stretchable applications.[37,196,260] The key benefits of photo-crosslinking in integrated devices can be categorized into three main aspects: (i) precise patterning, (ii) simplified fabrication and (iii) enhanced interfacial stability. First, photo-crosslinking enables precise patterning of organic materials,[261] allowing for the incorporation of complex geometric designs with finely tuned mechanical properties.[39] This capability is particularly beneficial for optimizing the sensitivity, stability, and selectivity of flexible and stretchable sensors. Additionally, by adjusting the degree of crosslinking, it is possible to modulate the material's modulus, which is essential for maintaining mechanical compliance in stretchable applications.[262] Second, photo-crosslinking simplifies and optimizes device fabrication by reducing reliance on traditional multi-step photolithography processes that require photoresists. Conventional fabrication methods necessitate careful control of solvent orthogonality to prevent film swelling or material diffusion during curing, which can lead to pattern inaccuracies and resolution limitations. In contrast, photo-crosslinking enables direct solution-based processing, allowing the fabrication of large-area devices with minimized defects.[263] Third, photo-crosslinking enhances interfacial stability between multiple electronic layers, ensuring robust adhesion and mechanical durability. Repeated processing steps in conventional methods can degrade thin films, posing challenges for reliable device integration. Photo-crosslinking improves the chemical resistance of organic layers by facilitating both lamination and patterning in a controlled manner, making them solvent-resistant and mechanically stable under deformation.

This section will focus on fully integrated flexible and stretchable devices utilizing photo-crosslinkable components. We will explore three major application categories: (i) physical sensors, which leverage changes in capacitance or material properties enabled by crosslinking, (ii) OFETs, the foundational circuits in organic electronics, and (iii) OSCs, where crosslinking ensures high efficiency and stability. Each category will highlight how photo-crosslinking contributes to both enhanced device performance and reliability.

6.1. Physical sensors

Stretchable physical sensors capable of measuring external stimuli in real time are essential components of E-skins, which play a critical role in applications such as soft robotics and skin-attachable healthcare devices.[264] Physical sensors, such as pressure and strain sensors, can be classified based on their transduction mechanisms, where mechanical deformation is detected through piezoresistive, capacitive, piezoelectric, or triboelectric methods. Ideal sensors should meet essential criteria, including high sensitivity, stable linearity, low hysteresis, and rapid response times. Unlike conventional rigid sensors, stretchable sensors utilizing elastic polymers as a matrix can withstand deformation while maintaining their electrical properties, thereby enhancing sensing accuracy and improving signal-to-noise (S/N) ratios under optimal conditions.[265–267] However, the elastic characteristics of the polymer matrix can lead to decreased linearity, low repeatability, and diminished durability in practical applications. Recent studies have demonstrated that crosslinking is an effective method for addressing these challenges, and this strategy can be applied to all components of the sensors, including the active layer and electrodes.

The photo-crosslinking approach is applicable to both structure-based[40] and material-based[111–113] strategies for fabricating active layers in stretchable tactile sensors. The structure-based approach, which involves geometric microengineering of the active layer into structures like micropyramids,[114,115,268] improves sensor performance parameters such as sensitivity, response time, relaxation time, and detection limit. A key advantage of photo-crosslinking in this context is its ability to precisely modulate material properties, making it an effective tool for optimizing sensor performance through a structure-based strategy. For example, Park *et al.* developed capacitive strain-insensitive pressure sensors by synthesizing a photo-crosslinkable polymer based on acrylates.[39] The soft acrylate

polymer enabled the selective formation of highly crosslinked rigid islands, exhibiting a 38 000% increase in modulus upon UV irradiation. The rigid region remains mechanically robust while the surrounding soft matrix preserved stretching durability under strain. By incorporating these rigid islands as the dielectric layer in a capacitor, they successfully fabricated a strain-insensitive pressure sensor (Fig. 3c).

Su *et al.* reported a wearable pyramidal-shaped, photo-patternable pressure sensor array integrated with a wearable measurement unit (Fig. 15a).[40] They employed a PDMS matrix with a benzophenone photoinitiator and observed an increase in viscosity as the system photo-crosslinked under UV light. The blended solution was cast onto a 3D-printed plastic mold, which was subsequently spun during photo-patterning under a photomask to create a thin shell pyramidal structure (Fig. 15b). By leveraging photo-crosslinking, they were able to efficiently fabricate this structure, which enhanced interfacial capacitive transduction and ultimately resulted in superior sensing performance. Consequently, the pressure sensor array exhibited remarkable sensing properties, with a maximum sensitivity of 104 kPa^{-1}, and demonstrated excellent repeatability, maintaining stable operation under 4 kPa for 1500 cycles.

In a material-based approach, various elastic materials can be used as candidates for the active layer, including viscoelastic elastomers and ionic conductive hydrogels.[116–118] In the first approach, researchers usually fabricate sensors by incorporating conductive fillers such as CNTs, silver nanowires into stretchable substrates such as polyurethane (PU) and PDMS. Certain photo-crosslinked viscoelastic polymers exhibit excellent cyclic durability, thermal stability, and chemical resilience, along with a low Young's modulus, making them suitable for attachment to human tissue. Due to the reduced glass transition temperature, crosslinked elastomers are deformable and resistant to fracture at room temperature, resulting in increased mechanical strength. The second approach involves ionic conductive hydrogels, which consist of biocompatible hydrophilic polymer gels combined with salts.[88,269,270] These ionic conductors facilitate ion transport, sharing the same electrical signal carriers with biological systems, thus making them suitable for real-time health monitoring. Similar to the structural approach, crosslinking methods are frequently employed to enhance cyclic durability and stability.

Guo *et al.* presented ionic conductive hydrogels fabricated through the photo-crosslinking of monomer blend solution,

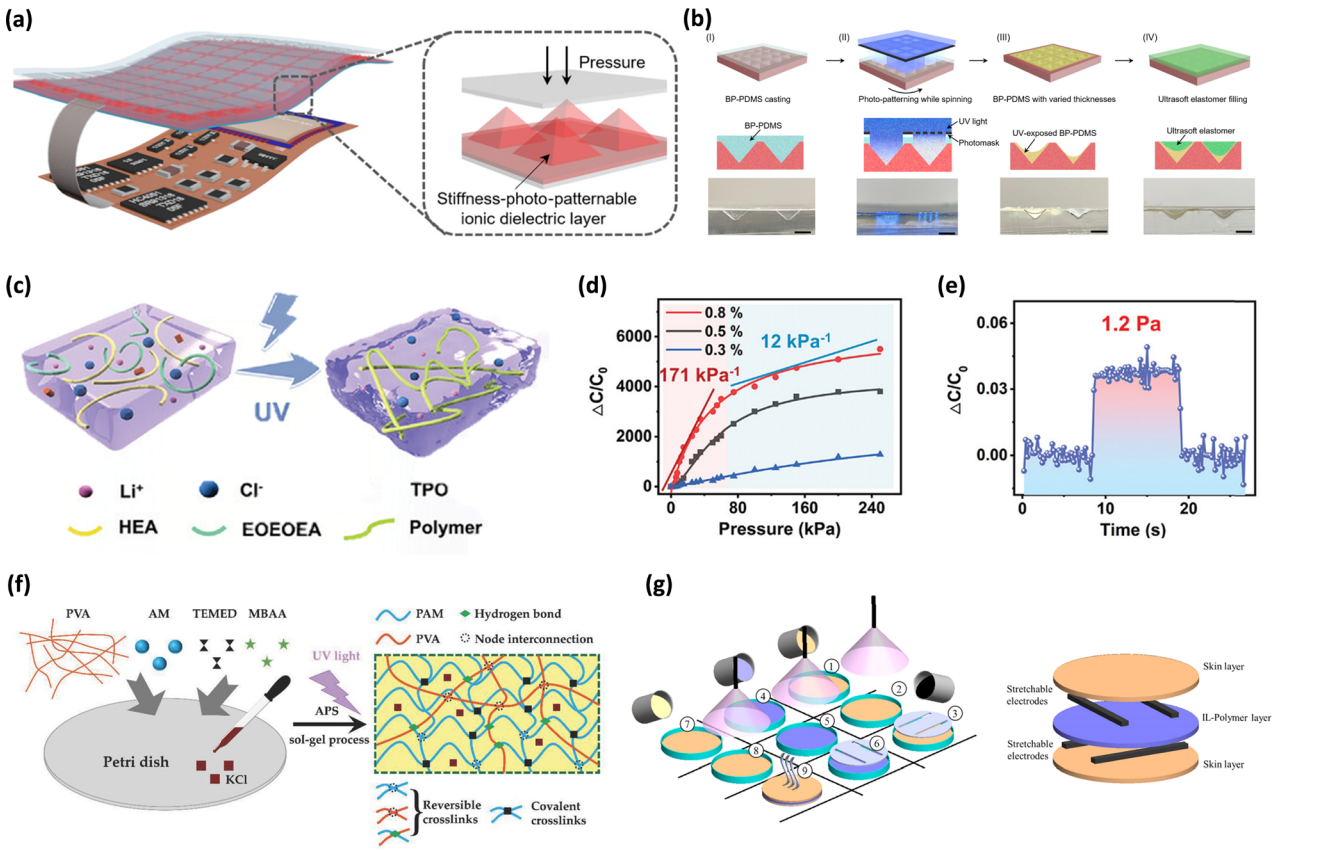

Fig. 15 Schematic diagram of the application of photo-crosslinked polymers in physical sensors. (a) Schematic illustration of a photo-patterned pressure sensor array. (b) Schematic illustration of the fabrication process and corresponding photographs. Scale bars, 2 mm.[40] Copyright 2022, American Chemical Society. (c) Schematic illustration of synthesis of the photocurable ionic hydrogel. (d) Relative capacitance variation as a function of ionic liquid concentration. (e) Relative capacitance variation when a limit of detection pressure is applied to the device.[111] Copyright 2023, Wiley-VCH. (f) Schematic illustration of synthetic process for binary networked hydrogel.[119] Copyright 2018, Wiley-VCH. (g) Schematic illustration of the sensor fabrication process and architecture.[121] Copyright 2017, IOP-Publishing.

which incorporates 2-HEA as a crosslinker, along with the 2-(2-ethoxyethoxy)ethyl acrylate (EOEOEA) monomer and lithium chloride (Fig. 15c).[111] The ionic liquid provides a source of ions, increasing the carrier concentration and the ion transport rate, which subsequently enhances the electrical conductivity of the material. Notably, sensitivity increased with higher concentrations of lithium chloride, with an optimal ion concentration of 0.8% required to preserve the hydrogel's transparency (Fig. 15d). Utilizing this pressure sensor, a minimal detectable pressure of 1.2 Pa was achieved, along with a sensitivity of 171 kPa^{-1} for pressures ranging from 0 to 60 kPa (Fig. 15e).

Similarly, Ge *et al.* developed a conductive dual-crosslinked hydrogel composed of PVA and polyacrylamide (PAM) through a sol–gel process using photo-crosslinking.[119] This process involved the use of PVA, acrylamide (AM), the chemical crosslinker *N*,*N*′-methylenebisacrylamide (MBAA), potassium chloride, and *N*,*N*,*N*′,*N*′-tetramethylethylenediamine (TEMED) as ionic materials to enhance the reaction rate and conductivity. In addition to the covalently crosslinked PVA polymer matrix, the *in situ* crosslinked PVA long chains formed dynamic, reversible crosslinks that further increase the flexibility of the network (Fig. 15f). This was achieved through sliding and unwrapping between the polymer chains, which facilitates energy dissipation. The resultant network exhibited notable piezoresistive behavior, characterized by a high sensitivity (0.05 kPa^{-1} for pressures ranging from 0 to 3.27 kPa), rapid response times, and exceptional stability for pressure sensor applications.

Zhang *et al.* presented a 3D-printable dual-crosslinked ionogel strain sensor characterized by high stretchability, self-healability, and self-adhesiveness.[113] They incorporated a multi-armed, vinyl-functionalized crosslinker, VPOSS, into a polymer matrix comprising the ionic liquid $EMIM(EtO)_2PO_2$ to facilitate efficient photo-crosslinking of polyacrylic acid (PAA). The PAA side chains induced physical crosslinking, which is sacrificial to the external strain. This dual-crosslinked ionogel exhibited remarkable stretchability and durability, demonstrating mechanical properties such as the absence of fatigue resistance and the ability to maintain performance at extreme temperatures (150 °C and −60 °C). The ionic liquid served to weaken the interactions between the polymer molecular chains, thereby enhancing the stretchability of the network, which contributes to a linear relationship between strain and electrical resistance ($\Delta R/R_0$).

Despite the significant potential of hydrogel-based materials for stretchable tactile sensors, current fabrication methods, such as mold curing, limit their applicability in stretchable devices. To address this challenge, some researchers have employed 3D printing technologies to construct intricate microstructures.[120] Lee *et al.* developed piezoelectric sensors using 3D-printable, photocurable materials.[121] Specifically, they utilized an ionic conductive hydrogel composed of acrylate-based monomer, 2-[[(butylamino)carbonyl]oxy]ethyl acrylate (BACOEA) and the ionic liquid 1-ethyl-3-methylimidazolium tetrafluoroborate (EMIMBF4), combined with the acrylate-based crosslinker, glyceryl propoxy triacrylate (GPTA). This mixture was cast into a rigid PTFE Petri dish and subsequently cured. For the substrate, TangoPlus, a rubber suitable for 3D printing, was molded on both sides of the composite, while MWCNTs were employed as electrodes (Fig. 15g). The sensor demonstrated a linear relationship between electrical resistance and strain (<30%) under a force of 15 N.

Similarly, Yan *et al.* developed an ionic conductive tactile sensor with high printability using DLP 3D printing technology.[112] They blended acrylamide (AA) and AM monomers with magnesium chloride and incorporated polyethylene glycol diacrylate (PEGDA) as a crosslinker, curing the material layer by layer to create complex structures. The hydrogel was constructed using a bottom-up printing approach, and the sensor exhibited a high sensitivity (0.06 kPa^{-1}) across a broad detection range (26 kPa–70 kPa) and exceptional stability, sustaining 200 cycles of pressure loading.

To develop fully elastic electronic devices, it is essential to create organic electrodes that conform to biological tissues and accommodate body movements. Several methods have been explored to enhance the elasticity of rigid conductive materials, including application of metallic thin films through structural engineering,[271,272] incorporation of conductive nanoparticles and nanowires into elastomers,[273–275] and fabrication of intrinsically elastic electrodes.[276] Among these strategies, the crosslinking method offers an effective approach for developing intrinsically stretchable organic electrodes while maintaining high conductivity by using brittle materials such as PEDOT:PSS. Although PEDOT exhibits high electrical conductivity and oxidation resistance, its intrinsic stretchability is limited to less than 10%, which hinders its application in wearable electronics. Wang *et al.* developed an elastic capacitive strain sensor using stretchable PEDOT:PSS electrode through the thermal crosslinking of PSS chains with poly(ethylene glycol) diglycidyl ether (PEGDE) as a crosslinker *via* esterification, resulting in a high-quality capacitance strain sensor electrode.[122] Wang *et al.* fabricated a strain sensor device with stretchable PEDOT:PSS electrodes positioned at both ends of the PVDF-HFP active layer. Contrast to the uncrosslinked PEDOT:PSS electrodes, crosslinked PEDOT:PSS electrodes showed low hysteresis under 50% strain and linear relationship between the capacitance variation and strain under 50%, indicating excellent sensing performance. Also, the sensor exhibited stable electrical performance after 2000 cycles.

6.2. OFETs

The simplicity of patterning offered by photo-crosslinkable elastomers,[32] as explained for the above physical sensors, also provides significant advantages for OFETs. This advancement is particularly noteworthy as it simplifies conventional photoresist-based fabrication processes, enhancing the resolution of transistor array patterns. Furthermore, the reduction in complex processing steps minimizes the risk of damage to dielectric[277] or semiconducting layers,[99] reducing current leakage and improving overall transistor performance.[77,278] Photo-crosslinking between layers also helps prevent layer

delamination, ensuring stable device operation. The improved stability enables the development of reliable electronic devices with complex circuits.[123,279–282] Assigning photo-crosslinkable characteristics to essential components, such as the gate dielectric[283–286] and the semiconductor layer functioning as the active matrix,[51,99,204] ensures effective circuit array isolation, further enhancing the reliability of the entire device. Consequently, recent research has increasingly focused on developing OFET arrays through all-solution processes and all-photolithography, highlighting the streamlined and efficient approach that photo-crosslinkable organic materials offer for next-generation device fabrication. Moreover, the self-healing properties[95] and improved interfacial adhesion[207,208] in thin film layers make photo-crosslinkers advantageous for developing stretchable devices. The application of photo-crosslinkers will likely play a critical role in enhancing the resolution of OTFTs and in the production of integrated flexible and stretchable devices in the future.

Using photo-crosslinkable organic materials in OFETs, Kim *et al.* introduced a versatile three-dimensional crosslinker, 4Bx, with a tetrahedral geometry containing four photo-crosslinkable azide moieties.[125] When mixed with solution-processable materials, 4Bx enables photo-patterning of all layers, including polymer semiconductors, polymer insulators, and metal nanoparticles. While crosslinkers typically reduce the intrinsic crystallinity of semiconductors, leading to decreased electrical performance, 4Bx is highly effective even at low concentrations (as little as 1 wt% in the semiconductor layer). Its azide groups enable the formation of a photo-crosslinked network, providing strong solvent resistance without significantly compromising performance. Fig. 16a shows the fabrication of all-photo-patterned OFETs and logic circuits on a flexible plastic substrate, using materials such as the PEN elastomer and AgNPs for the substrate and electrodes. The dielectric and organic semiconducting layers were made flexible by employing PMMA and P(DPP2DT-TVT), respectively. The average hole mobility was estimated to be 0.81 ± 0.18 $cm^2 V^{-1} s^{-1}$. It is noteworthy that a maximum mobility of 1.03 $cm^2 V^{-1} s^{-1}$ was obtained even though all electronic components were photo-patterned. Fig. 16b shows an optical image of a functional logic gate fabricated using this process, with a 4Bx crosslinker incorporated into the n-type semiconductor to enable photo-patterning.

In the study reported by Zheng *et al.*, direct optical polymer patterning was used to fabricate high-density monolithic elastic circuits.[126] The researchers developed an optical microlithography technology by incorporating a branched-diazirine crosslinker into a semiconductor polymer, enabling precise photo-crosslinking. This approach controlled the local solubility of the polymer, allowing the fabrication of micrometer-scale

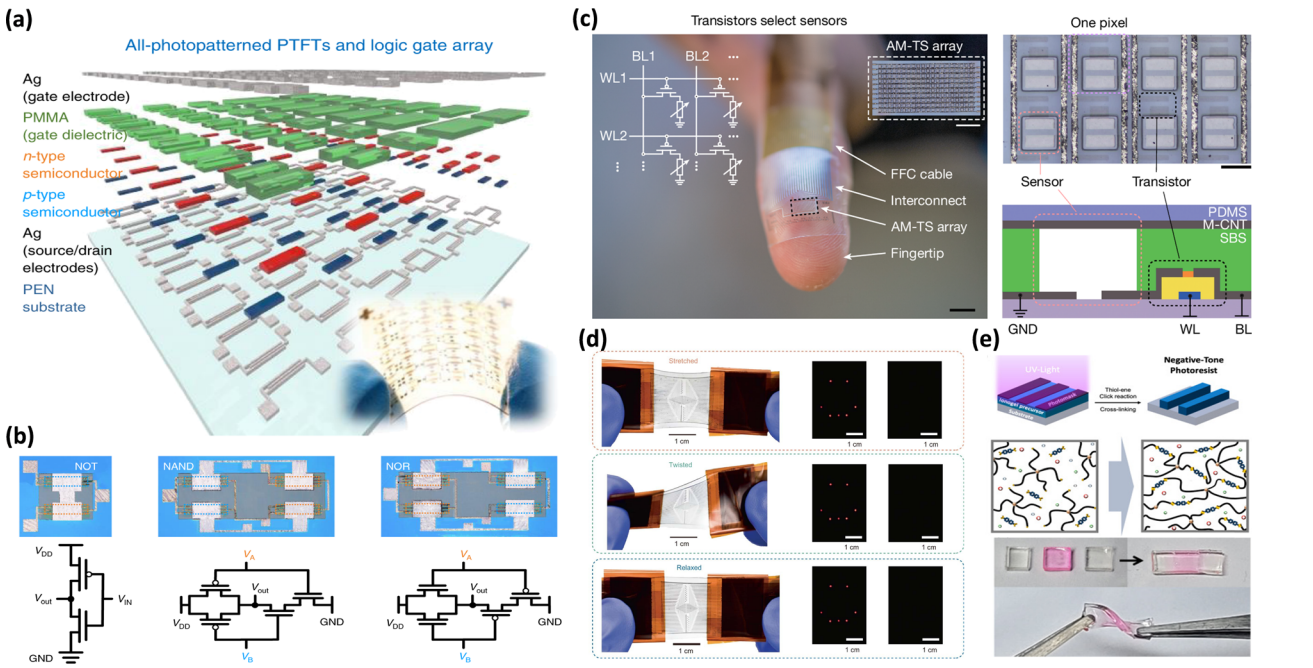

Fig. 16 Schematic diagram of application of photo crosslinked polymers in OFETs. (a) Schematic drawing and photographic image of all-photo-patterned OTFTs and logic circuits fabricated on a plastic substrate by patterning of the semiconducting channel, gate dielectric, and electrode materials. (b) Optical images and schematic circuit diagrams of NOT, NAND, and NOR logic gates based on all-photo-patterned p-type and n-type OTFTs.[125] Copyright 2020, Springer Nature. (c) Schematic illustrating the central role of intrinsically stretchable transistors and circuits for e-skin applications and the high-performance requirements (left). Photo image and schematic of an active-matrix sensor array (right). (d) Photography of the display system and intrinsically stretchable transistor array under deformed/released and corresponding LED display images.[123] Copyright 2024, Springer Nature. (e) Schematics representing the formation of photo-patterns and the corresponding network structure through a thiol–ene click reaction between the polymer ionogels and the crosslinker in an ionic liquid (left). Schematic of an ionogel block after self-healing, and a twisted self-healed ionogel (right).[87] Copyright 2023, Elsevier.

transistors with excellent uniformity and high yield. With the mechanism of the PhotoAssist strategy, based on UV-triggered crosslinking, they facilitated the production of an elastic transistor array comprising 10 000 transistors, which could seamlessly attach to the skin. A 10 × 10 transistor array, fabricated using the same strategy, demonstrated ideal p-type transfer characteristics with minimal hysteresis and an average saturation mobility of 0.255 $cm^2\ V^{-1}\ s^{-1}$. Furthermore, the array withstood 100% strain both parallel and perpendicular to the charge transport direction without showing any visible cracks or delamination and electrical performance degradation.

Zhong *et al.* conducted systematic research on each thin film layer to develop high-density, intrinsically stretchable transistors and integrated circuits with high driving ability, fast operation speed, and large-scale integration.[123] Their intrinsically stretchable transistors demonstrated an impressive average field-effect mobility of over 20 $cm^2\ V^{-1}\ s^{-1}$ under 100% strain, with a device density of 100 000 transistors cm^{-2} (Fig. 16c). The performance was enhanced by incorporating crosslinkable moieties into the dielectric, semiconductor, and electrode layers. Notably, the dielectric layer was photopatterned through a straightforward thiol–ene reaction using a high-κ elastic dielectric material, nitrile-butadiene rubber (NBR) with C=C bonds, and a thiol-containing crosslinker. This study demonstrated the fabrication of high-density, intrinsically stretchable transistors by employing different materials and patterning methods for each layer. These transistors were further used to build several applications, including intrinsically stretchable pseudo-CMOS inverters, active-matrix tactile sensor arrays, and LED displays driven by intrinsically stretchable transistors (Fig. 16d). The work highlighted the potential of photo-crosslinking strategies and material innovations in advancing next-generation stretchable electronic devices.

Furthermore, flexible and stretchable OFETs hold significant potential for bioelectronic applications.[287,288] Jiang *et al.* focused on developing an ideal interface for seamless and biocompatible integration with the human body.[103] Their research led to two key biomedical innovations, which are a soft and stretchable electrode array capable of stable electrophysiological monitoring of deformable tissues and a stretchable high-density array that enables localized neuromodulation for precise control of individual muscle activities. These advancements demonstrated the potential of stretchable OFETs to bridge electronics and biology, paving the way for high-performance, adaptable biomedical devices designed for dynamic interaction with living tissues. Photo-crosslinking offers not only the advantage of creating high-resolution patterns but also introducing self-healing properties. In the recent paper of Kim *et al.*, 3D polymer networks based on a thiol–ene click reaction were used to fabricate self-healing ionogels, which serve as high-capacitance gate dielectrics for OTFTs.[87] The resulting ionogels exhibited self-healing capability under mild conditions of 60 °C for 3 minutes. Fig. 16e illustrates the formation of a crosslinked network *via* UV-induced disulfide bonds, allowing for both photo-patternability and self-healing, as demonstrated by the disulfide metathesis reaction.

6.3. OSCs

Due to environmental concerns and fossil fuel depletion, OSCs have gained significant research interest.[289,290] The photoelectric conversion process in OSCs begins with the photoexcitation in the photoactive layer, where photon absorption generates excitons. These excitons diffuse to the donor–acceptor (D–A) interface and dissociate into holes and electrons, rapidly transferred to the electrodes. Through photo-crosslinking, the thermodynamically metastable state can be preserved, ensuring the morphology of the photoactive layer remains stable under external stimuli, which is essential for advanced OSC applications.[36,101,291,292] Leveraging the stabilizing effect of photo-crosslinking, researchers have applied this strategy in various studies, such as constructing stable BHJs in the active layer and substituting fullerene acceptors with non-fullerene alternatives.

For the practical application of stretchable OSCs, an increase in power conversion efficiency (PCE) resulting from the stabilized morphology of the BHJ in the active layer, along with robust mechanical properties under external strain, is essential. However, high-efficiency OSCs typically require extended π-conjugated backbone molecules and highly ordered crystallinity, which can reduce the device's stretchability. To address the challenge of balancing mechanical and optoelectronic performance in OSCs, many researchers are employing crosslinking reactions in the side chains and main backbone to stabilize both morphology and device performance. Ma *et al.* highlighted the thermal stability benefits provided by the crosslinker DTODF-4F with the BHJ active layer.[293] This crosslinker with a conjugated fluorene-based backbone and epoxy side chains formed a stable network structure through *in situ* crosslinking under UV radiation, which enhances exciton dissociation and reduces traps and defects, leading to improved PCE. While BHJ films are typically optimized through thermal annealing, they suffer from morphological instability under heating or solar radiation, resulting in phase separation and performance degradation (Fig. 17a). The incorporation of C-DTODF-4F, which is photo-crosslinked DTODF-4F, allowed for thermal annealing-induced optimization, followed by UV radiation to fix the morphology, ensuring stability even under continuous heating. Furthermore, they demonstrated that PCE is more stable with DTODF-4F, maintaining 72.7% of its original value after 50 hours of aging, compared to 27.5% for the device without crosslinker (Fig. 17b). This indicated improved thermal stability due to crosslinking. They also demonstrated that adding 0.5% DTODF-4F reduces trap-assisted recombination, as evidenced by the reduction in the V_{oc} slope from 1.19 $kT\ q^{-1}$ to 1.11 $kT\ q^{-1}$. After aging, the V_{oc} slope of devices without crosslinker increased from 1.19 to 1.25, while the DTODF-4F-based devices showed a minimal change from 1.11 to 1.13, demonstrating the superior long-term stability of DTODF-4F-based devices (Fig. 17c).

Inspired by the stabilizing effects of photo-crosslinking on OSCs, researchers have explored the substitution of fullerene-based materials with non-fullerene alternatives.[294–298] While fullerene acceptors have been widely used in OSCs due to their electron affinity and light absorption, they have limitations

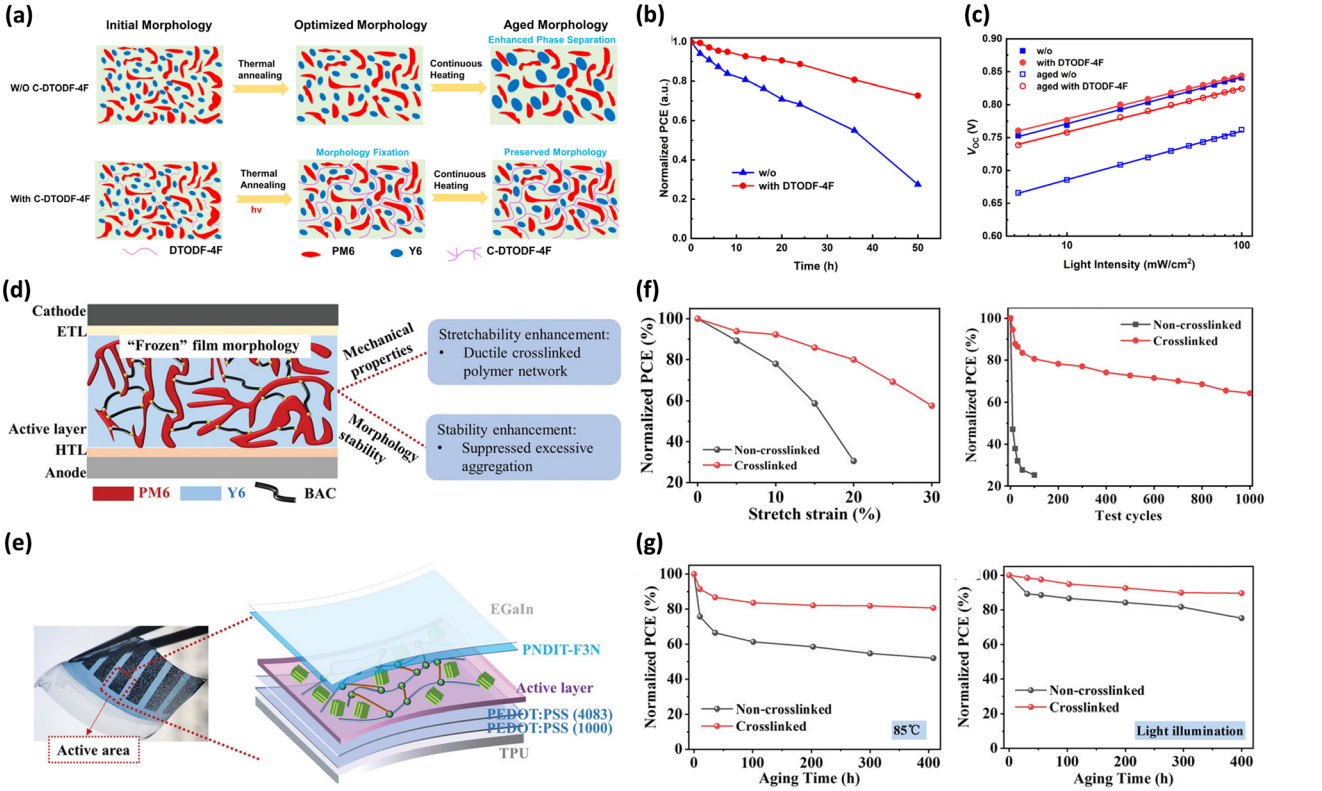

Fig. 17 Schematic diagram of application of photo crosslinked polymers in OSCs. (a) Schematic illustration of the mechanism for crosslinker induced morphological stability. (b) Efficiency evolution of devices w/o and with crosslinker under a thermal condition of 150 °C. (c) Relationship between V_{oc} with the light intensity.[293] Copyright 2022, American Chemical Society. (d) Schematic illustration of crosslinked active layer films. (e) Optical image of intrinsically stretchable OSCs and the corresponding device structure. (f) Normalized PCE variation of intrinsically stretchable OSCs as a function of strain and stretching test cycles. (g) Stability of OSCs under thermal aging and light illumination.[102] Copyright 2022, Wiley-VCH.

such as uncontrollable energy levels and instability. To address these issues, Wang *et al.* introduced crosslinker small molecules 2,6-bis(4-azidobenzylidene)cyclohexanone (BAC) into the donor polymer PM6 and developed the device with an Y6 acceptor molecule (Fig. 17d).[102] Using this active layer, Wang *et al.* fabricated an intrinsically stretchable OSC device with other all-stretchable device components (Fig. 17e). It is important to note that a high density of direct photo-crosslinking can adversely affect the optoelectronic properties of OSCs due to steric hindrance. Therefore, the incorporation of a small amount of crosslinker was critical, for achieving the optimized fill factor (FF), short-circuit current density (J_{sc}), and PCE (Fig. 17f). The OSC maintained its photovoltaic performance of 80% PCE under 20% strain and 64% PCE retention after strain-release cycles under 20% strain. Furthermore, in order to ensure long-term device stability, which encompasses the ability to withstand high temperatures and light exposure, crosslinked layers exhibited significantly slower degradation of PCE, even under harsh conditions (Fig. 17g).

7. Conclusion and outlook

This review has explored recent advancements in photo-crosslinking technologies for flexible and stretchable electronics, which offer effective methods for controlling the physical, chemical, electrical, and mechanical properties of materials. We began by discussing how photo-crosslinking strategies have been employed to enhance the performance of essential components—insulators, semiconducting polymers, and conductors—each presenting unique challenges and requirements. We also highlighted the role of these strategies in facilitating the fabrication of integrated stretchable devices.

For individual components, insulators require distinct crosslinking approaches depending on their function as substrates, dielectrics, or adhesives. For substrates, improving energy dissipation and controlling chain mobility through photo-crosslinking is crucial for enhancing mechanical durability. In dielectric materials, reducing charge trapping and minimizing defects are key objectives, while for adhesives, photo-crosslinking enables precise control over adhesion strength. In semiconducting polymers, photo-crosslinking enhances mechanical durability, electrical performance, and chemical resistance through three key strategies: molecular design, direct crosslinking, and the development of self-crosslinking networks. We also investigated how these strategies impart additional functionalities, further improving both stability and performance. Finally, in conductors, the functionalization of molecular structures and the incorporation of conductive fillers into photo-crosslinkable polymers enable

precise micropatterning and advanced 3D printing, ensuring the integrity of electrical connections even under mechanical deformation.

We further explored how integrated devices benefit from the reliable and facile integration enabled by photo-crosslinking. For example, physical sensors demonstrate excellent durability and conductivity under mechanical stress, with potential applications in 3D printing. In OFETs, photo-crosslinking enhances the resolution of transistor arrays while simplifying the manufacturing process, thereby improving the reliability of high-density integrated devices. Similarly, in OSCs, crosslinked photoactive layers minimize charge traps and defects, ensuring thermodynamic metastability and consistent performance over prolonged operation.

While significant progress has been made in applying photo-crosslinking to stretchable electronics, several considerable challenges remain. For instance, residual small molecules such as photoinitiators and crosslinkers may degrade device electrical properties and adversely affect biocompatibility by causing skin irritation. Additionally, operating conditions in various environments where prolonged exposure to light or high temperatures may trigger additional crosslinking reactions that compromise environmental stability and long-term reliability. Balancing the conflicting demands for flexibility and durability is challenging, and achieving a uniformly controllable crosslinking density remains difficult. Moreover, as device systems become more complex, integrating photo-crosslinkable materials becomes increasingly demanding, requiring careful consideration of adhesion, interfacial compatibility, and process scalability. Overcoming these challenges is essential to fully realize the potential of photo-crosslinkable materials in next-generation flexible and stretchable electronic devices. One promising direction is the precise molecular design of photo-crosslinkable materials, which could unlock advanced functionalities such as self-healing, seamless attachment, molecular passivation, and reversible crosslinking. These innovations are particularly relevant for human body sensors, where they could improve comfort, extend lifespan, and maintain high sensitivity with reliable electrical performance. Additionally, there is great potential in developing advanced applications, such as 3D and 4D printed electronics, where materials can not only offer flexibility and stretchability but also exhibit dynamic, stimuli-responsive behavior, enabling structural and functional transformations over time. By programming crosslinking-induced shape morphing and mechanical adaptability, 4D printing can facilitate the development of reconfigurable and self-adaptive devices with enhanced performance. Such innovations are especially valuable in fields that require both functional complexity and stretchability, including soft robotics and multi-sensor systems.

Beyond fabrication advancements, integrating photo-crosslinking with frontier technologies such as machine learning-driven material design and dynamically reconfigurable devices holds significant promise. Machine learning approaches can facilitate the rapid optimization of crosslinkable material formulations by predicting the relationships between molecular structure, crosslinking density, and final device performance. This data-driven approach could accelerate the discovery of novel crosslinkable systems tailored for specific applications, optimizing mechanical compliance, conductivity, and chemical stability. Furthermore, in dynamically reconfigurable electronics, photo-crosslinking could enable adaptable and reprogrammable materials that respond to external stimuli, such as heat, light, or mechanical strain, paving the way for advanced smart materials with tunable properties. The integration of photo-crosslinking with 4D printing methodologies further expands the possibilities of dynamically changing electronic architectures, enabling multifunctional devices capable of real-time adaptation to environmental conditions.

To fully exploit the potential of photo-crosslinking technology, further research must focus on broadening the range of material functionalities and deepening our understanding of the complex relationships between molecular structure, reactivity, and microphase transitions during the crosslinking process. By optimizing these factors, photo-crosslinking technologies can achieve both precision and functionality, driving new innovations in stretchable electronics. This progress will open up new possibilities across diverse fields, including medical technology, neuroscience, robotics, and environmental monitoring.

Author contributions

J. H. O. proposed the topic of the review and supervised the writing. M. K. and H. P. equally contributed to writing the following main sections: introduction; photo-crosslinkable insulator/semiconductor/conductor for stretchable electronics; and conclusion and outlook. E. K. and M. C. wrote the application section. All authors contributed to the discussion and revision of the manuscript.

Data availability

Data sharing is not applicable, since no new data were created or analyzed in this review.

Conflicts of interest

There are no conflicts to declare.

Acknowledgements

This work was supported by the National Research Foundation of Korea (NRF) grant (2023R1A2C3007715, RS-2024-00398065) through the NRF by the Ministry of Science and ICT (MSIT), Korea. The Institute of Engineering Research at Seoul National University provided research facilities for this work.

References

1 J. A. Rogers, T. Someya and Y. Huang, *Science*, 2010, **327**, 1603–1607.
2 S. Hou, C. Chen, L. Bai, J. Yu, Y. Cheng and W. Huang, *Small*, 2024, **20**, 2306749.
3 K. K. Kim, Y. Suh and S. H. Ko, *Adv. Intell. Syst.*, 2021, **3**, 2000157.
4 H. Kim, J. Lee, U. Heo, D. K. Jayashankar, K.-C. Agno, Y. Kim, C. Y. Kim, Y. Oh, S.-H. Byun and B. Choi, *Sci. Adv.*, 2024, **10**, eadk5260.
5 Q. Zhao, E. Gribkova, Y. Shen, J. Cui, N. Naughton, L. Liu, J. Seo, B. Tong, M. Gazzola and R. Gillette, *Sci. Adv.*, 2024, **10**, eadn7202.
6 D. Liu, X. Tian, J. Bai, S. Wang, S. Dai, Y. Wang, Z. Wang and S. Zhang, *Nat. Electron.*, 2024, **7**, 1176–1185.
7 S. J. Woodman, D. S. Shah, M. Landesberg, A. Agrawala and R. Kramer-Bottiglio, *Sci. Robot.*, 2024, **9**, eadn6844.
8 D. Hu, F. Giorgio-Serchi, S. Zhang and Y. Yang, *Nat. Mach. Intell.*, 2023, **5**, 261–272.
9 Z. Wang and J. Zhu, *Small*, 2024, **20**, 2311012.
10 J. Pu, Q. Cao, Y. Gao, Q. Wang, Z. Geng, L. Cao, F. Bu, N. Yang and C. Guan, *Adv. Mater.*, 2024, **36**, 2305812.
11 S. Xu, Y. Zhang, J. Cho, J. Lee, X. Huang, L. Jia, J. A. Fan, Y. Su, J. Su and H. Zhang, *Nat. Commun.*, 2013, **4**, 1543.
12 S. Naficy, F. Oveissi, B. Patrick, A. Schindeler and F. Dehghani, *Adv. Mater. Technol.*, 2018, **3**, 1800137.
13 Y. Fu, H. He, Y. Liu, Q. Wang, L. Xing and X. Xue, *J. Mater. Chem. C*, 2017, **5**, 1231–1239.
14 G. Zhou, J.-H. Byun, Y. Oh, B.-M. Jung, H.-J. Cha, D.-G. Seong, M.-K. Um, S. Hyun and T.-W. Chou, *ACS Appl. Mater. Interfaces*, 2017, **9**, 4788–4797.
15 D. C. Kim, H. J. Shim, W. Lee, J. H. Koo and D. H. Kim, *Adv. Mater.*, 2020, **32**, 1902743.
16 H. Cho, B. Lee, D. Jang, J. Yoon, S. Chung and Y. Hong, *Mater. Horiz.*, 2022, **9**, 2053–2075.
17 X. Yang, C. Forró, T. L. Li, Y. Miura, T. J. Zaluska, C.-T. Tsai, S. Kanton, J. P. McQueen, X. Chen and V. Mollo, *Nat. Biotechnol.*, 2024, **42**, 1836–1843.
18 J. Gu, Y. Jung, J. Ahn, J. Ahn, J. Choi, B. Kang, Y. Jeong, J.-H. Ha, T. Kim and Y. Jung, *Nano Energy*, 2024, **130**, 110124.
19 X. Huang, L. Liu, Y. H. Lin, R. Feng, Y. Shen, Y. Chang and H. Zhao, *Sci. Adv.*, 2023, **9**, eadh9799.
20 Y. Li, W. Liu, Y. Deng, W. Hong and H. Yu, *npj Flexible Electron.*, 2021, **5**, 3.
21 Y. Wang, Q. Liu, J. Zhang, T. Hong, W. Sun, L. Tang, E. Arnold, Z. Suo, W. Hong and Z. Ren, *Adv. Mater.*, 2019, **31**, 1902955.
22 H. Gao, Z. Wang, F. Yang, X. Wang, S. Wang, Q. Zhang, X. Liu, Y. Sun, J. Kong and J. Yao, *Nat. Commun.*, 2024, **15**, 2321.
23 T. Q. Trung and N. E. Lee, *Adv. Mater.*, 2017, **29**, 1603167.
24 Q. Zhang, J. Liang, Y. Huang, H. Chen and R. Ma, *Mater. Chem. Front.*, 2019, **3**, 1032–1051.
25 H. Hu, C. Zhang, Y. Ding, F. Chen, Q. Huang and Z. Zheng, *Small Methods*, 2023, **7**, 2300671.
26 G. Balakrishnan, J. Song, C. Mou and C. J. Bettinger, *Adv. Mater.*, 2022, **34**, 2106787.
27 Y. Li, N. Li, W. Liu, A. Prominski, S. Kang, Y. Dai, Y. Liu, H. Hu, S. Wai and S. Dai, *Nat. Commun.*, 2023, **14**, 4488.
28 S. Chen, L. Sun, X. Zhou, Y. Guo, J. Song, S. Qian, Z. Liu, Q. Guan, E. Meade Jeffries and W. Liu, *Nat. Commun.*, 2020, **11**, 1107.
29 Q. Xu, P. McMichael, J. Creagh-Flynn, D. Zhou, Y. Gao, X. Li, X. Wang and W. Wang, *ACS Macro Lett.*, 2018, **7**, 509–513.
30 Y. Liu, M. Pharr and G. A. Salvatore, *ACS Nano*, 2017, **11**, 9614–9635.
31 Y. Lee, J. W. Chung, G. H. Lee, H. Kang, J.-Y. Kim, C. Bae, H. Yoo, S. Jeong, H. Cho and S.-G. Kang, *Sci. Adv.*, 2021, **7**, eabg9180.
32 J. S. Kwon, H. W. Park, D. H. Kim and Y.-J. Kwark, *ACS Appl. Mater. Interfaces*, 2017, **9**, 5366–5374.
33 Q. Li, X. Wan, Z. Xu, Y. He, Q. Xue and C. Yang, *Extreme Mech. Lett.*, 2024, **67**, 102128.
34 X. He, J. Cheng, Z. Li, H. Ye, X. Wei, H. Li, R. Wang, Y.-F. Zhang, H. Y. Yang and C. Guo, *ACS Appl. Mater. Interfaces*, 2022, **15**, 3455–3466.
35 D. Wu, S. Wu, P. Narongdej, S. Duan, C. Chen, Y. Yan, Z. Liu, W. Hong, I. Frenkel and X. He, *Adv. Mater.*, 2024, **36**, 2307632.
36 M. Li, Y. G. Yang, Z. K. Wang, T. Kang, Q. Wang, S. H. Turren-Cruz, X. Y. Gao, C. S. Hsu, L. S. Liao and A. Abate, *Adv. Mater.*, 2019, **31**, 1901519.
37 W. Wang, S. Wang, R. Rastak, Y. Ochiai, S. Niu, Y. Jiang, P. K. Arunachala, Y. Zheng, J. Xu, N. Matsuhisa, X. Yan, S. Kwon, M. Miyakawa, Z. Zhang, R. Ning, A. M. Foudeh, Y. Yun, C. Linder, J. B.-H. Tok and Z. Bao, *Nat. Electron.*, 2021, **4**, 143–150.
38 W. Wang, Y. Jiang, D. Zhong, Z. Zhang, S. Choudhury, J.-C. Lai, H. Gong, S. Niu, X. Yan and Y. Zheng, *Science*, 2023, **380**, 735–742.
39 H. G. Park, M. Kim, H. Park and J. H. Oh, *Adv. Funct. Mater.*, 2024, **34**, 2312034.
40 Q. Su, C. Liu, T. Xue and Q. Zou, *ACS Appl. Mater. Interfaces*, 2022, **14**, 33641–33649.
41 A. Ribas-Massonis, M. Cicujano, J. Duran, E. Besalú and A. Poater, *Polymers*, 2022, **14**, 2856.
42 K. S. Lim, J. H. Galarraga, X. Cui, G. C. Lindberg, J. A. Burdick and T. B. Woodfield, *Chem. Rev.*, 2020, **120**, 10662–10694.
43 M. Körner, O. Prucker and J. Rühe, *Macromolecules*, 2016, **49**, 2438–2447.
44 G. Becker, Z. Deng, M. Zober, M. Wagner, K. Lienkamp and F. R. Wurm, *Polym. Chem.*, 2018, **9**, 315–326.
45 Q. Liu and J. L. Locklin, *ACS Omega*, 2020, **5**, 9204–9211.
46 Z. Geng, J. J. Shin, Y. Xi and C. J. Hawker, *J. Polym. Sci.*, 2021, **59**, 963–1042.
47 C. E. Hoyle, A. B. Lowe and C. N. Bowman, *Chem. Soc. Rev.*, 2010, **39**, 1355–1387.
48 M. L. Lepage, C. Simhadri, C. Liu, M. Takaffoli, L. Bi, B. Crawford, A. S. Milani and J. E. Wulff, *Science*, 2019, **366**, 875–878.

49 C. Wu, C. Li, X. Yu, L. Chen, C. Gao, X. Zhang, G. Zhang and D. Zhang, *Angew. Chem.*, 2021, **133**, 21691–21698.
50 S.-S. Ge, B. Chen, Y.-Y. Wu, Q.-S. Long, Y.-L. Zhao, P.-Y. Wang and S. Yang, *RSC Adv.*, 2018, **8**, 29428–29454.
51 S. H. Kim, S. Chung, M. Kim, D. Yoo, E. Ok, S. Kim, K. C. Song, Y. J. Song, B. Kang and K. Cho, *Adv. Funct. Mater.*, 2023, **33**, 2212127.
52 J. Lee, S. Z. Hassan, S. Lee, H. R. Sim and D. S. Chung, *Nat. Commun.*, 2022, **13**, 7021.
53 N. Zivic, P. K. Kuroishi, F. Dumur, D. Gigmes, A. P. Dove and H. Sardon, *Angew. Chem., Int. Ed.*, 2019, **58**, 10410–10422.
54 T. Sun, L. Kang, H. Zhao, Y. Zhao and Y. Gu, *Adv. Sci.*, 2024, **11**, 2302875.
55 T. Tsuchimura, *J. Photopolym. Sci. Technol.*, 2020, **33**, 15–26.
56 N. Klikovits, P. Knaack, D. Bomze, I. Krossing and R. Liska, *Polym. Chem.*, 2017, **8**, 4414–4421.
57 F. Dumur, *Polymers*, 2023, **15**, 4202.
58 L.-Y. Peng, S.-L. Xiang, J.-D. Huang, Y.-Y. Ren, P. Hong, C. Li, J. Liu and M.-Q. Zhu, *Chem. Eng. J.*, 2024, **482**, 148810.
59 J. Deng, S. Bailey, S. Jiang and C. K. Ober, *J. Am. Chem. Soc.*, 2022, **144**, 19508–19520.
60 Y. Liu, D. Wang, Q. Wang and W. Kang, *Small Methods*, 2024, **8**, 2400112.
61 Y. Liu, D. Wang, H. Wang, H. Chen, Q. Wang and W. Kang, *Small*, 2025, 2412297.
62 L. Di Terlizzi, A. Martinelli, D. Merli, S. Protti and M. Fagnoni, *J. Org. Chem.*, 2022, **88**, 6313–6321.
63 W. Xu, T. Li, G. Li, Y. Wu and T. Miyashita, *J. Photochem. Photobiol., A*, 2011, **219**, 50–57.
64 L. Zhang, B. Feng, S. Pang, H. Xin, K. Li and Y. Jin, *J. Mol. Struct.*, 2024, **1304**, 137653.
65 C. J. Martin, G. Rapenne, T. Nakashima and T. Kawai, *J. Photochem. Photobiol., C*, 2018, **34**, 41–51.
66 N. A. Romero and D. A. Nicewicz, *Chem. Rev.*, 2016, **116**, 10075–10166.
67 F. Mohamadpour and A. M. Amani, *RSC Adv.*, 2024, **14**, 20609–20645.
68 C. K. Prier, D. A. Rankic and D. W. MacMillan, *Chem. Rev.*, 2013, **113**, 5322–5363.
69 M. Reckenthaeler and A. G. Griesbeck, *Adv. Synth. Catal.*, 2013, **355**, 2727–2744.
70 B. R. Pfund and O. S. Wenger, *JACS Au*, 2025, **5**, 426–447.
71 N. Zivic, M. Bouzrati-Zerelli, A. Kermagoret, F. Dumur, J. P. Fouassier, D. Gigmes and J. Lalevée, *ChemCatChem*, 2016, **8**, 1617–1631.
72 S. Poplata, A. Tröster, Y.-Q. Zou and T. Bach, *Chem. Rev.*, 2016, **116**, 9748–9815.
73 T. Hughes, G. Simon and K. Saito, *Mater. Horiz.*, 2019, **6**, 1762–1773.
74 S. Pruksawan, J. W. R. Lim, Y. L. Lee, Z. Lin, H. L. Chee, Y. T. Chong, H. Chi and F. Wang, *Commun. Mater.*, 2023, **4**, 75.
75 H. Xu, Y. Zhang, J. Yang, L. Ye, Q. Wu, B. Qu, Q. Wang and Z. Wang, *Polym. Chem.*, 2013, **4**, 3028–3038.
76 S.-H. Kang, J.-W. Jo, J. M. Lee, S. Moon, S. B. Shin, S. B. Choi, D. Byeon, J. Kim, M.-G. Kim and Y.-H. Kim, *Nat. Commun.*, 2024, **15**, 2814.
77 H.-j Kwon, X. Tang, S. Shin, J. Hong, W. Jeong, Y. Jo, T. K. An, J. Lee and S. H. Kim, *ACS Appl. Mater. Interfaces*, 2020, **12**, 30600–30615.
78 M.-J. Kim, H. Park, J. Ha, L. N. T. Ho, E. C. Kim, W. Lee, S. Park, J. C. Won, D.-G. Kim and Y. H. Kim, *J. Mater. Chem. C*, 2021, **9**, 4742–4747.
79 J. Ma, Y. Zhang, Y. Zhang, L. Zhang, S. Zhang, X. Jiang and H. Liu, *J. Energy Chem.*, 2022, **68**, 195–205.
80 K. Kim, H. W. Song, K. Shin, S. H. Kim and C. E. Park, *J. Phys. Chem. C*, 2016, **120**, 5790–5796.
81 H. R. Byun, E. A. You and Y. G. Ha, *Appl. Phys. Lett.*, 2019, **114**, 013301.
82 A. Perinot, F. Scuratti, A. D. Scaccabarozzi, K. Tran, J. M. Salazar-Rios, M. A. Loi, G. Salvatore, S. Fabiano and M. Caironi, *ACS Appl. Mater. Interfaces*, 2023, **15**, 56095–56105.
83 S. Wang, J. Xu, W. Wang, G.-J. N. Wang, R. Rastak, F. Molina-Lopez, J. W. Chung, S. Niu, V. R. Feig and J. Lopez, *Nature*, 2018, **555**, 83–88.
84 K. Kallitsis, D. Thuau, T. Soulestin, C. Brochon, E. Cloutet, F. D. Dos Santos and G. Hadziioannou, *Macromolecules*, 2019, **52**, 5769–5776.
85 G. Lee, S. C. Jang, J. H. Lee, J. M. Park, B. Noh, H. Choi, H. Kweon, D. H. Kim, H. Y. Kim and H. S. Kim, *Adv. Funct. Mater.*, 2024, **34**, 2405530.
86 Y. Liu, J.-Q. Zhao, W.-J. Sun, Y.-K. Huang, S.-J. Chen, X.-J. Guo and Q. Zhang, *Chin. J. Polym. Sci.*, 2018, **36**, 918–924.
87 S. Kim, J. Yeo, S. J. Kim, S. Park, K. G. Cho, K. Paeng, K. H. Lee and M. Kim, *Org. Electron.*, 2023, **122**, 106895.
88 M.-J. Yin, Z. Yin, Y. Zhang, Q. Zheng and A. P. Zhang, *Nano Energy*, 2019, **58**, 96–104.
89 B. T. Michal, E. J. Spencer and S. J. Rowan, *ACS Appl. Mater. Interfaces*, 2016, **8**, 11041–11049.
90 J.-H. Lee, K.-M. Kim, H.-J. Kim and Y. Kim, *Polymer*, 2021, **237**, 124324.
91 S.-W. Kim, Y. H. Ju, S. Han, J. S. Kim, H.-J. Lee, C. J. Han, C.-R. Lee, S.-B. Jung, Y. Kim and J.-W. Kim, *J. Mater. Chem. A*, 2019, **7**, 22588–22595.
92 D. Kim, H. Kim, W. Jeon, H. J. Kim, J. Choi, Y. Kim and M. S. Kwon, *Adv. Mater.*, 2024, **36**, 2309891.
93 A. Nyayachavadi, A. K. Sur, P. Kulatunga, Y. Wang, T. C. Gomes, M. Mooney, G. T. Mason, A. Hu, X. Gu and S. Rondeau-Gagné, *Chem. Mater.*, 2023, **35**, 9682–9691.
94 C. Gao, D. Shi, C. Li, X. Yu, X. Zhang, Z. Liu, G. Zhang and D. Zhang, *Adv. Sci.*, 2022, **9**, 2106087.
95 X. Yu, C. Li, C. Gao, L. Chen, X. Zhang, G. Zhang and D. Zhang, *J. Polym. Sci.*, 2022, **60**, 517–524.
96 H. J. Kim, A.-R. Han, C.-H. Cho, H. Kang, H.-H. Cho, M. Y. Lee, J. M. Frechet, J. H. Oh and B. J. Kim, *Chem. Mater.*, 2012, **24**, 215–221.
97 H. C. Tien, X. Li, C. J. Liu, Y. Li, M. He and W. Y. Lee, *Adv. Funct. Mater.*, 2023, **33**, 2211108.

98 X. Xue, C. Li, Q. Zhou, X. Yu, C. Gao, K. Chenchai, J. Liao, Z. Shangguan, X. Zhang and G. Zhang, *Adv. Mater.*, 2024, **36**, 2407305.
99 R. Chen, X. Wang, X. Li, H. Wang, M. He, L. Yang, Q. Guo, S. Zhang, Y. Zhao and Y. Li, *Sci. Adv.*, 2021, **7**, eabg0659.
100 B. Wang, W. Huang, S. Lee, L. Huang, Z. Wang, Y. Chen, Z. Chen, L.-W. Feng, G. Wang and T. Yokota, *Nat. Commun.*, 2021, **12**, 4937.
101 N. Y. Kwon, S. H. Park, H. Kang, Y. U. Kim, H. D. Chau, A. K. Harit, H. Y. Woo, H. J. Yoon, M. J. Cho and D. H. Choi, *ACS Appl. Mater. Interfaces*, 2021, **13**, 16754–16765.
102 Z. Wang, D. Zhang, M. Xu, J. Liu, J. He, L. Yang, Z. Li, Y. Gao and M. Shao, *Small*, 2022, **18**, 2201589.
103 Y. Jiang, Z. Zhang, Y.-X. Wang, D. Li, C.-T. Coen, E. Hwaun, G. Chen, H.-C. Wu, D. Zhong and S. Niu, *Science*, 2022, **375**, 1411–1417.
104 J. Kim, J. You and E. Kim, *Macromolecules*, 2010, **43**, 2322–2327.
105 N. M. Bojanowski, C. Huck, L. Veith, K.-P. Strunk, R. Bäuerle, C. Melzer, J. Freudenberg, I. Wacker, R. R. Schröder and P. Tegeder, *Chem. Sci.*, 2022, **13**, 7880–7885.
106 M. Wang, S. Kee, P. Baek, M. S. Ting, Z. Zujovic, D. Barker and J. Travas-Sejdic, *Polym. Chem.*, 2019, **10**, 6278–6289.
107 M. Yi, J. Wang, A. Li, Y. Xin, Y. Pang and Y. Zou, *Adv. Mater. Technol.*, 2023, **8**, 2201939.
108 T. Xiao, C. Qian, R. Yin, K. Wang, Y. Gao and F. Xuan, *Adv. Mater. Technol.*, 2021, **6**, 2000745.
109 X. He, B. Zhang, Q. Liu, H. Chen, J. Cheng, B. Jian, H. Yin, H. Li, K. Duan and J. Zhang, *Nat. Commun.*, 2024, **15**, 6431.
110 Z. Yu, N. Bao, H. Liu, X. Zhou, H. Yu, Y. Sun, D. Meng, L. Zhu, N. Aminov and H. Li, *ACS Appl. Mater. Interfaces*, 2023, **15**, 51833–51845.
111 Y. Guo, F. Yin, Y. Li, G. Shen and J. C. Lee, *Adv. Mater.*, 2023, **35**, 2300855.
112 H. Yan, J. Zhou, C. Wang, H. Gong, W. Liu, W. Cen, G. Yuan and Y. Long, *Smart Mater. Struct.*, 2021, **31**, 015019.
113 J. Zhang, E. Liu, S. Hao, X. Yang, T. Li, C. Lou, M. Run and H. Song, *Chem. Eng. J.*, 2022, **431**, 133949.
114 Y. X. Zhang, Y. He, Y. Liang, J. Tang, Y. Yang, H. M. Song, M. Zrínyi and Y. M. Chen, *Appl. Surf. Sci.*, 2023, **615**, 156328.
115 Y. Sun, Q. Li, J. Gong, Z. Li and J. Zhang, *Chem. Eng. Sci.*, 2023, **281**, 119119.
116 C. Luo, Y. Chen, Z. Huang, M. Fu, W. Ou, T. Huang and K. Yue, *Adv. Funct. Mater.*, 2023, **33**, 2304486.
117 X. Zhang, Q. Fu, Y. Wang, H. Zhao, S. Hao, C. Ma, F. Xu and J. Yang, *Adv. Funct. Mater.*, 2024, **34**, 2307400.
118 X. Yao, S. Zhang, L. Qian, N. Wei, V. Nica, S. Coseri and F. Han, *Adv. Funct. Mater.*, 2022, **32**, 2204565.
119 G. Ge, Y. Zhang, J. Shao, W. Wang, W. Si, W. Huang and X. Dong, *Adv. Funct. Mater.*, 2018, **28**, 1802576.
120 Z. Wang, J. Zhang, J. Liu, S. Hao, H. Song and J. Zhang, *ACS Appl. Mater. Interfaces*, 2021, **13**, 5614–5624.
121 J. Lee, M. O. F. Emon, M. Vatani and J.-W. Choi, *Smart Mater. Struct.*, 2017, **26**, 035043.
122 L. Wang, B.-L. Hu, F. Zhang, Y. Zhang, J. Li, T. Xu and R.-W. Li, *J. Mater. Chem. C*, 2023, **11**, 4235–4242.
123 D. Zhong, C. Wu, Y. Jiang, Y. Yuan, M.-G. Kim, Y. Nishio, C.-C. Shih, W. Wang, J.-C. Lai and X. Ji, *Nature*, 2024, **627**, 313–320.
124 Y. Zheng, Z. Yu, S. Zhang, X. Kong, W. Michaels, W. Wang, G. Chen, D. Liu, J.-C. Lai and N. Prine, *Nat. Commun.*, 2021, **12**, 5701.
125 M. J. Kim, M. Lee, H. Min, S. Kim, J. Yang, H. Kweon, W. Lee, D. H. Kim, J.-H. Choi and D. Y. Ryu, *Nat. Commun.*, 2020, **11**, 1520.
126 Y.-Q. Zheng, Y. Liu, D. Zhong, S. Nikzad, S. Liu, Z. Yu, D. Liu, H.-C. Wu, C. Zhu and J. Li, *Science*, 2021, **373**, 88–94.
127 Y. Zheng, L. Michalek, Q. Liu, Y. Wu, H. Kim, P. Sayavong, W. Yu, D. Zhong, C. Zhao and Z. Yu, *Nat. Nanotechnol.*, 2023, **18**, 1175–1184.
128 J. Wang, C. Wang, X. Zhang, H. Wu and S. Guo, *RSC Adv.*, 2014, **4**, 20297–20307.
129 S.-W. Jung, J. B. Koo, C. W. Park, B. S. Na, N.-M. Park, J.-Y. Oh, Y. G. Moon, S. S. Lee and K.-W. Koo, *J. Mater. Chem. C*, 2016, **4**, 4485–4490.
130 Y. Cao, G. Zhang, Y. Zhang, M. Yue, Y. Chen, S. Cai, T. Xie and X. Feng, *Adv. Funct. Mater.*, 2018, **28**, 1804604.
131 J. Park, J. Kim, S.-Y. Kim, W. H. Cheong, J. Jang, Y.-G. Park, K. Na, Y.-T. Kim, J. H. Heo and C. Y. Lee, *Sci. Adv.*, 2018, **4**, eaap9841.
132 L. Luo, Z. Wu, Q. Ding, H. Wang, Y. Luo, J. Yu, H. Guo, K. Tao, S. Zhang, F. Huo and J. Wu, *ACS Nano*, 2024, **18**, 15754–15768.
133 Z. Wu, S. Zhang, A. Vorobyev, K. Gamstedt, K. Wu, C. Guo and S. H. Jeong, *Mater. Today Phys.*, 2018, **4**, 28–35.
134 D. H. Lee, J. Yea, J. Ha, D. Kim, S. Kim, J. Lee, J.-U. Park, T. Park and K.-I. Jang, *ACS Nano*, 2024, **18**, 13061–13072.
135 R. Moser, G. Kettlgruber, C. M. Siket, M. Drack, I. M. Graz, U. Cakmak, Z. Major, M. Kaltenbrunner and S. Bauer, *Adv. Sci.*, 2016, **3**, 1500396.
136 M. Cai, S. Nie, Y. Du, C. Wang and J. Song, *ACS Appl. Mater. Interfaces*, 2019, **11**, 14340–14346.
137 D. Cotton, A. Popel, I. Graz and S. Lacour, *J. Appl. Phys.*, 2011, **109**, 054905.
138 G. Cantarella, V. Costanza, A. Ferrero, R. Hopf, C. Vogt, M. Varga, L. Petti, N. Münzenrieder, L. Büthe and G. Salvatore, *Adv. Funct. Mater.*, 2018, **28**, 1705132.
139 S. Xu, Y. Zhang, L. Jia, K. E. Mathewson, K.-I. Jang, J. Kim, H. Fu, X. Huang, P. Chava and R. Wang, *Science*, 2014, **344**, 70–74.
140 J. C. Yang, S. Lee, B. S. Ma, J. Kim, M. Song, S. Y. Kim, D. W. Kim, T.-S. Kim and S. Park, *Sci. Adv.*, 2022, **8**, eabn3863.
141 W. Fan, Y. Du, Z. Yuan, P. Zhang and W. Fu, *Macromolecules*, 2023, **56**, 6482–6491.
142 Y. Wang, X. Huang, T. Li, Z. Wang, L. Li, X. Guo and P. Jiang, *J. Mater. Chem. A*, 2017, **5**, 20737–20746.

143 F. Li, L. Wang, L. Gao, D. Zu, D. Zhang, T. Xu, Q. Hu, R. Zhu, Y. Liu and B. L. Hu, *Adv. Mater.*, 2024, **36**, 2411082.
144 S. Wang, C. Yang, X. Li, H. Jia, S. Liu, X. Liu, T. Minari and Q. Sun, *J. Mater. Chem. C*, 2022, **10**, 6196–6221.
145 X. Wang, H. Wang, Y. Li, T. Xu, W. Wang, J. Cheng, Z. Shi, D. Yan and Z. Cui, *New J. Chem.*, 2018, **42**, 10969–10975.
146 S. Kumar and A. Dhar, *Mater. Res. Bull.*, 2015, **70**, 590–594.
147 H. J. Kwon, H. Ye, K. Shim, H. G. Girma, X. Tang, B. Lim, Y. Kim, J. Lee, C. E. Park and S. H. Jung, *Adv. Funct. Mater.*, 2021, **31**, 2007304.
148 S. Park, A. K. Palai, J. Park, J. H. Jung and S. Pyo, *Org. Electron.*, 2019, **66**, 169–174.
149 J. E. Q. Quinsaat, M. Alexandru, F. A. Nüesch, H. Hofmann, A. Borgschulte and D. M. Opris, *J. Mater. Chem. A*, 2015, **3**, 14675–14685.
150 M. R. Beaulieu, J. K. Baral, N. R. Hendricks, Y. Tang, A. L. Briseño and J. J. Watkins, *ACS Appl. Mater. Interfaces*, 2013, **5**, 13096–13103.
151 Y.-Z. Yan, S. S. Park, H. R. Moon, W.-J. Zhang, S. Yuan, L. Shi, D. G. Seong and C.-S. Ha, *ACS Appl. Nano Mater.*, 2021, **4**, 8217–8230.
152 J. Su and J. Zhang, *RSC Adv.*, 2015, **5**, 78448–78456.
153 J. Ma, U. Azhar, C. Zong, Y. Zhang, A. Xu, C. Zhai, L. Zhang and S. Zhang, *Mater. Des.*, 2019, **164**, 107556.
154 E. Lee, J. Jung, A. Choi, X. Bulliard, J.-H. Kim, Y. Yun, J. Kim, J. Park, S. Lee and Y. Kang, *RSC Adv.*, 2017, **7**, 17841–17847.
155 J. S. Hur, J. O. Kim, H. A. Kim and J. K. Jeong, *ACS Appl. Mater. Interfaces*, 2019, **11**, 21675–21685.
156 Y. Zhang, K. Zhang, X. Hou, L. Liu and J. Zhang, *New J. Chem.*, 2023, **47**, 2886–2898.
157 H. Ye, E. Park, S. C. Shin, G. Murali, D. Kim, J. Lee, I. H. Kim, S. J. Kim, S. H. Kim and Y. J. Jeong, *Adv. Funct. Mater.*, 2023, **33**, 2214865.
158 Y. Sheima, Y. Yuts, H. Frauenrath and D. M. Opris, *Macromolecules*, 2021, **54**, 5737–5749.
159 J. Mao, J. Li, W. Lin and F. Luo, *Macromol. Rapid Commun.*, 2023, **44**, 2200971.
160 X. Yuan and T. Chung, *Appl. Phys. Lett.*, 2011, **98**, 062901.
161 W. Xu and S.-W. Rhee, *J. Mater. Chem.*, 2009, **19**, 5250–5257.
162 M. N. Tousignant, B. Ronnasi, V. Tischler and B. H. Lessard, *Adv. Mater. Interfaces*, 2023, **10**, 2300079.
163 M. N. Tousignant, Z. S. Lin, J. Brusso and B. H. Lessard, *ACS Appl. Mater. Interfaces*, 2023, **15**, 3680–3688.
164 E. K. Lee, J. Y. Kim, J. W. Chung, B.-L. Lee and Y. Kang, *RSC Adv.*, 2014, **4**, 293–300.
165 F. Huang, Y. Xu, Z. Pan, W. Li and J. Chu, *IEEE Electron Device Lett.*, 2020, **41**, 1082–1085.
166 Y. Li, H. Sun, Y. Shi and K. Tsukagoshi, *Sci. Technol. Adv. Mater.*, 2014, **15**, 024203.
167 C. H. Park, G. Tarsoly, D. Park and S. Pyo, *Polym. Adv. Technol.*, 2023, **34**, 2597–2605.
168 Z. Wang, X. Zhuang, Y. Chen, B. Wang, J. Yu, W. Huang, T. J. Marks and A. Facchetti, *Chem. Mater.*, 2019, **31**, 7608–7617.
169 B. C. Popere, G. E. Sanoja, E. M. Thomas, N. S. Schauser, S. D. Jones, J. M. Bartels, M. E. Helgeson, M. L. Chabinyc and R. A. Segalman, *J. Mater. Chem. C*, 2018, **6**, 8762–8769.
170 Z. Robert Czech, *ChemTexts*, 2024, **10**, 6.
171 Y. Park, J. Kim, D. Kim, S. Lee, D. Hwang and M. S. Kwon, *Soft Sci.*, 2024, **4**, 28.
172 A. B. Croll, N. Hosseini and M. D. Bartlett, *Adv. Mater. Technol.*, 2019, **4**, 1900193.
173 N. D. Blelloch, H. J. Yarbrough and K. A. Mirica, *Chem. Sci.*, 2021, **12**, 15183–15205.
174 C. Bandl, W. Kern and S. Schlögl, *Int. J. Adhes. Adhes.*, 2020, **99**, 102585.
175 X. Wan, Y. He and C. Yang, *Soft Matter*, 2022, **18**, 272–281.
176 Y. Gao, X. Jiang, P. Wang, Y. Zhong and T. Lu, *Extreme Mech. Lett.*, 2023, **61**, 102016.
177 Z. Zhou, Q. Yan, Y. Guo, L. Bai, T. Kalantar, A. Song, W. Zhang and Y. Yu, *ACS Appl. Polym. Mater.*, 2024, **6**, 6788–6799.
178 P. Karnal, A. Jha, H. Wen, S. Gryska, C. Barrios and J. Frechette, *Langmuir*, 2019, **35**, 5151–5161.
179 Y. Gao, K. Wu and Z. Suo, *Adv. Mater.*, 2019, **31**, 1806948.
180 T. Nakamura, Y. Takashima, A. Hashidzume, H. Yamaguchi and A. Harada, *Nat. Commun.*, 2014, **5**, 4622.
181 B. Lee, I. Son, J. H. Kim, C. Kim, J. Y. Yoo, B. W. Ahn, J. Hwang, J. Lee and J. H. Lee, *J. Appl. Polym. Sci.*, 2018, **135**, 46586.
182 H. Zhang and M. Guo, *ACS Appl. Mater. Interfaces*, 2024, **16**, 43180–43188.
183 J. Bonaldo, M. Banea, R. Carbas, L. Da Silva and S. De Barros, *J. Adhes.*, 2019, **95**, 995–1014.
184 S. Lu, Z. Ma, M. Ding, Y. Wu, Y. Chen, M. Dong and L. Qin, *Chem. Eng. J.*, 2024, **486**, 150393.
185 S. Leijonmarck, A. Cornell, C.-O. Danielsson, T. Åkermark, B. D. Brandner and G. Lindbergh, *Int. J. Adhes. Adhes.*, 2012, **32**, 39–45.
186 Y.-Z. Wang, L. Li, F.-S. Du and Z.-C. Li, *Polymer*, 2015, **68**, 270–278.
187 Y. Wu, B. D. Clarke, K. M. Liechti and Z. A. Page, *Chem. Mater.*, 2024, **36**, 8066–8075.
188 T.-H. Lee, J.-H. Back, J.-S. Lim, G.-Y. Han, M.-B. Yi, Y. Kim, J.-H. Lee, S. Kim and H.-J. Kim, *Composites, Part B*, 2024, **272**, 111175.
189 T.-H. Lee, G.-Y. Han, M.-B. Yi, H.-J. Kim, J.-H. Lee and S. Kim, *ACS Appl. Mater. Interfaces*, 2021, **13**, 43364–43373.
190 S. Saito, S. Nobusue, E. Tsuzaka, C. Yuan, C. Mori, M. Hara, T. Seki, C. Camacho, S. Irle and S. Yamaguchi, *Nat. Commun.*, 2016, **7**, 12094.
191 H.-W. Park, H.-S. Seo, K. Kwon and S. Shin, *RSC Adv.*, 2023, **13**, 11874–11882.
192 G. Wang, X. Huang, Z. Zhou, Y. Zhang and Y. Yu, *Chem. Eng. J.*, 2024, **499**, 155820.
193 K. Boga, A. F. Patti, J. C. Warner, G. P. Simon and K. Saito, *ACS Appl. Polym. Mater.*, 2023, **5**, 4644–4653.
194 D. Yoo, D. J. Won, W. Cho, S. Kim and J. Kim, *Small Methods*, 2021, **5**, 2101049.

195 C. Hwang, J.-H. Back, D. Ahn, H.-J. Paik, W. Lee and Y. Yu, *Polym. Chem.*, 2022, **13**, 193–200.
196 H.-C. Tien, Y.-W. Huang, Y.-C. Chiu, Y.-H. Cheng, C.-C. Chueh and W.-Y. Lee, *J. Mater. Chem. C*, 2021, **9**, 2660–2684.
197 J. C. Yang, J. Mun, S. Y. Kwon, S. Park, Z. Bao and S. Park, *Adv. Mater.*, 2019, **31**, 1904765.
198 L. Ding, Z.-D. Yu, X.-Y. Wang, Z.-F. Yao, Y. Lu, C.-Y. Yang, J.-Y. Wang and J. Pei, *Chem. Rev.*, 2023, **123**, 7421–7497.
199 Y. Zheng, S. Zhang, J. B.-H. Tok and Z. Bao, *J. Am. Chem. Soc.*, 2022, **144**, 4699–4715.
200 H. Ren, Y. Tong, M. Ouyang, J. Wang, L. Zhang, Y. Fu and Q. Tang, *J. Mater. Chem. C*, 2022, **10**, 14921–14928.
201 J. Mun, Y. Ochiai, W. Wang, Y. Zheng, Y.-Q. Zheng, H.-C. Wu, N. Matsuhisa, T. Higashihara, J. B.-H. Tok and Y. Yun, *Nat. Commun.*, 2021, **12**, 3572.
202 Z. Ding, D. Liu, K. Zhao and Y. Han, *Macromolecules*, 2021, **54**, 3907–3926.
203 N. Sun, Y. Han, W. Huang, M. Xu, J. Wang, X. An, J. Lin and W. Huang, *Adv. Mater.*, 2024, **36**, 2309779.
204 Z. Ma, B. Zhao, H. Gao, Y. Gong, R. Yu and Z. A. Tan, *J. Mater. Chem. A*, 2022, **10**, 18542–18576.
205 J. Freudenberg, D. Jänsch, F. Hinkel and U. H. Bunz, *Chem. Rev.*, 2018, **118**, 5598–5689.
206 G.-J. N. Wang, Y. Zheng, S. Zhang, J. Kang, H.-C. Wu, A. Gasperini, H. Zhang, X. Gu and Z. Bao, *Chem. Mater.*, 2018, **31**, 6465–6475.
207 J. Kang, J. Mun, Y. Zheng, M. Koizumi, N. Matsuhisa, H.-C. Wu, S. Chen, J. B.-H. Tok, G. H. Lee and L. Jin, *Nat. Nanotechnol.*, 2022, **17**, 1265–1271.
208 J. Liu, J. Wang, Z. Zhang, F. Molina-Lopez, G.-J. N. Wang, B. C. Schroeder, X. Yan, Y. Zeng, O. Zhao and H. Tran, *Nat. Commun.*, 2020, **11**, 3362.
209 C. J. Mueller, T. Klein, E. Gann, C. R. McNeill and M. Thelakkat, *Macromolecules*, 2016, **49**, 3749–3760.
210 D. Zhang, C. Li, G. Zhang, J. Tian and Z. Liu, *Acc. Chem. Res.*, 2024, **57**, 625–635.
211 F. J. Kahle, C. Saller, A. Köhler and P. Strohriegl, *Adv. Energy Mater.*, 2017, **7**, 1700306.
212 C.-Y. Nam, Y. Qin, Y. S. Park, H. Hlaing, X. Lu, B. M. Ocko, C. T. Black and R. B. Grubbs, *Macromolecules*, 2012, **45**, 2338–2347.
213 N. Haberkorn, J. S. Gutmann and P. Theato, *ACS Nano*, 2009, **3**, 1415–1422.
214 X. Guo, Q. Tan, S. Liu, D. Qin, Y. Mo, L. Hou, A. Liu, H. Wu and Y. Ma, *Nano Energy*, 2018, **46**, 150–157.
215 A. Nyayachavadi, A. Langlois, M. N. Tahir, B. Billet and S. Rondeau-Gagne, *ACS Appl. Polym. Mater.*, 2019, **1**, 1918–1924.
216 J. Farinhas, Q. Ferreira, R. E. Di Paolo, L. Alcácer, J. Morgado and A. Charas, *J. Mater. Chem.*, 2011, **21**, 12511–12519.
217 K. Zhang, C. Zhong, S. Liu, C. Mu, Z. Li, H. Yan, F. Huang and Y. Cao, *ACS Appl. Mater. Interfaces*, 2014, **6**, 10429–10435.
218 M. Schock and S. Bräse, *Molecules*, 2020, **25**, 1009.
219 Z.-S. Tan, Z. Jamal, D. W. Teo, H.-C. Ko, Z.-L. Seah, H.-Y. Phua, P. K. Ho, R.-Q. Png and L.-L. Chua, *Nat. Commun.*, 2024, **15**, 6354.
220 D. W. Teo, Z. Jamal, H.-Y. Phua, C. G. Tang, R.-Q. Png and L.-L. Chua, *ACS Appl. Mater. Interfaces*, 2019, **11**, 48103–48112.
221 R.-Q. Png, P.-J. Chia, J.-C. Tang, B. Liu, S. Sivaramakrishnan, M. Zhou, S.-H. Khong, H. S. Chan, J. H. Burroughes and L.-L. Chua, *Nat. Mater.*, 2010, **9**, 152–158.
222 S. F. Musolino, M. Mahbod, R. Nazir, L. Bi, H. A. Graham, A. S. Milani and J. E. Wulff, *Polym. Chem.*, 2022, **13**, 3833–3839.
223 K. Dey, S. R. Chowdhury, E. Dykstra, A. Koronatov, H. P. Lu, R. Shinar, J. Shinar and P. Anzenbacher, *J. Mater. Chem. C*, 2020, **8**, 11988–11996.
224 A. F. Gomes and F. C. Gozzo, *J. Mass Spectrom.*, 2010, **45**, 892–899.
225 S. Choi, S. I. Han, D. Kim, T. Hyeon and D.-H. Kim, *Chem. Soc. Rev.*, 2019, **48**, 1566–1595.
226 W. C. Gao, J. Qiao, J. Hu, Y. S. Guan and Q. Li, *Responsive Mater.*, 2024, **2**, e20230022.
227 N. Matsuhisa, X. Chen, Z. Bao and T. Someya, *Chem. Soc. Rev.*, 2019, **48**, 2946–2966.
228 S. Nagels and W. Deferme, *Materials*, 2018, **11**, 375.
229 L. Wang, Z. Yi, Y. Zhao, Y. Liu and S. Wang, *Chem. Soc. Rev.*, 2023, **52**, 795–835.
230 Y. Wang, C. Zhu, R. Pfattner, H. Yan, L. Jin, S. Chen, F. Molina-Lopez, F. Lissel, J. Liu and N. I. Rabiah, *Sci. Adv.*, 2017, **3**, e1602076.
231 L. V. Kayser and D. J. Lipomi, *Adv. Mater.*, 2019, **31**, 1806133.
232 D. J. Lipomi, J. A. Lee, M. Vosgueritchian, B. C.-K. Tee, J. A. Bolander and Z. Bao, *Chem. Mater.*, 2012, **24**, 373–382.
233 H. Stoyanov, M. Kollosche, S. Risse, R. Waché and G. Kofod, *Adv. Mater.*, 2013, **25**, 578–583.
234 Y. Shi, M. Wang, C. Ma, Y. Wang, X. Li and G. Yu, *Nano Lett.*, 2015, **15**, 6276–6281.
235 J. Hur, K. Im, S. W. Kim, J. Kim, D.-Y. Chung, T.-H. Kim, K. H. Jo, J. H. Hahn, Z. Bao and S. Hwang, *ACS Nano*, 2014, **8**, 10066–10076.
236 J. Lowe and S. Holdcroft, *Macromolecules*, 1995, **28**, 4608–4616.
237 J. Lowe and S. Holdcroft, *Synth. Met.*, 1997, **85**, 1427–1430.
238 J. Kim, Y. Kim and E. Kim, *Macromol. Res.*, 2009, **17**, 791–796.
239 B. Lussem, C.-M. Keum, D. Kasemann, B. Naab, Z. Bao and K. Leo, *Chem. Rev.*, 2016, **116**, 13714–13751.
240 M. D. Dickey, *Adv. Mater.*, 2017, **29**, 1606425.
241 X. Wang and J. Liu, *Micromachines*, 2016, **7**, 206.
242 Y. G. Park, G. Y. Lee, J. Jang, S. M. Yun, E. Kim and J. U. Park, *Adv. Healthcare Mater.*, 2021, **10**, 2002280.
243 S. Chen, Z. Cui, H. Wang, X. Wang and J. Liu, *Appl. Phys. Rev.*, 2023, **10**, 021308.
244 G.-H. Lee, H. Kim, J. Lee, J.-Y. Bae, C. Yang, H. Kim, H. Kang, S. Q. Choi, S. Park and S.-K. Kang, *Mater. Today*, 2023, **67**, 84–94.

245 B. Llerena Zambrano, A. F. Renz, T. Ruff, S. Lienemann, K. Tybrandt, J. Vörös and J. Lee, *Adv. Healthcare Mater.*, 2021, **10**, 2001397.
246 J. Chen, Q. Yu, X. Cui, M. Dong, J. Zhang, C. Wang, J. Fan, Y. Zhu and Z. Guo, *J. Mater. Chem. C*, 2019, **7**, 11710–11730.
247 S. Peng, Y. Yu, S. Wu and C.-H. Wang, *ACS Appl. Mater. Interfaces*, 2021, **13**, 43831–43854.
248 O. Kanoun, A. Bouhamed, R. Ramalingame, J. R. Bautista-Quijano, D. Rajendran and A. Al-Hamry, *Sensors*, 2021, **21**, 341.
249 S. K. Eshkalak, A. Chinnappan, W. Jayathilaka, M. Khatibzadeh, E. Kowsari and S. Ramakrishna, *Appl. Mater. Today*, 2017, **9**, 372–386.
250 A. Mora, P. Verma and S. Kumar, *Composites, Part B*, 2020, **183**, 107600.
251 K. Gnanasekaran, T. Heijmans, S. Van Bennekom, H. Woldhuis, S. Wijnia, G. De With and H. Friedrich, *Appl. Mater. Today*, 2017, **9**, 21–28.
252 B. Podsiadły, P. Matuszewski, A. Skalski and M. Słoma, *Appl. Sci.*, 2021, **11**, 1272.
253 T. E. Glier, L. Akinsinde, M. Paufler, F. Otto, M. Hashemi, L. Grote, L. Daams, G. Neuber, B. Grimm-Lebsanft and F. Biebl, *Sci. Rep.*, 2019, **9**, 6465.
254 N. Sharma, N. M. Nair, G. Nagasarvari, D. Ray and P. Swaminathan, *Flexible Printed Electron.*, 2022, **7**, 014009.
255 D. J. Finn, M. Lotya and J. N. Coleman, *ACS Appl. Mater. Interfaces*, 2015, **7**, 9254–9261.
256 Y. Qian, C. Li, Y. Qi and J. Zhong, *Carbon*, 2021, **171**, 777–784.
257 A. Chiappone, I. Roppolo, E. Naretto, E. Fantino, F. Calignano, M. Sangermano and F. Pirri, *Composites, Part B*, 2017, **124**, 9–15.
258 J. Huang, Z. Yu and P. Wu, *Adv. Sci.*, 2023, **10**, 2302891.
259 J. Cheng, R. Wang, Z. Sun, Q. Liu, X. He, H. Li, H. Ye, X. Yang, X. Wei and Z. Li, *Nat. Commun.*, 2022, **13**, 7931.
260 H. Mu, W. Wang, L. Yang, J. Chen, X. Li, Y. Yuan, X. Tian and G. Wang, *Energy Storage Mater.*, 2021, **39**, 130–138.
261 J. Shi, Z. Wang, T. Zheng, X. Liu, B. Guo and J. Xu, *Mater. Horiz.*, 2022, **9**, 3070–3077.
262 G. Zhao, J. Sun, M. Zhang, S. Guo, X. Wang, J. Li, Y. Tong, X. Zhao, Q. Tang and Y. Liu, *Adv. Sci.*, 2023, **10**, 2302974.
263 Y. Sun, H. Jiang, L. Zhu and C. Wong, *IEEE Trans. Compon. Packag. Technol.*, 2008, **31**, 135–142.
264 J. W. Gu, J. H. Lee and S. K. Kang, *Adv. Sens. Res.*, 2023, **2**, 2300013.
265 Y.-S. Guan, F. Ershad, Z. Rao, Z. Ke, E. C. da Costa, Q. Xiang, Y. Lu, X. Wang, J. Mei and P. Vanderslice, *Nat. Electron.*, 2022, **5**, 881–892.
266 X. Liu, X. Chen, X. Chi, Z. Feng, C. Yang, R. Gao, S. Li, C. Zhang, X. Chen and P. Huang, *Nano Energy*, 2022, **92**, 106735.
267 S. Shen, Z. Du, P. Zhou, Z. Zou and X. Lyu, *Adv. Funct. Mater.*, 2024, **34**, 2408017.
268 K. Kang, H. Jung, S. An, H. W. Baac, M. Shin and D. Son, *Polymers*, 2021, **13**, 3272.
269 H. Liu, X. Wang, Y. Cao, Y. Yang, Y. Yang, Y. Gao, Z. Ma, J. Wang, W. Wang and D. Wu, *ACS Appl. Mater. Interfaces*, 2020, **12**, 25334–25344.
270 J.-Y. Yu, S. E. Moon, J. H. Kim and S. M. Kang, *Nano-Micro Lett.*, 2023, **15**, 51.
271 S. Jang, C. Kim, J. J. Park, M. L. Jin, S. J. Kim, O. O. Park, T.-S. Kim and H.-T. Jung, *Small*, 2018, **14**, 1702818.
272 D.-H. Kim, N. Lu, R. Ma, Y.-S. Kim, R.-H. Kim, S. Wang, J. Wu, S. M. Won, H. Tao and A. Islam, *Science*, 2011, **333**, 838–843.
273 W. Hu, R. Wang, Y. Lu and Q. Pei, *J. Mater. Chem. C*, 2014, **2**, 1298–1305.
274 T. Sekitani, Y. Noguchi, K. Hata, T. Fukushima, T. Aida and T. Someya, *Science*, 2008, **321**, 1468–1472.
275 D. Jung, C. Lim, H. J. Shim, Y. Kim, C. Park, J. Jung, S. I. Han, S.-H. Sunwoo, K. W. Cho and G. D. Cha, *Science*, 2021, **373**, 1022–1026.
276 P. Zhao, Q. Tang, X. Zhao, Y. Tong and Y. Liu, *J. Colloid Interface Sci.*, 2018, **520**, 58–63.
277 J. Choi, J. Kang, C. Lee, K. Jeong and S. G. Im, *Adv. Electron. Mater.*, 2020, **6**, 2000314.
278 S. Otep, K. Ogita, N. Yomogita, K. Motai, Y. Wang, Y.-C. Tseng, C.-C. Chueh, Y. Hayamizu, H. Matsumoto and K. Ishikawa, *Macromolecules*, 2021, **54**, 4351–4362.
279 L. Liu, S. Li, L. Wu, D. Chen, K. Cao, Y. Duan and S. Chen, *Org. Electron.*, 2021, **89**, 106047.
280 W. Wu, *Sci. Technol. Adv. Mater.*, 2019, **20**, 187–224.
281 K. Tang, W. Miao and S. Guo, *ACS Appl. Polym. Mater.*, 2021, **3**, 1436–1444.
282 P. A. Lopes, B. C. Santos, A. T. de Almeida and M. Tavakoli, *Nat. Commun.*, 2021, **12**, 4666.
283 R. Teruel-Juanes, B. Pascual-Jose, C. del Río, O. García and A. Ribes-Greus, *React. Funct. Polym.*, 2020, **155**, 104715.
284 M. Cruz, S. McKillop, V. Tischler and B. H. Lessard, *Macromol. Rapid Commun.*, 2024, **45**, 2400205.
285 H. Burgoon, C. Cyrus, D. Skilskyj, J. Thoresen, C. Ebner, G. A. Meyer, P. Filson, L. F. Rhodes, T. Backlund and A. Meneau, *ACS Appl. Polym. Mater.*, 2020, **2**, 1819–1826.
286 J. Peng, C. Guo, X. Hu, H. Du, Q. Peng, H. Hu, W. Yuan, J. Yang and J. Ma, *RSC Appl. Polym.*, 2024, **2**, 606–611.
287 B. van Bochove and D. W. Grijpma, *J. Biomater. Sci., Polym. Ed.*, 2019, **30**, 77–106.
288 H. Tetsuka, L. Pirrami, T. Wang, D. Demarchi and S. R. Shin, *Adv. Funct. Mater.*, 2022, **32**, 2202674.
289 K. Fukuda, K. Yu and T. Someya, *Adv. Energy Mater.*, 2020, **10**, 2000765.
290 L. Duan and A. Uddin, *Adv. Sci.*, 2020, **7**, 1903259.
291 S. Tu, X. Lin, L. Xiao, H. Zhen, W. Wang and Q. Ling, *Mater. Chem. Front.*, 2022, **6**, 1150–1160.
292 M. H. Jee, B. Park, A. Y. Lee, S. Rhee, M. Lim, J. M. Ha, N. Kim, F. Zhang, J. W. Ha and H. Ahn, *Chem. Eng. J.*, 2024, **490**, 151624.

293 Z. Ma, Y. Dong, Y.-J. Su, R. Yu, H. Gao, Y. Gong, Z.-Y. Lee, C. Yang, C.-S. Hsu and Z. A. Tan, *ACS Appl. Mater. Interfaces*, 2021, **14**, 1187–1194.
294 A. Armin, W. Li, O. J. Sandberg, Z. Xiao, L. Ding, J. Nelson, D. Neher, K. Vandewal, S. Shoaee and T. Wang, *Adv. Energy Mater.*, 2021, **11**, 2003570.
295 F. Zhao, H. Zhang, R. Zhang, J. Yuan, D. He, Y. Zou and F. Gao, *Adv. Energy Mater.*, 2020, **10**, 2002746.
296 K. An, W. Zhong, F. Peng, W. Deng, Y. Shang, H. Quan, H. Qiu, C. Wang, F. Liu and H. Wu, *Nat. Commun.*, 2023, **14**, 2688.
297 C. Li, J. Zhou, J. Song, J. Xu, H. Zhang, X. Zhang, J. Guo, L. Zhu, D. Wei and G. Han, *Nat. Energy*, 2021, **6**, 605–613.
298 D. Luo, W. Jang, D. D. Babu, M. S. Kim, D. H. Wang and A. K. K. Kyaw, *J. Mater. Chem. A*, 2022, **10**, 3255–3295.